Hydrogen Recovery and Utilization from Water Splitting Processes

Wasserstoffrückgewinnung und -nutzung aus Wasserspaltungsprozessen

Von der Fakultät für Maschinenwesen
der Rheinisch-Westfälischen Technischen Hochschule Aachen
zur Erlangung des akademischen Grades
eines Doktors der Ingenieurwissenschaften genehmigte Dissertation

vorgelegt von
Sari Alsayegh

Berichter:
Univ.-Prof. Dr.-Ing. Matthias Wessling
Prof. Eric Favre, Ph.D.

Tag der mündlichen Prüfung: 3 Juli 2018

Acknowledgment

First of all, I would like to express my sincere gratitude to my advisor Prof. Matthias Wessling for the continuous support of my Ph.D study and related research, for his patience, motivation, and immense knowledge. His guidance helped me in all the time of research and in writing of this thesis. He has been supportive and has given me the freedom to pursue my Ph.D topic without objection. At the same time, he has provided insightful discussions about each step, which has lead to my success.

Besides my advisor, I would like to thank the rest of my thesis committee: Prof. Eric Favre, and Prof. Stefan Pischinger for their review, insightful comments and encouragement during my PhD defense.

Similar, profound gratitude goes to Dr. J.R. Johnson, who has been a truly dedicated mentor. I am particularly indebted to J.R. for his constant faith in my work, and for his support and encouragement.

My sincere thanks also goes to Burkhard Ohs and Johannes Lohaus for their guidance through the modeling and simulation work, to my office mate Bander Bawareth who shared with me all the ups and downs during our time together and to all my colleagues in the department for their support.

Also, I would like to thank SABIC (Saudi Arabian Basic Industrial Cooperation) for sponsoring my higher education program at RWTH university.

Last but not the least, I would like to thank my wife Hanaa, my sons Omar & Emad and my parents for supporting me spiritually throughout writing this thesis and my life in general.

Thank you!

Sari Alsayegh July 2018

Abstract

Renewable energy sources must be adopted in order to satisfy the increase in global energy demand all the while minimizing the carbon footprint. One obvious energy source is solar. Aside from traditional electricity generation technologies, solar energy can be utilized to produce H_2 (as an energy carrier) via photocatalytic water splitting. In a typical process, both H_2 and O_2 are produced in the same reactor environment, thereby creating a potentially hazardous scenario. This obstacle can be avoided by utilizing flammability suppressants to recover the product outside the flammability regime. The scope of this thesis is to identify membrane-based processes to recover and utilize H_2 generated from photocatalytic water splitting while maintaining safety and flammability constraints throughout the separation process.

Two flammability suppressants were investigated, namely: N_2 and CO_2. Detailed information about H_2 flammability in these two diluents and the impact of the operating conditions were described in order to identify the parametric range that ensures a safe separation process. To be more genuine in designing the membrane-based process, an optimization study for the whole process economic was implemented using commercially available membrane materials. These membrane units were incorporated in different process layouts to achieve high purity and recovery values while applying flammability constraints in all pertinent streams. The results for both suppressants revealed the advantage of CO_2 over N_2 as a suppressant, where the H_2 product was recovered at a higher purity with lower specific cost and O_2 concentration. However, both diluent systems revealed imposing recovery costs due to the low H_2 concentration in the feed. Further studies were conducted to show the impact of varying feed compositions, high performance polymeric membrane materials (not commercialized), and alternative membrane configurations (hollow fiber / spiral wound) on the process economics.

As a conceptual culmination of the initial process design work, a renewable methanol production route was proposed to integrate technologies into a complete petrochemical facility. Through integration, the aim was to improve the overall process economics through the production of a more value-added product. This approach utilized H_2 from photocatalytic water splitting and captured CO_2 (e.g. flue gas). Contrary to the previous approach, the membrane-based separation process was optimized to produce a 3:1 H_2 and CO_2 mixture. This binary mixture was used as the feedstock for a conceptual direct CO_2 hydrogenation methanol synthesis plant. Based on a detailed economic analysis, the break-even value of the methanol produced using this approach is higher than the current market of methanol. However, it is very comparable to other renewable methanol routes proposed in the literature. Sensitivity analysis was carried out on different economic and energy parameters to show their impact on both economic and energy efficiencies of the proposed process. The sensitivity analysis revealed the strong influence of CO_2 market price on the process economics over other considered parameters.

The design approach and the optimization models developed in this study are not limited to H_2 recovery from photocatalytic water splitting. Other gas separation applications, that involve flammability constraints, can be easily implemented. Hence, these models provide a strong tool for similar future works.

Kurzfassung

Der Einsatz von erneuerbarer Energie ist entscheidend um den gesteigerten Energiebedarf zu decken und gleichzeitig den globalen CO_2 Ausstoß zu minimieren. Sonnenenergie kann neben der direkten Erzeugung von Elektrizität auch für die Produktion von H_2 durch das photokatalytische Aufspalten von Wasser genutzt werden. In diesem Prozess entsteht ein explosives H_2 sowie ein O_2 Gemisch. Um die Entzündung zu verhindern, werden Inertgase eingesetzt, wodurch das Gemisch nicht in dem Entflammbarkeitsbereich liegt. Ziel der Arbeit ist die Identifizierung membranbasierter Prozesse, die das in einem photokatalytischen Prozess gewonnene H_2 anreichern unter Gewährleistung von Sicherheits- und Entflammbarkeitsgrenzen.

Zwei Inertgase (CO_2, N_2) zur Unterdrückung der Entflammbarkeit werden untersucht. Detaillierte Informationen zu der Entflammbarkeit von H_2 mit diesen beiden Inertgase und Bereiche der sicheren Betriebsbedingungen werden beschrieben. Um den Membranprozess effizienter und realistischer zu gestalten, wurde eine globale Optimierung des gesamten Prozesses mit kommerziell erhältlichen Membranmaterialien durchgeführt. Um hohe Ausbeuten und Reinheiten unter gleichzeitiger Einhaltung der Entflammbarkeitsgrenzen zu generieren, wurden unterschiedliche Verschaltungsschemen der Membraneinheiten evaluiert. Die Ergebnisse zeigen, dass CO_2 durch die stärkere Unterdrückung der Entflammbarkeit Vorteile gegenüber N_2 bietet. Mit CO_2 können höhere H_2 Reinheiten bei geringeren spezifischen Kosten und geringeren O_2 Konzentrationen erzielt werden. Allerdings führt der Einsatz beider Inertgas und die damit verbundene geringere H_2 Konzentration des Feeds zu höheren Aufbereitungskosten. Weitere ökonomische Studien wurden durchgeführt, um den Einfluss der Feedzusammensetzung, leistungsstärkerer Polymermembranen (nicht kommerziell) und alternative Membrankonfiguration (Spiralwickelmembran/ Hohlfasermembran) zu evaluieren.

Als anfängliche Prozessdesignarbeit wurde ein erneuerbares Methanolproduktionsverfahren vorgeschlagen, um Technologien in eine komplette petrochemische Anlage zu integrieren. Ziel der Integration war es, die Gesamtprozessökonomie durch die Herstellung eines höherwertigen Produktes zu verbessern. Bei diesem Ansatz wurde H_2 aus einer photokatalytischer Wasserspaltung und gespeichertes CO_2 verwendet. Im Gegensatz zum vorherigen Ansatz wurde der membranbasierte Trennungsprozess optimiert, um ein 3:1 H_2- und CO_2-Gemisch zu erzeugen. Diese binäre Mischung wurde als Ausgangsmaterial für eine direkte CO_2 -Hydrierungs-Methanolsyntheseanlage verwendet. Basierend auf einer ökonomischen Analyse ist der Break-even-Wert des mit diesem Ansatz hergestellten Methanols höher als der aktuelle Marktpreis. Allerdings ist es mit denen in der Literatur vorgeschlagenen erneuerbaren Methanolrouten vergleichbar. Eine Sensitivitätsanalyse wurde an wirtschaftlichen und energetischen Parametern durchgeführt, um ihre Auswirkungen auf die Wirtschaftlichkeit und Energieeffizienz des vorgeschlagenen Verfahrens zu zeigen. Der CO_2 Marktpreis zeigt sich als der dominante Faktor für die Ökonomie des Prozesses.

Der Entwurfsansatz und die entwickelten Optimierungsmodelle beschränken sich nicht auf die H_2-Rückgewinnung aus der photokatalytischen Wasserspaltung. Andere Gastrennungsanwendungen, die Entflammbarkeitseinschränkungen beinhalten, sind leicht implementierbar. Daher bieten die Modelle ein starkes Werkzeug für zukünftige Arbeiten.

CONTENTS

CHAPTER 1

Introduction

1.1 Motivation

The global energy demand has been increasing dramatically for the past decades as indicated in Figure 1.1 [1]. To satisfy this increase, greater consumption of fossil fuels will be required to provide a steady and reliable source of energy. In fact, it is estimated that 38% increase in fossil fuel production and consumption will be required by 2040 in order to satisfy the demands [1] - unless alternative solutions are adopted. Fossil fuel resources are finite and combustion thereof has negative environmental impacts, such as increasing greenhouse gas (GhG) emissions . Accounting for more than 60% of GhG, CO_2 emissions are the main contributor to global climate change [2, 3]. Countless studies and observations show the potential harmful impacts of these gases on our environment including rising sea levels and superstorms [4–6]. To minimize anthropogenic influence on the environment, industrial nations must take the lead and implement global efforts to reduce CO_2 emissions and limit the temperature increase to 2°C [3, 7]. Therefore, researchers must focus on further developing sustainable and green energy sources [8].

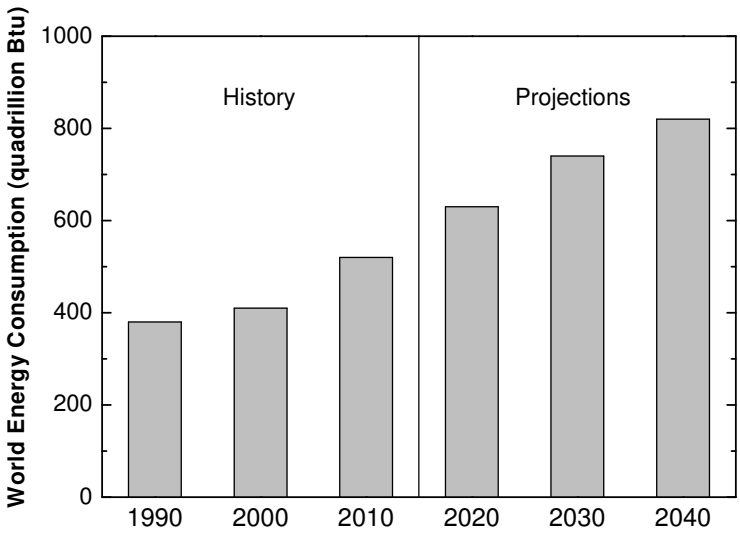

Figure 1.1: World energy consumption growth between 1990 and 2040 [1].

Solar energy, for example, has the potential of being a primary energy source for many regions in the future. For instance, the amount of potential energy from one hour of sunlight is enough to satisfy the energy demand for an entire year [9, 10]. In order to utilize such an ideal source, more efficient and cost effective technologies have to be established to convert, capture and store the energy. Utilization of solar energy can be achieved in two forms: (1) direct production of electrical energy (e.g. photovoltaic) or (2) creation of energy carriers (e.g. H_2). Per mole, the energy value released from H_2 combustion is 2.75 times greater than typical hydrocarbon fuels [10, 11]. Not only that, the primary combustion product is water, instead of carbon dioxide. These two advantages make H_2 an attractive candidate to supplement future energy demand and potentially reduce environmental impact [8, 12, 13].

1.2 Water splitting processes

Nowadays, most of the global H_2 production is produced via steam reforming of natural gas [11, 14]. Other methods include coal gasification, partial oxidation of ethanol and water electrolysis [11]. Additional techniques can be utilized using solar energy, which includes solar cells, reforming of biomass and water splitting [15–18]. Water splitting holds particular interest since it utilizes water, an inexpensive and abundant resource. H_2 production from solar and water splitting can be classified into three main types: thermochemical, photobiological, and photocatalytic water splitting processes [19, 20].

Thermochemical water splitting utilizes solar heat directly. The reaction operates at elevated temperatures using collected and/or concentrated heat from sunlight. This reaction is typical carried out over a metal/metal oxide catalyst, such as Zn/ZnO [21]. The thermochemical cycle starts when the solar heat is used to reduce the metal oxide to its metallic form, thereby releasing O_2. The highly active metal species will readily react with water to form H_2 and revert back to the metal oxide [21, 22]:

$$\mathrm{ZnO} + \mathrm{Heat}(\sim 2000\,^{\circ}\mathrm{C}) \longrightarrow \mathrm{Zn} + \mathrm{O_2}$$

$$\mathrm{Zn} + \mathrm{H_2O} + \mathrm{Heat}(\sim 500\,^{\circ}\mathrm{C}) \longrightarrow \mathrm{ZnO} + \mathrm{H_2}$$

Zinc is one example; researchers are actively exploring other catalytic materials (e.g. Fe_3O_4/FeO and CeO_2/CeO_3) [23, 24]. Challenges facing this approach include high heat management and control, heat-resistant materials selection and the capital cost of large-scale solar concentrators.

Biological routes for H_2 production can be classified based on the microorganisms selected, products generated and reaction mechanism(s) [19, 25]. For example, oxygenic photosynthesis process converts water into H_2 and O_2 using green algae or cyanobacteria along with a particular enzyme (hydrogenase or nitrogenase) under anaerobic conditions. These organisms can survive under sunlight and CO_2 without organic carbon source [26]. The process produces both H_2 and O_2 as shown in the following simplified reaction [25]:

$$4\,\mathrm{H_2O} + \mathrm{Light\,Energy} \longrightarrow 2\,\mathrm{O_2} + 4\,\mathrm{H_2}$$

Photocatalytic water splitting is a light-induced conversion reaction of water to its constituent gases, H_2 and O_2. This reaction is initiated when solar photons are absorbed by a semiconductor material that can convert photon energy into a current that electrolyzes water [27]. Fundamentally, the minimum potential difference (voltage) needed to split water is 1.23 eV [28]:

$$\mathrm{H_2O} + 1.23\,\mathrm{V} \rightleftharpoons \mathrm{H_2} + \frac{1}{2}\mathrm{O_2}$$

This process has attracted significant attention from the scientific community for more than 40 years. The first paper described this approach was presented by Fujishima and Honda in 1972 using a TiO_2 photoelectrode [29, 30]. Two primary approaches can be applied to produce H_2 via photocatalytic water splitting - depending on the type of catalyst [12, 31].

The one-step approach splits water using a single catalyst, which coproduces H_2 and O_2 in a reactor (see Figure 1.2). Although a straightforward concept on paper, this configuration introduces an out of the ordinary risk of explosion. Moreover, no technology has been developed so far to separate H_2 and O_2 mixtures [31]. The two-step approach, also known as 'Z-Scheme', requires two catalysts to produce H_2 and the O_2 in separate chambers. Such a configuration does mitigate the explosion hazard. However, there are substantial materials challenges remaining regarding electron transfer between the two chambers and prevention of the backward reactions [12, 32].

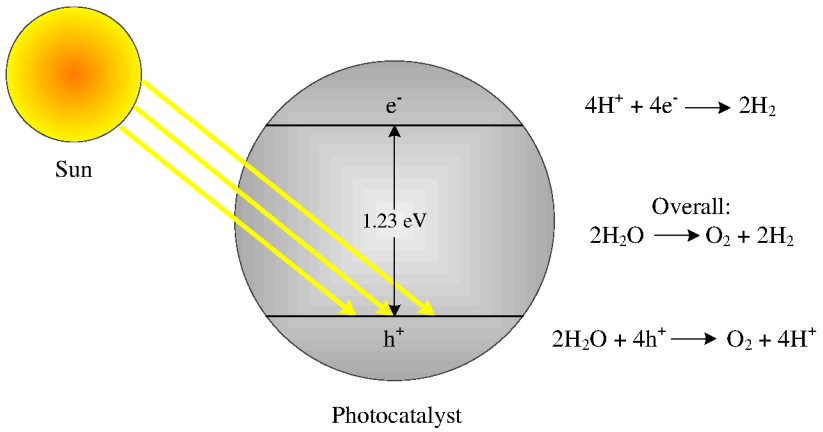

Figure 1.2: Photocatalytic water splitting (one-step approach) [20, 27].

Recently, a full techno-economic analysis of four different technologies utilizing the photo-electrochemical (PEC) approach for water splitting was reported by the US Department of Energy (DOE) [27, 28]. The findings of this study showed that the single-bed colloidal suspension reactor, which utilizes photocatalytic nanoparticles (one-step approach), has the lowest estimated H_2 production price of $\$1.6/kg_{H_2}$. In this concept, a transparent slurry reactor, made of high-density polyethylene (HDPE), is used to permit sunlight penetration. The semiconductor, nano-sized catalysts are suspended in a potassium hydroxide (KOH) electrolyte solution. An example catalyst is 40 nm iron oxide (Fe_2O_3) with a 5nm shell layer of TiO_2 [28]. Upon reacting with sunlight, the catalysts produce electron-hole pairs that react with water to drive both the H_2 and O_2 evolution reactions. While the chemistry is sound and reactor design is an effective solution, the study discounted the explosion hazards of the product mixture. Such hazards make the process industrially unrealistic, as presented in the DOE report.

1.3 Thesis objective and outline

The scientific objective of this thesis is to identify a membrane-based separation process that can recover and utilize the H_2 produced from photocatalytic process (one-step approach). Recovered H_2 can be either used as an energy source or in the production for

more value-added chemicals. Two different gases, namely: N_2 and CO_2, are explored as possible flammability suppressant to overcome the flammability constraints raised from the simultaneous production of H_2 and O_2. A full techno-economic analysis is conducted for all possible scenarios proposed in this study to genuinely evaluate the commercialization of this approach.

Chapter 2 provides an overview on the latest development of H_2 production including conventional processes and renewable routes. Membrane and other separation techniques are briefly discussed to address the relevant separation of H_2 from the tertiary mixture of ($H_2/O_2/N_2$) and ($H_2/O_2/CO_2$). Moreover, list of commercially available membrane materials is developed for comparison purposes. The chapter concludes with the importance of H_2 in the field of energy and petrochemical industry with more emphasis on the use of H_2 in the production of ammonia and methanol.

Chapter 3 describes the utilization of N_2 diluent for the recovery of H_2 from water splitting. Before investigation this scenario, detailed information is given about the flammability limits of H_2 in the tertiary mixture of $H_2/O_2/N_2$ and the influence of both temperature and pressure on these limits values. This step is essential to identify the safe operating conditions to design the membrane separation and minimize the computational time required for the optimization study. The investigation is carried in three steps: (1) ambient/vacuum pressure process, (2) high/vacuum pressure process and (3) optimization. Influence on the process economics as a function of feed concentration and membrane material performance are addressed in the optimization study.

Chapter 4 highlights the advantages of utilizing CO_2 over N_2 as a diluent for the photocatalytic reactor. The optimization study is carried on several membrane cascade designs using commercially available composite polymer membrane from MTR in the spiral wound architecture. Both H_2-selective and CO_2-selective membrane materials are used in designing the proposed layouts. The chapter concludes with a comparative cost analysis between the operation of spiral wound and hollow fiber membrane architectures. Hypothetical hollow fibers based on the MTR materials were used in this investigation.

Chapter 5 demonstrates a conceptual process and its economic viability of a novel methanol production route utilizing captured CO_2 (i.e. from flue gas) and H_2 produced via photocatalytic water splitting. This conceptual process comprised of integrated facilities to produce methanol. The first process unit supplies captured CO_2, which is used as a raw material and a diluent to recover H_2 safely from the photocatalytic reactors. The tertiary mixture ($H_2/O_2/CO_2$) is safely processed in a membrane-based separation plant, which was optimized to produce a 3:1 H_2 and CO_2 mixture. This binary mixture is then used as feedstock for methanol production via the direct CO_2 hydrogenation approach. Both economic and energy analysis will be carried for this process in order to compare it with other alternative renewable methanol routes.

CHAPTER 2

State of the Art: H_2 Production, Purification and Applications

2.1 Introduction

H_2 is a promising alternative as future energy carrier due to diverse advantages. It has a higher energy yield compared to conventional fossil fuels. In addition, it is extremely abundant as it can be found on both water and biomass. Finally, it can be stored in different forms (e.g., gaseous, liquid, metal hydride) [16, 19]. However, the major drawback of H_2 applicability for transportation fuel is its low energy density, which results in the requirement of compressing into liquid form at low temperatures. This step has a significant energy penalty and requires capital intensive equipment. Storing H_2 in metal hydride has its own challenges as these metals are usually heavy, expensive, and have a limited lifetime [19].

The majority of the H_2 global production is derived from four conventional routes: 48% produced from methane reforming, 30% from oil reforming, 18% from coal gasification and 3.9% from water electrolysis [33]. Other non-conventional methods only account for 0.1% of the global H_2 production [16, 34]. However, most of these production routes produce by-products (e.g., CO_2, CO) that need to be removed for environmental reasons or preventing catalyst poisoning in the downstream processes. These purification techniques commonly include pressure swing adsorption (PSA), polymeric/inorganic membranes, and metal hydrides.

This chapter will provide an overview on the latest development of H_2 production including the conventional processes listed above and renewable routes. Membrane and other separation techniques are briefly discussed to address the relevant recovery of H_2 from tertiary mixtures of $H_2/O_2/N_2$ and $H_2/O_2/CO_2$, as they apply to photocatalytic water splitting applications. The chapter concludes with an overview of H_2 utilization in the production of ammonia and methanol. Figure 2.1 shows an overview of production, purification and utilization technologies for H_2 [35].

2.2 H_2 production

2.2.1 Conventional routes

As stated before, reforming of methane, which contains the highest H_2 to carbon ratio among hydrocarbons, is the most common production route for H_2. The process industrially occurs at elevated temperatures (700-1100°C) and pressures (20-40 bar) [36]. Two distinguished techniques are utilized. Steam methane reforming (SMR) processes convert both methane and steam into syngas over Ni-based catalysts, as described by the following endothermic reaction [37]:

$$CH_4 + H_2O \rightleftharpoons CO + 3\,H_2$$

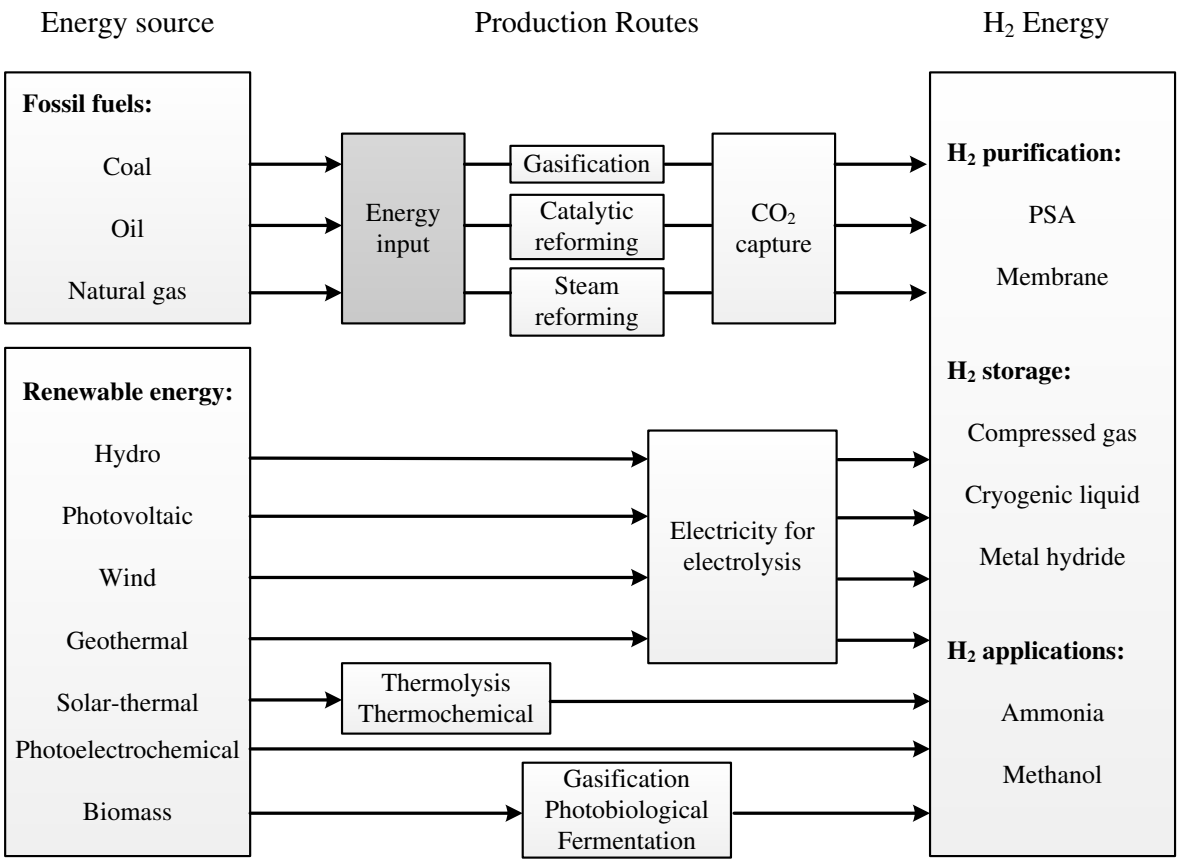

Figure 2.1: H_2 production, purification, storage, and applications (adopted from [35]).

The heat of reaction required must be supplied externally. More H_2 can be obtained by reacting additional steam with carbon monoxide via water gas shift reaction (WGS) at lower temperature over a Cu-based catalyst [19]:

$$CO + H_2O \rightleftharpoons CO_2 + H_2$$

Autothermal reforming (ATR) is the other traditional methane reforming technique. In this process, O_2 is used directly in the reaction along with steam to partially oxidize methane into syngas [38, 39]:

$$CH_4 + \frac{1}{2}O_2 \rightleftharpoons 2\,H_2 + CO$$

$$CO + H_2O \rightleftharpoons CO_2 + H_2$$

In many cases, SMR and ATR are used in series to optimize the syngas products for chemical production. Both technologies are well established and very mature. However, there is ongoing research focusing on different supporting materials / promoters for the Ni-based catalyst [40, 41], renewable energy sources to drive the reforming reaction [42], and membrane reactors to combine H_2 production and purification in one step [43, 44].

The second largest source of H_2 is the catalytic reforming of oil (heavy naphtha) to increase

the octane number in the automobiles' gasoline production. The main feed entering the catalytic reforming section contains paraffins, olefins, naphthenes and aromatics [45]. Higher gasoline octane number can be obtained by converting paraffins, olefins and naphthenes into aromatics through three different reactions [45]:

- Dehydrogenation of naphthenes into aromatics

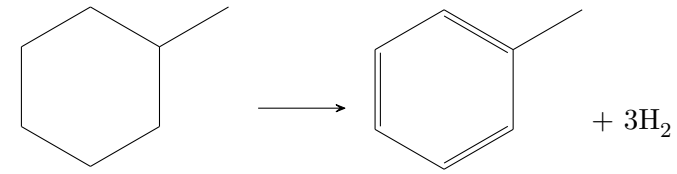

- Dehydrocyclization of paraffins into aromatics

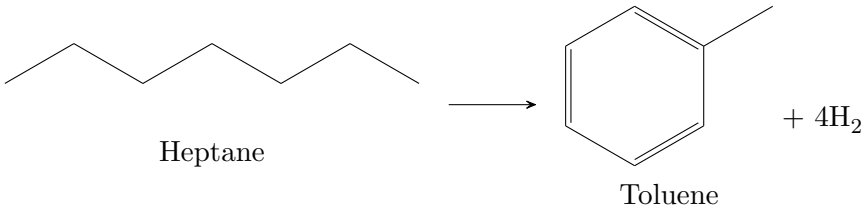

- Hydrocracking of olefins and large paraffins into smaller paraffins, which are then converted to aromatics

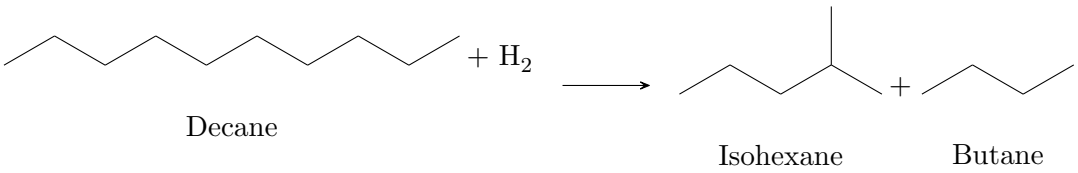

The net production of H_2 is about 50-200 m^3/m^3 of liquid naphtha despite the consumption in the hydrocracking step reaction [46]. The excessed H_2 is used mainly in other processes involved in the oil refinery complex [47].

Countries rich in coal feedstocks, such as China and South Africa, use coal gasification systems to generate energy, H_2, and/or syngas [48, 49]. For this process, partial oxidation of coal occurs at high temperatures and pressures in the presence of both O_2 and steam as shown in the following net reactions:

$$C + \frac{1}{2}O_2 \longrightarrow CO$$

$$C + H_2O \longrightarrow CO + H_2$$

Coal gasification is considered one of the cheapest routes for H_2 production given the abundance and price of coal feedstocks [22]. Nevertheless, this approach leads to higher

CO_2 emissions compared to other technologies. Integrating carbon capture and storage technologies are the main focus of research for coal gasification facilities [50–52].

The final conventional production method is water electrolysis. It is considered the only conventional route that produce pure H_2 product. The basic principle for this technique is the use of an external electricity source connected to two electrodes (cathode and anode) immersed in water. This external source will provide the necessary electrons to initiate the water electrolysis:

Reduction at cathode: $2\,H^+(aq) + 2\,e^- \longrightarrow H_2(g)$

Oxidation at anode: $2\,H_2O(l) \longrightarrow O_2(g) + 4\,H^+(aq) + 4\,e^-$

Table 2.1 summarizes three different technologies that are actively used for water electrolysis: alkaline, polymer electrolyte membrane (PEM), and solid oxide electrolyzes (SOE) [53].

Table 2.1: Comparison between three different technologies for water electrolysis (adopted from [53]).

Specification	Alkaline	PEM	SOE
Principle	Two electrodes immersed in a liquid alkaline solution (NaOH).	Polymer electrolyte used for protons conduction and product separation.	High temperature electrolysis of steam to increase efficiencies.
Technology maturity	State of the art	Demonstration	R&D
Current density (A/cm^2)	0.2-0.4	0.6-2.0	0.3-1.0
Cell Voltage (V)	1.8-2.4	1.8-2.2	0.95-1.3
Voltage efficiency (%)	62-82	67-82	81-86
Specific energy (kWh/Nm^3)	4.5-7.0	4.5-7.0	2.5-3.5

2.2.2 Non-conventional routes

Most of the conventional routes consume considerable quantities of energy, which is usually derived from fossil fuels; further contributing to CO_2 emissions. In order to consider H_2 as a clean fuel for the future, it must be generated from alternative energies such as solar, wind, hydro and geothermal. The developing technologies for H_2 production emphasize the use of these alternative energies, especially solar energy [54]. Utilization of these alternative energies can be achieved by subsequent transformation of energy from one form to another. One example is the transformation of wind (mechanical) energy to electricity, which is used to operate water electrolyzers to produce H_2 (mechanical - electrical - chemical transformation).

Another example is the utilization of photovoltaic (PV) based electrolysis (solar - electrical - chemical transformation). This technique is based on excitation of electrons to a higher-energy state in a semiconducting material which results in electricity generation. It consists of solar panels, electricity grid, battery storage, water electrolyzer, and H_2 storage [16]. Due to the capital complexity, PV based electrolysis is considered one of the most expensive production route for H_2 (at this time). A H_2 production facility of this kind is about 6 times more expensive than a traditional natural gas facility [35, 54].

Photoelectrochemical (PEC) techniques utilize solar photon energy to directly electrolyze water into H_2 and O_2. Thus, eliminating electrical current collection and transportation and thus resulting in lower estimated costs and a simpler production route [27]. There are several essential requirements for direct PEC water decompositions. The most essential requirement is the supply of sufficient photon energy to overcome the bandgap of the water splitting reaction (1.23V) and associated resistance losses. Other requirements include fast electron transfer and corrosion resistance materials. Photocatalytic water splitting is considered one type of PEC, which was described in Section 1.2.

A full comprehensive study of 19 different H_2 production routes, both conventional and non-conventional, was conducted by Dincer and Acar [16]. The study briefly described each technology and reported six different assessment variables namely: global warming potential (GWP), acidification potential (AP), social cost of carbon (SCC), production cost, energy consumption and energy efficiencies. The finding of this study showed that fossil fuel reforming has the highest energy efficiency with lowest production cost. However as expected, it has very high environmental impact in terms of GWP, AP and SCC [16].

2.3 H_2 purification

The increasing demands of H_2 require more efficient and low cost separation processes to obtain H_2 in the required purities. In line with this demand, there have been tremendous efforts on the development of H_2 separation/recovery technologies. For example, technology development in this area has yielded more than 500 patents between 2000 and 2011 in the field of H_2 membrane separation only [14].

There are multiple commercialized solutions for the separation and purification of H_2 used today. The selection criteria is based on the type of the impurities and the required degree of the H_2 purification in the product stream [39]. Table 2.2 shows the most common techniques, their respective operating conditions, targeted impurities, H_2 recovery rates, and purity values. More details will be provided for the most common techniques namely: pressure swing adsorption (PSA) and membranes.

Table 2.2: Summary of industrial H_2 purification techniques (adopted from [39, 55, 56]).

Technique	Operating Conditions		H_2 Purity	H_2 Recovery	Impurities
	Temp. (°C)	Press.(bar)	(%)	(%)	
Partial Condensation	-183	20 - 50	Up to 98	95	CH_4, CO
Physical Absorption	25	10 - 150	Up to 95	90 - 95	Hydrocarbons
Chemical Absorption	25 - 107	3 - 30	98	> 95	CO_2 removal
PSA	25	20 - 150	> 99.9	70 - 90	Hydrocarbons
	25	10 - 40	> 99.999	70 - 85	CO_2, H_2O, CH_4, CO
Polymeric Membranes	25 - 150	20 - 200	Up to 99	85 - 95	Hydrocarbons, CO
Metallic Membrane	300 - 450	< 20	99.99999	< 99	N_2, O_2, CO, CO_2
Metal Hydrides	> 25	1 - 40	> 99.5	> 90	Hydrocarbons, N_2

2.3.1 Pressure swing adsorption (PSA)

Adsorption is a process that utilizes the differences between components' affinity and molecular attraction towards an absorbent material such as zeolites, activated carbon and silica gel. If the attraction between a certain gas molecule and the absorbent is very strong that result in an electron transfer, this phenomena is defined as chemisorption. On the other hand, if the attraction is weak and involve only electrostatic bonding, then it is called physical adsorption [57]. The use of PSA for H_2 purification started in the late 1950's. However in early 1970's, a breakthrough emerged in the PSA technology when multi-layer PSA for H_2 purification, in methane steam reforming plants, was developed [39].

Two separation mechanisms are applied for PSA operation. Equilibrium based separation is based on the affiliation of the impurities concentration in the bulk phase and in the adsorbed phase. In this case, the selected adsorbent should have the weakest attraction forces with the product. The kinetic based separation is based on the mass transfer rates of species between the bulk phase and in the adsorbed phase [57, 58].

PSA based on physical adsorption has one main advantage over other adsorption techniques in that pressure can be rapidly changed leading to faster adsorption/desorption cycles. Nevertheless, strongly attached species on the adsorbent surface usually lead to higher operating cost as high vacuum is required in the desorption step [58]. For this reason, it is crucial to select the right adsorbent materials based on the H_2 feed impurities. Currently, multi-layer PSA is used to purify H_2 up to 99.99% in different application. Each layer is specific to remove certain impurities. In methane steam reforming, silica gel and alumina are utilized to remove water, activated carbon for CO_2 removal and zeolites for CH_4, CO

and N_2 removal [39, 56]. The use of activated carbon to remove CO_2 prior to the use of zeolites is critical since CO_2 is strongly attached to zeolites, which will lead to high vacuum regeneration step [56]. Figure 2.2 shows the adsorption isotherms of the four gases involved in our study (H_2, O_2, N_2 and CO_2) on zeolites 5A.

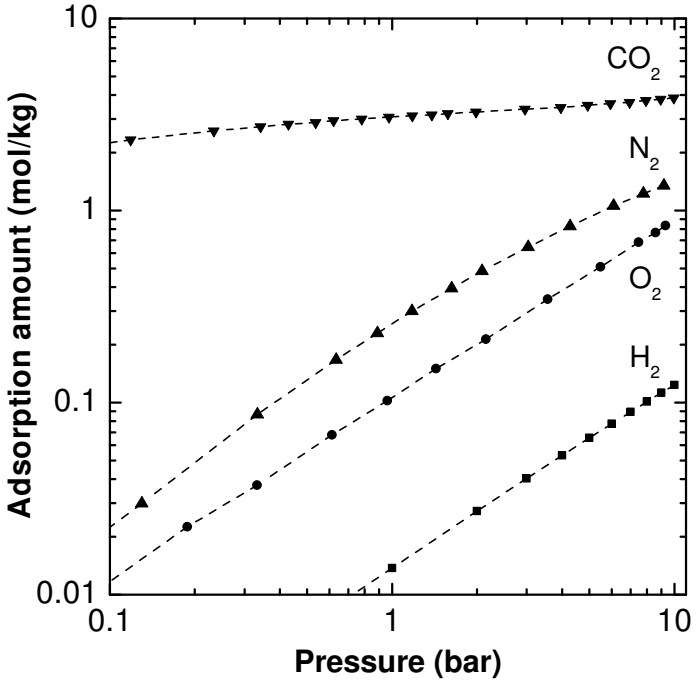

Figure 2.2: Adsorption isotherms of pure components (H_2, O_2, N_2 and CO_2) on zeolite 5A at 30°C [59–61].

The research and development efforts in this separation technique focus on process modification and integration to increase product recoveries while maintain the high purities and reduction of operating cost and adsorption/desorption cycles times [56]. One approach to achieve these objectives is by developing more selective absorbents for the impurities. Metal-organic frameworks (MOFs) and zeolitic imidazolate frameworks (ZIFs) are being investigated for CO_2 selective adsorption [62–64] and Cu-based absorbents for CO adsorption [65, 66]. Membrane-PSA hybrid systems have the potential to increase the recovery of products. This can be achieved by recovering H_2 from PSA off-gas using membranes, which then recycled back to the PSA-feed. This will results in an additional of 7-9% H_2 recovery when compared to PSA system only [67, 68]. Another integration design was studied for separation enhancement by introducing membrane units prior to PSA to decrease the amount of impurities captured in the adsorbent which allows for more gas processing or more purification [67, 69].

2.3.2 Membranes

Membrane technology has the potential to overcome other conventional separation processes due to its advantages, such as lower capital and operating costs, ease of installation and

operations as well as minimal footprints. The main advantage of membrane over PSA is the continuous operation based on pressure driven separation unlike PSA where it is considered a cyclic process that rotate between adsorption/desorption steps.

2.3.2.1 Membranes types

Four major membrane types are discussed in the literature for H_2 separation, namely: metal, ion transport, Nano-porous and dense polymeric membranes, which will be discussed briefly and highlight their commercial availability.

Dense metal membrane is considered a H_2 selective membrane where H_2 can be obtained with very high purity ($> 99.9\%$). The transport phenomena depend on the solution-diffusion mechanism which is usually occurred at elevated temperatures (300-800°C). The most used metal is palladium (Pd), which has both acceptable flux and the ability to enhance H_2 dissociation and re-association reaction. The major drawbacks of metal membranes include: high cost, H_2 embrittlement, sulfur poising and producing thin films with no defects or pinholes. To overcome these challenges, Pd alloys are being investigated (e.g. PdInRu). Commercial systems are available by Johnson Matthey technology which is sold by SAES Pure Gas Inc. [39, 70, 71]

Ion transport membrane is another type of H_2 selective membrane. The membrane surface must be proton conductive in which have the ability of charge transfer between the high and low pressure sides. The considered materials can be of any conductive type including hydrated or water containing compounds (e.g. polyoxometallates). Operating temperature and materials compositions play a major role in the mechanical and chemical stability of these membranes. Currently there is no commercial available membrane from this type. [70, 72]

Nano-porous membranes act as molecular sieve that can separate H_2 (d = 2.83Å) from other gases up to a moderate purity ($< 95\%$). Organic and inorganic materials including ceramics, glasses and carbon can be utilized to fabricate different types of membranes. Carbon Molecular Sieve (CMS) membranes are produced pyrolysis of some polymeric precursors like polyimides and polyacrylonitrile. The best separation performance can be obtained when the pore diameters is between (3-5Å). High cost, pore blocking and brittleness are the reasons that there is no commercial membrane from CMS [70, 72]. Silica, zeolites and other porous ceramics can also be used as membrane materials. Some zeolites have the ability of gas adsorption which will enhance the H_2 separation beside the molecular sieve effects. Some post treatments and modification are required in order to have a stable and high separation performance. For example, silyation (adding silyl group R_3Si) was performed on MFI zeolite membrane, which results in increasing the separation factor of H_2/N_2 from 4.5 to 140. The high cost of the inorganic materials is one of the major drawbacks, where the membrane module cost is more than $\$1000/m^2$. Only prototypes of tubular silica membrane are available up to 90cm [39, 70–72]. A new class of polymer was developed to mimic the structure of zeolites which is known as Polymer of Intrinsic Microporosity (PIMs). These glassy rigid polymers have high free volume with interconnected pores, which result in a very high gas permeability with low selectivity.

Recent researches focus on improving the selectivity of these polymers by modifying or adding materials and function groups [70, 73].

Polymeric membranes are the most widely used materials for gas separation [74]. The driving force is the difference in chemical potentials of the components in the feed and permeates side. For both glassy and rubbery polymers, the transport phenomena depends on the solution-diffusion mechanism where the permeability (P) of a species in the membrane is the product of the solubility (S) and diffusivity (D). Glassy membranes (where diffusion is more dominate) are the preferred option for separating H_2 from gas mixtures. These polymers show more selectivity values for light gases than rubbery polymers but as a tradeoff, they have less permeability. Typically though, higher H_2 selectivities are more important than flux for most H_2 based applications [74, 75].

2.3.2.2 Membranes material selection

Due to the tradeoff between selectivity and permeability for polymeric membranes, it is crucial to identify the right membrane material for the investigated study based on their separation performance and commercial availability. Four different gases are involved in this study: H_2 and O_2 as the product from water splitting while N_2 and CO_2 are used as diluents. Here, an overview will be provided about membrane materials for the related gases pairs: H_2/O_2, H_2/N_2 and H_2/CO_2.

The idea of separating H_2/O_2 has been discussed by few researchers using membranes [27, 76–78]. Leelachaikul, *et al.* investigated a liquid membrane technology for the separation of H_2/O_2 [78]. It was mentioned that the application could be photocatalytic water splitting. Argon was used as a carrier gas, but not analysed as a permeate product because it was also used to sweep the permeate. Hence, the system was not designed to recover H_2 instead; it was for measuring the liquid membrane general performance. Similar study was carried by T. Yamaguchi, *et al.* with different liquid membrane materials [79]. Nevertheless, there is no commercial technology available for this separation [31].

The separation of H_2/N_2 has been discussed by many researches for its importance in ammonia production [80, 81]. In gas separation industry, four glassy polymers are commercially utilized for this separation namely: polysulfones (PSF), cellulose acetates (CA), polyaramids and polyimides [81]. Table 2.3 summarizes these polymers for their permeability values of the $H_2/O_2/N_2$ gas mixture and the supplied companies.

In Chapter 3, the investigation will focus on the use of the commercial polyimide membrane from UBE® (Japan) [82]. It shows the highest permeability and permselectivities for H_2 in Table 2.3 for the investigated tertiary mixture $H_2/O_2/N_2$ in Chapter 3.

Table 2.3: Commercial available membrane materials for $H_2/O_2/N_2$ separation [14, 74, 81–83].

	PSF	CA	Polyaramids	Polyimides
Trade name	Prism	Separex	Medal	UBE®
Company	Air Products	UOP	Air Liquid	UBE Industries
Membrane type	Composite	Asymmetric	Asymmetric	Asymmetric
Module type	Hollow fiber	Spiral wound	Hollow fiber	Hollow fiber
Data point temperature (°C)	35	25	-	60
H_2 permeability (Barrers)	14.00	24.00	40.00	50.00
N_2 permeability (Barrers)	0.25	0.33	-	0.60
O_2 permeability (Barrers)	1.40	1.60	-	3.00
Permselectivity (P_{H_2}/P_{N_2})	56.00	72.00	-	83.33
Permselectivity (P_{H_2}/P_{O_2})	10.00	15.00	-	16.67
Permselectivity (P_{O_2}/P_{N_2})	5.60	4.85	-	5.00

H_2 and CO_2 separation has been discussed widely for its application in H_2 production from methane reforming and CO_2 capture from power plants [84–86]. Typically, PSA units are used to purify H_2 in these systems. However, recovery rates are usually less than desired [68]. Alternatively, there are numerous, commercially available membrane materials that can be utilized for these two applications (H_2 purification and CO_2 capture). The CO_2-selective membranes are usually comprised of a rubbery polymer, which ideally operates at ambient or even sub-ambient temperatures [87, 88]. H_2-selective membranes, on the other hand, are formed from glassy polymers and are operated at elevated temperatures. Unfortunately, neither membrane type provides excellent separation due to the countering effects of solubility (CO_2 dominant) and diffusivity (H_2 dominant). As such, there have been considerable research efforts to develop an improved membrane material [89, 90].

The membrane materials investigated to carry out the separation process in Chapter 4&5 are based on commercially available composite polymer membranes from MTR in the spiral wound architecture. Both the H_2-selective membrane (Proteus^{TM}) and CO_2-selective (Polaris^{TM}) were utilized [85, 91, 92]. Table 2.4 shows the permeability and selectivity values of these membranes for $H_2/O_2/CO_2$ gas mixture.

Table 2.4: Gas permeation properties for Proteus^{TM} and Polaris^{TM} [85, 91, 92].

Component	Proteus^{TM}		Polaris^{TM}	
	Permeance (GPU)	Selectivity (Q_{H_2}/Q_i)	Permeance (GPU)	Selectivity (Q_{CO_2}/Q_i)
H_2	300	-	100	10
O_2	6	50	50	20
CO_2	20	15	1000	-

2.4 H_2 applications

The estimated annual H_2 production for 2016 is around 73.5 million tonnes with a global market value estimated at $118 billion [93, 94]. The majority of H_2 is utilized in ammonia synthesis (50%), petroleum processing (37%), methanol production (8%) and other small-size consumers (5%) [33, 95]. The demand of H_2 in these applications is expected to grow even further. Particularly for ammonia production, which is utilized in the food industry, as the world population increases and for petroleum processing as more environmental regulations are implemented on the industry [33, 94].

2.4.1 Ammonia production

Ammonia is the main building block for different fertilizers including urea, ammonium sulphate and ammonium phosphate [47]. The annual production rate of ammonia is around 146 million tonnes [96], in which more than 85% is consumed to produce these different fertilizers [36]. Other usages include production of acrylonitrile, nylons and SO_2 removal from flue gases.

Ammonia synthesis is based on simple reaction where N_2 and H_2 are combined in a stoichiometric ratio of 1:3. The process was first described by two German Scientists Haber and Bosch [97]. The reaction occurs are elevated pressure (150-250 bar) and high temperature (350-550°C) over an iron-based catalyst [36]:

$$N_2 + 3H_2 \longleftrightarrow 2\,NH_3$$

Two different criteria distinguished the current commercial technologies used for ammonia production. The first criteria is the source of H_2 used in the process, which has been discussed earlier in Section 2.2. The other criteria is the catalyst utilized for ammonia synthesis, which is either a modified version of the iron-based catalyst developed by Haber and Bosch (e.g. Uhde Dual Pressure Process) or ruthenium catalyst (e.g. KBR PuriferPlus^{TM} Process) [36]. The most common H_2 source for ammonia synthesis comes from natural gas steam reforming process. The process consist of five major steps as illustrated in Figure 2.3 [36, 98].

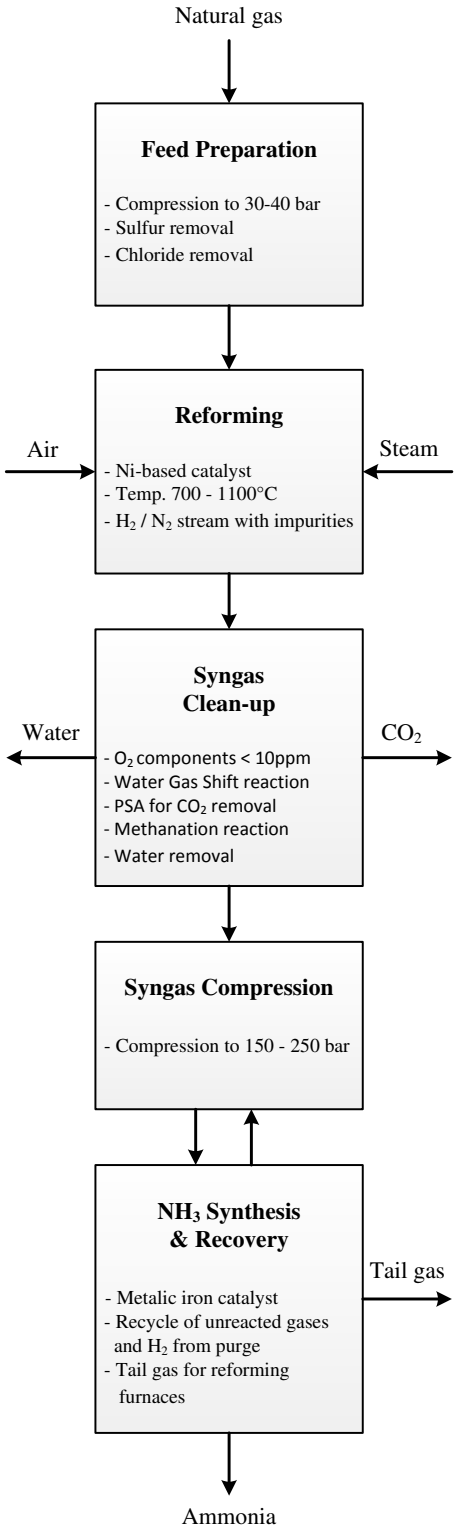

Figure 2.3: Block flow diagram for typical ammonia synthesis process from natural gas (adopted from [36, 98]).

As any fossil fuel driven process, the release of CO_2 to the atmosphere is the main issue facing the ammonia production. It is estimated that around 1.9 metric tons of CO_2 release to the atmosphere per metric ton of ammonia produced [96]. To address this obstacle, the scientific community investigated two approaches to reduce the energy consumption and CO_2 emission of ammonia process. The first approach is by the production of H_2 from renewable resources and energy. However, recent studies showed that the production cost of ammonia from this approach is about 2.5 to 5 times more than the natural gas driven ammonia and consume more energy [99, 100]. The second approach is the development of a new catalyst and reaction pathway to activate N_2 so that lower temperature and pressure operation is viable [96]. Under this approach, electrochemical [101, 102] and photocatalytic [103, 104] ammonia production were investigated.

2.4.2 Methanol production

Methanol is one of the major chemical products, which has a potential market of more than 80 million tons per year globally [105]. It is a key building block for numerous commodity chemicals (i.e. MTBE, acetic acid, formaldehyde) [106]. As a liquid fuel, methanol is considered a suitable energy storage component due to its high energy density by volume and weight, and easy handling and storage compared to H_2 [23, 107, 108].

Methanol is produced from a mixture of CO, H_2 and CO_2 commonly known as synthesis gas or syngas. This syngas gas mixture is converted to methanol over a metal-based catalyst (e.g. $CuO/ZnO/Al_2O_3$) catalyst according to the following reactions [106]:

$$CO + 2H_2 \longleftrightarrow CH_3OH$$

$$CO_2 + 3H_2 \longleftrightarrow CH_3OH + H_2O$$

$$CO_2 + H_2 \longleftrightarrow CO + H_2O$$

Most of the world's syngas is generated from natural gas via steam reforming and/or partial oxidation (autothermal reforming) [109, 110] as in ammonia process. However, both CO and CO_2 are removed in ammonia plants to prevent catalyst (iron-based) poisoning unlike the methanol process, where both are required according to the stoichiometry number (S), which describe the syngas compositions [111]:

$$S = \frac{[H_2] - [CO_2]}{[CO] - [CO_2]}$$

where the gases concentrations are expressed in volume percent. The targeted value of S should be between 2.05 - 2.10. Lower S value will indicate H_2 deficiency, which leads to lower methanol production. On the other hand, higher value of S indicate access of H_2, which leads to higher recycle loop [110, 111].

Conventionally, methanol production worldwide utilizes low-pressure catalytic conversion process. The low-pressure processes have the advantages of lower investment, improved operational reliability and lower production cost. The process can be divided into three

main sections as shown in Figure 2.4. Some of the current licensers are Lurgi, JM/Davy, and JM/Uhde [111].

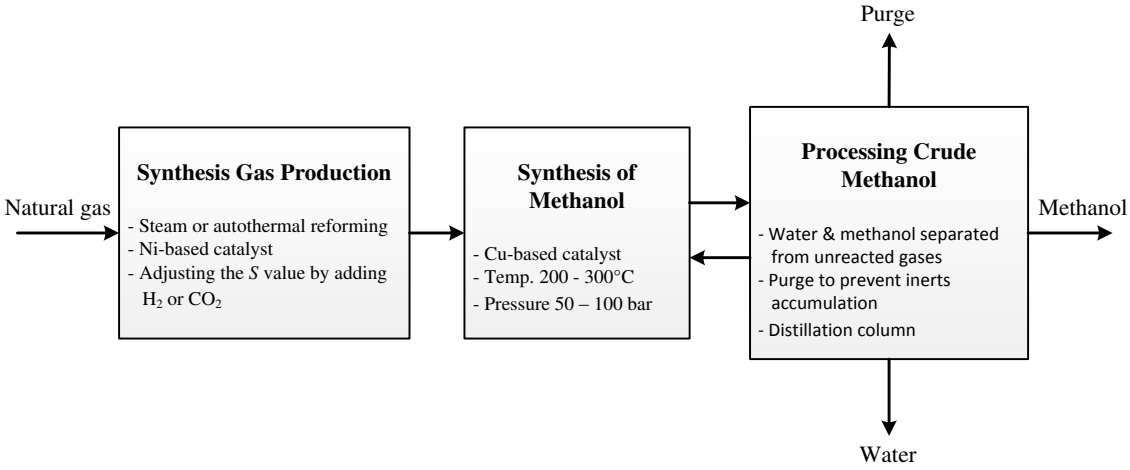

Figure 2.4: Block flow diagram for typical methanol synthesis process from natural gas [111, 112].

The first step in methanol process (syngas production) accounts for more than 60% of the capital investment and requires substantial amounts of water and energy, around 35 GJ/ton_{MeOH}, which is also provided from fossil fuels [113, 114]. Moreover, an estimated CO_2 emission from this process is around 0.5 t_{CO_2}/t_{MeOH} [113]. Recent studies focus on the production of renewable syngas and the utilization of CO_2 capture to produce methanol [3, 106, 107]. It must be noted that in order to achieve an overall CO_2 reduction while synthesizing methanol, a renewable source of energy and/or feedstock must be utilized [115, 116].

Solar energy has the potential to provide a sustainable syngas source for the methanol production using captured CO_2 and water based feedstock. One method is water splitting wherein H_2 is produced and then partially utilized to produce CO through a reverse water gas shift (RWGS) reaction using captured CO_2. Alternatively, the produced H_2 can be utilized for the direct hydrogenation of CO_2 to produce methanol [107, 112, 113]. A second method is using solar energy to reduce CO_2 directly to form CO in a catalytic system. After CO formation, conventional water gas shift (WGS) is performed to produce H_2 from water and CO. These two approaches can be accomplished by either thermochemical or electrochemical conversions via solar energy.

Using the thermochemical approach to activate CO_2 to form CO, Kim, *et al.* [115, 117] reported a full techno-economic analysis of this approach. The findings of this study show that the required break-even price for the methanol is $\$1.22/kg_{MeOH}$ compared to the current price of $\$0.38/kg_{MeOH}$ [118]. The high production cost is driven by the solar concentrator/reactor, which accounts for more than 90% of the capital investment. Similarly, the same technique can be used to generate H_2 from water as described in Section 1.2.

For the electrochemical approach (including photocatalysis and photoelectrolysis), suitable semiconductor materials generate electrons and holes via solar energy, which are used to react with water and CO_2. The main obstacle facing this approach is the dissolution of CO_2 in aqueous solution to enable the reduction to CO. Elevated pressures are needed to overcome limited CO_2 solubility (33mM at 25°C and 1 atm), which adds considerable processing costs [6]. Other challenges include formation of byproducts in the aqueous solution, challenging separations, and catalyst deactivation.

CHAPTER 3

H_2 Recovery using N_2 Diluent

Part of this chapter has been published:
S. Alsayegh, J. Johnson, B. Ohs, J. Lohaus, M. Wessling *Systematic optimization of H_2 recovery from water splitting process using membranes and N_2 diluent*, International Journal of Hydrogen Energy (2017), DOI: 10.1016/j.ijhydene.2016.11.186

3.1 Introduction

There is a growing interest in the production of H_2 using solar energy. As mentioned before, photocatalytic water splitting will produce both H_2 and O_2 with a ratio of 2:1 respectively in the same environment, which will drastically increase the risk of explosion [27, 119]. To mitigate this problem, an inert gas (e.g. N_2) can be used as a diluent to transition into a safe operating environment. Consequently, a suitable separation process must be utilized to recover the H_2 under safe conditions. N_2 gas can be obtained from air, a cheap abundant source, by different technologies including cryogenic distillation, PSA and membranes [120] with high purity up to 99.9%. Before utilizing N_2 as a diluent for the photocatalytic process, a detailed investigation must be carried on the flammability limits of H_2 in the tertiary mixture ($H_2/O_2/N_2$) and the influence of both temperature and pressure on these limits values. This step is essential to identify the safe operating conditions to design the membrane separation.

This chapter will describe the utilization of N_2 diluent for the recovery of H_2 from water splitting using commercial membrane materials. The investigation is carried in three steps: (1) ambient/vacuum pressure process, (2) high/vacuum pressure process and (3) optimization. The first two steps will assist in determining the variables range, process layouts, and assumptions for the optimization step, which will result in computational time reduction and output precision.

3.2 H_2 flammability limits

Great attention must be given when working with flammable mixtures in order to ensure a safe working environment. H_2 has a very wide flammable range in both pure O_2 and air mixtures. At normal (ambient) operating conditions, the Lower Flammability Limit (LFL) of H_2 is 4% in both mixtures, while the Upper Flammability Limit (UFL) is 75% for an air mixture and 94% for a binary mixture of O_2 and H_2 [121, 122]. The Limiting Oxygen Concentration (LOC) is defined as the minimum O_2 concentration that is required for a mixture to be explosive [123]. This value can be calculated from the UFL. At normal operating conditions, the LOC is equal to 5 mol-% for H_2 and air mixture [122, 123]. For this reason, the investigated gas mixtures will be flammable only if the O_2 concentration in a stream is above 5% and the H_2 concentration is between the LFL and UFL of the air mixture, as illustrated in Figure 3.1. Based on these findings, two gas mixtures with different molar concentration of $H_2/O_2/N_2$ will be investigated in this chapter to show the effects of feed concentration on the separation process design and economic (see Table 3.1).

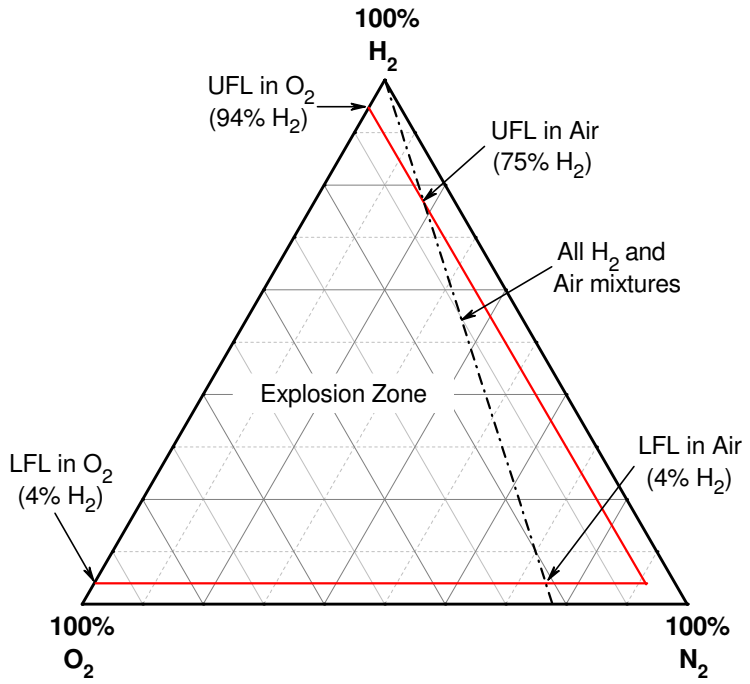

Figure 3.1: H_2 flammability diagram under normal operating conditions [124].

Table 3.1: Feed compositions for the investigated mixtures.

Gas	Mixture (1)	Mixture (2)
Nitrogen (N_2)	94%mol	91%mol
Hydrogen (H_2)	4%mol	6%mol
Oxygen (O_2)	2%mol	3%mol

H_2 recovery can be increased by reducing the permeate pressure to vacuum range in order to increase the driving force. Unfortunately, as pressure decreases, the 5% O_2 limit will slightly decrease resulting in a higher risk of explosion [125]. However, if the permeate is operated under 50mmHg (0.065 bar) absolute, no flame can propagate and the minimum ignition energy is increased dramatically [122]. For that reason, it will be assumed there is no explosion risk at vacuum range as long as the O_2 concentration remains below LOC value.

There is a strong influence of temperature and pressure on the explosion limits of H_2 both in air or pure O_2 mixtures. As temperature increases, the explosive range widens as shown in Figure 3.2. Assuming that our investigated mixtures behave as a H_2 and air mixture, Figure 3.2 also shows how the LOC decreases as temperature increases at atmospheric pressure [121, 124]. When pressure is increased, a different behavior is observed. As pressure increases, the explosive range decreases at lower pressures (up to 20 bar) then expands again. For pressures above 50 bar, the explosive range remains relatively constant for the mixture. The O_2 limits at these pressure values can be seen in Figure 3.3.

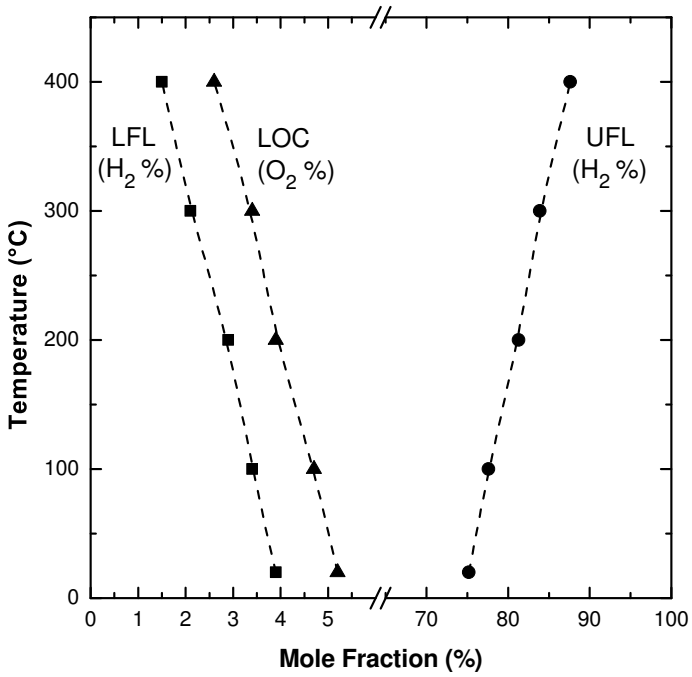

Figure 3.2: Temperature influence on the explosion limits of H_2-air mixtures (at atmospheric pressure) [121].

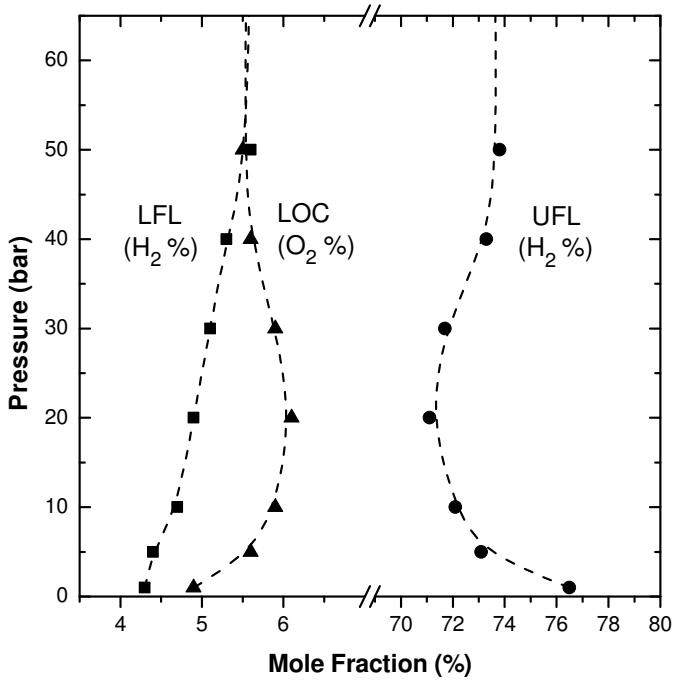

Figure 3.3: Pressure influence on the explosion limits of H_2-air mixtures (at room temperature) [121].

Considering these values and the trends, it is safe to assume that the O_2 limit stays at 5% as long as a proper design of the multi-stage compression or an isothermal compressor is used. When pressurizing the feed or the permeate streams, the temperature should be kept below 200°C. This temperature limit is more tolerant at lower O_2 concentrations and higher stream pressures. Using Aspen Plus process simulation software (with SRK thermodynamic package), a simple flow sheet was built to determine the number of stages required to pressurize the two mixtures. Both feed flow rate and compositions have minor influence on the outlet temperature since the molar heat capacity for the three components are very similar. The pressure increase factor should be limited to two (P_{out}/P_{in}=2) to prevent exceeding the above mentioned temperature limits. Therefore, pressurizing the feed from 1 to 8 bar requires three stages of compression. For the remainder of the investigation, the feed pressure will be limited to 4 bar (two stage compression) in order to minimize the capital and operating cost of the process.

3.3 Ambient/vacuum pressure process

The aim of this part of the investigation is to explore the maximum recovery that can be achieved for the two gas mixtures without the risk of pressurizing the feed using the commercial polyimide membrane from UBE® (Japan). For constant feed conditions (P=1bar, T=60°C and F=1kmol/hr), membrane area and permeate pressure for different membrane stages will be manipulated to recover the H_2 while keeping the O_2 concentration below 5% in the permeate outlet streams.

3.3.1 Membrane model

A simple membrane model was utilized in this investigation. Aspen Custom Modeler (ACM) was used to write the model with SRK equation as the thermodynamic package. The model is based on a simplified model done by Marco Scholz [126] considering only a material balance. It describes the steady state permeation for each gas component independently through the membrane in a countercurrent flow configuration. The membrane model is illustrated in Figure 3.4.

The differential mole balances for the retentate and permeate are:

$$\frac{d\dot{n}_{P,i}}{dx} = -\dot{n_i}^{"} W \tag{3.1}$$

$$\frac{d\dot{n}_{R,i}}{dx} = -\dot{n_i}^{"} W \tag{3.2}$$

where $\dot{n}_{P,i}$ and $\dot{n}_{R,i}$ are the molar flow of component i in the permeate and the retentate (mol/s), respectively, $\dot{n_i}^{"}$ is the molar flux of component i (mol/m^{2}s), x is the coordinate of the flow direction (m), W is the membrane width (m) and L is the channel length (m).

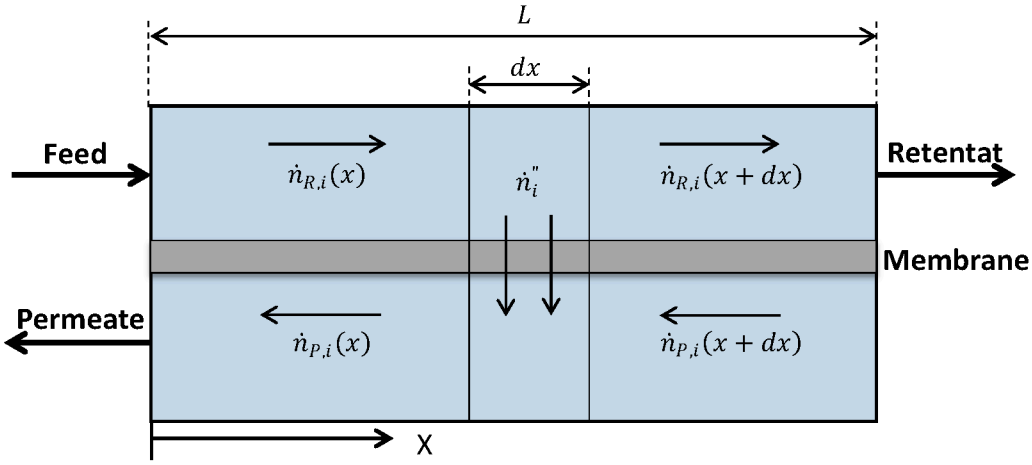

Figure 3.4: Illustration of the membrane model used in section 3.3.

The negative sign of the material balance indicates that the retentate flow decreases along the membrane while the permeate (downstream) flow is increasing in the negative direction of the coordinate plane (x). The material transfer through the membrane (flux), which is designated as $\dot{n}_i^{"}$, is calculated from the solution diffusion module as follow:

$$\dot{n}_i^{"} = Q_i \left(x_i \, p_F \; - \; y_i \, p_P\right) \tag{3.3}$$

where Q_i is the membrane permeance of component i (GPU), x_i and y_i are the mole fraction of component i in the retentate and the permeate, respectively and p_F and p_P are the feed and permeate pressure (bar).

The required boundary conditions are:

$$\dot{n}_{P,i}(x = L) = 0 \tag{3.4}$$

$$\dot{n}_{R,i}(x = 0) = x_i \, F \tag{3.5}$$

where F is the feed molar flow rate (mol/s).

The described membrane model was used under the following assumptions:

- The system is in steady state
- Solution-diffusion mechanism for the hollow fiber membrane
- No temperature and pressure drop along and across the membrane
- No interactions between the components were considered (no flux coupling)
- Constant selectivity and permeability along the membrane
- UBE® (Polyimide) membrane permeability data was measured at 60°C
- Membrane thickness of 0.36 μm was used to calculate the permeance(Table 3.2)

Table 3.2: UBE® membrane parameters [82].

Component	Permeability (Barrers)	Permeance (GPU)	Permselectivity (P_{H_2}/P_i)
Hydrogen (H_2)	50.0	140.0	-
Oxygen (O_2)	3.0	8.4	16.7
Nitrogen (N_2)	0.6	1.7	83.3

3.3.2 Results

Mixture (1) results:

Adding the flammability limitation as a process boundary condition heavily constrains the cascade design. Using the composition for Mixture (1), a double pass membrane module was utilized, as shown in Figure 3.5, to determine if a high purity stream could produce within the flammability limits. The concentration of O_2 and H_2 in the permeate stream were calculated as a function of variable membrane area and the driving force (pressure difference, Δp) across the membrane.

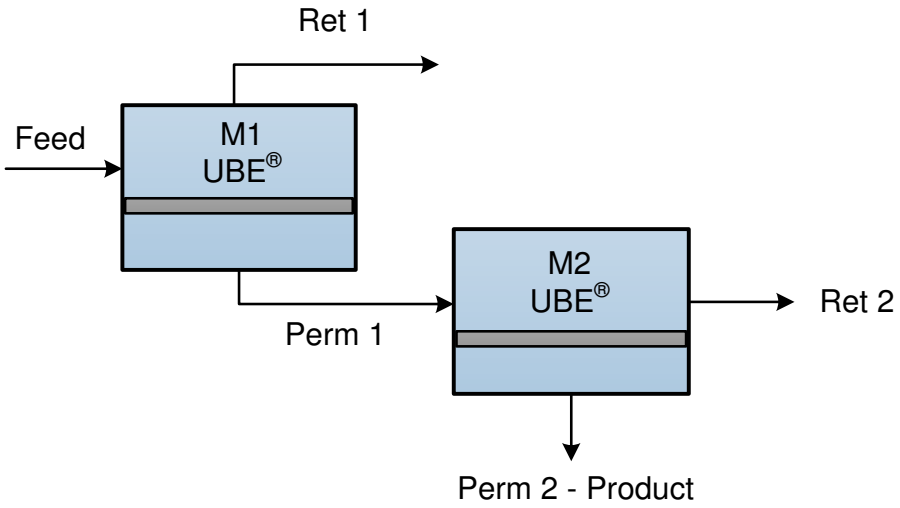

Figure 3.5: Double pass membrane cascade design.

The area of the primary unit (M1) was considered from 100-250 m^2. Moreover, the secondary unit (M2) was considered from 8-14 m^2 when M1 was 100 & 150 m^2 and 16-22 m^2 when M1 was 200 & 250 m^2. The O_2 and H_2 concentrations and the final H_2 recovery were calculated. Component concentrations and H_2 recovery, as measured in the M2 permeate, are shown in Figures 3.6 and 3.7 as a function of membrane area. Additionally, the calculated O_2 concentrations in the M1 permeate stream are provided in Table 3.3. Two pressure systems values were considered in this investigation: $p_p = 0.1$ and 0.05 bar.

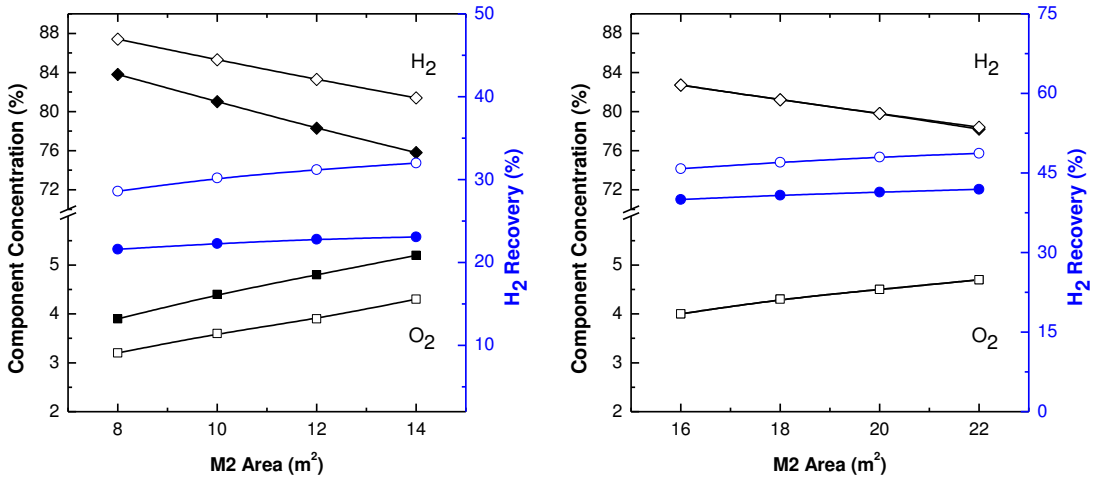

Figure 3.6: O_2 and H_2 concentrations and H_2 recovery in the M2 permeate as a function of membrane area. p_p at 0.1 bar. (a) For M1 area 100 m^2 (closed symbols), 150 m^2 (open symbols). (b) For M1 area 200 m^2 (closed symbols), 250 m^2 (open symbols). Note that the O_2 and H_2 concentration data points overlap

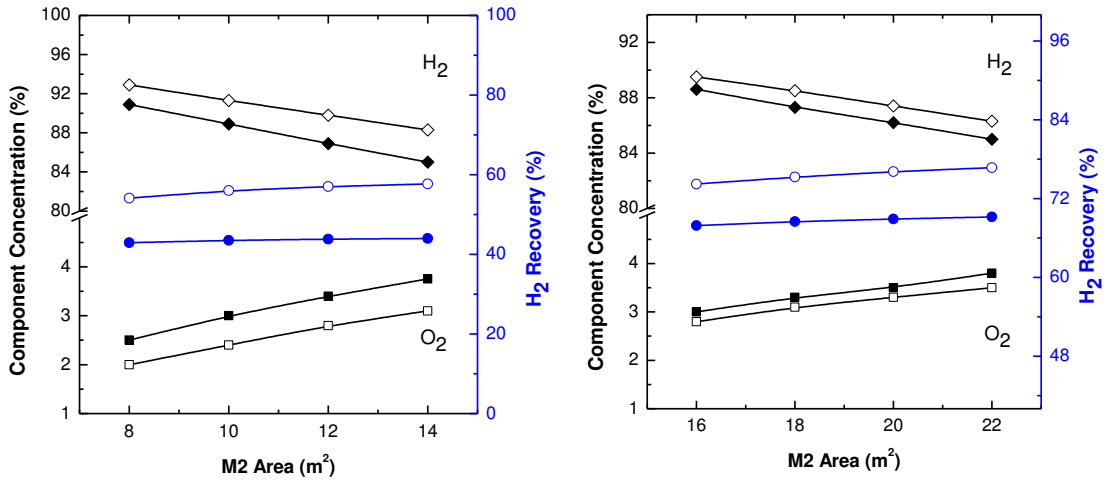

Figure 3.7: O_2 and H_2 concentrations and H_2 recovery in the M2 permeate as a function of membrane area. p_p at 0.05 bar. (a) For M1 area 100 m^2 (closed symbols), 150 m^2 (open symbols). (b) For M1 area is 200 m^2 (closed symbols), 250 m^2 (open symbols).

Table 3.3: O_2 concentration in M1 permeate stream as a function of membrane area and permeate pressure.

M1 Area	100 m^2	150 m^2	200 m^2	250 m^2
M1 $p_P = 0.1$ bar				
O_2 Concentration in Permeate 1	5.1%	5.0%	5.0%	5.0%
M1 $p_P = 0.05$ bar				
O_2 Concentration in Permeate 1	4.5%	4.7%	4.8%	4.9%

Promising results were obtained when $p_p = 0.05$ bar. In this condition, the O_2 concentration was kept below the flammability limit in both units. Moreover, the H_2 recovery rate was higher when comparing both figures since the driving force is increased. Unfortunately, in all cases, we see a trade-off between product purity and product recovery. The H_2 recovery rate increases with increasing membrane area, however, this comes at the expense of lower purity as more O_2 and N_2 permeates. In this situation, careful attention must be given to the permeate streams if more H_2 recovery is desired since the O_2 concentration is close to the flammability limits.

We observed that the double pass configuration in the previous example is capable of recovering most of the H_2. What if we used an auxiliary membrane unit to process the retentate from M1? Additional H_2 could be recovered, especially if a small area unit is used in the first stage to avoid the flammability limit (as evidenced in Table 3.3). We may consider this case (Figure 3.8) as a simplified cascade design from the first scenario.

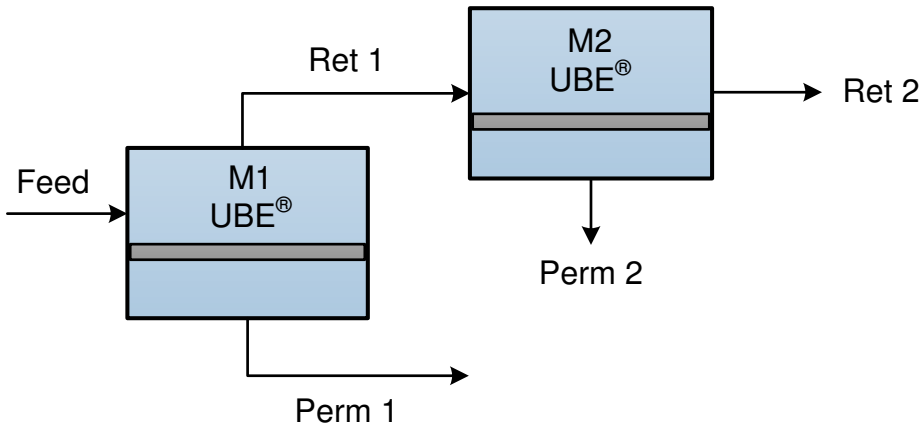

Figure 3.8: Two membrane modules in series.

From the previous results, it was shown that when $p_p = 0.05$ bar, the O_2 content in the permeate was minimized. Therefore we only this pressure value for this study. The retentate of the M1 is fed to the second module. One major difference between the feed compositions of the two modules is that the ratio of H_2 to O_2 is no longer 2:1. Since more

H_2 permeates through the first module than O_2, the ratio decreases. For the simulations, membrane area in both stages were varied. Process stream properties for the final permeate are presented in Figure 3.9.

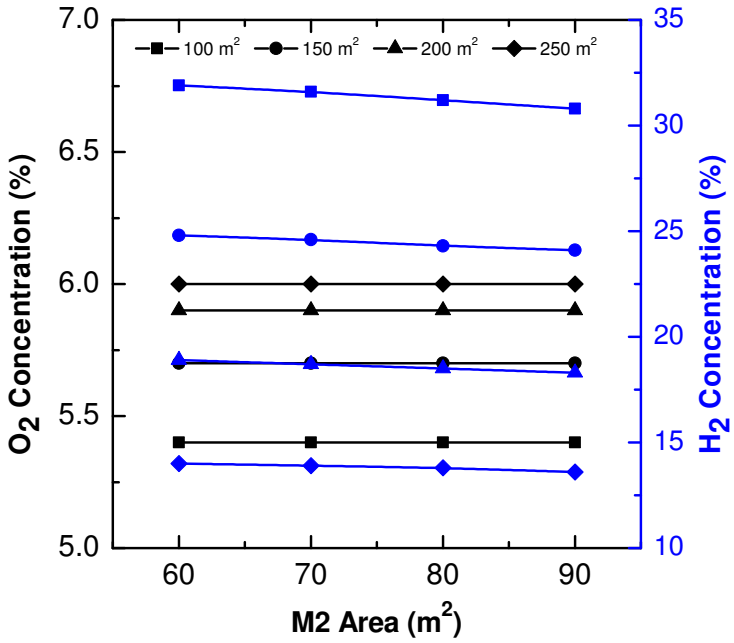

Figure 3.9: O_2 and H_2 concentrations in the M2 permeate as a function of membrane area. M1 area (100, 150, 200 and 250 m^2). p_p= 0.05 bar.

All of the scenarios resulted in streams concentrations that exceed the flammability limit. This is a direct result of the higher O_2 content feeding the second module. This result is exacerbated when the membrane area in the first stage is increased. Increasing the Δp is necessary for this scenario to be feasible.

Mixture (2) results:

The investigation of Mixture (2) was carried using only one membrane unit. Due to higher O_2 content in the feed, none of the operating variables (membrane are and permeate pressure) satisfy the flammability limitations. The lowest O_2 concentration (5.2%) was observed for the highest driving force (p_p = 0.05 bar) as shown in Figure 3.10.

The following remarks can represent the findings from this section:

- For Mixture (1), the best promising results were obtained for the double pass cascade design with p_p = 0.05 bar. The maximum recovery obtained was 76.7%.
- No results were obtained for Mixture (2) as all considered operating variables will lead to high O_2 concentration in the permeate.
- Greater driving force (Δp) between the feed and permeate streams is required for better performance and safer operating conditions.

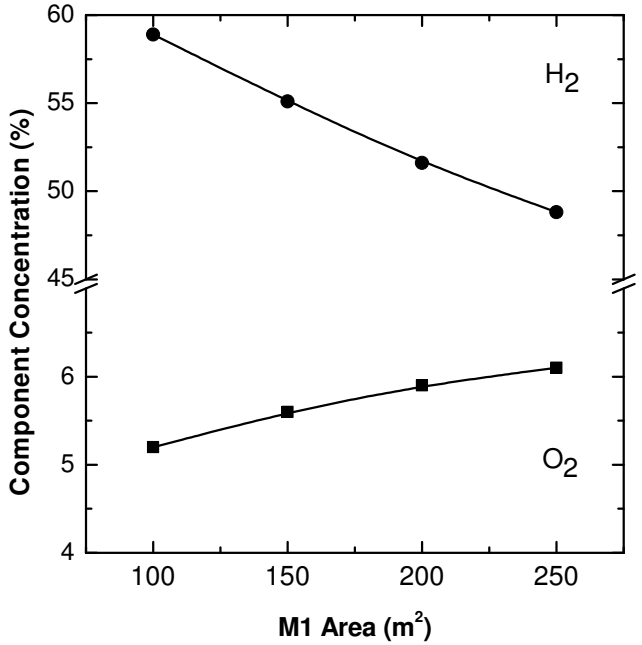

Figure 3.10: O_2 and H_2 concentrations in the M1 permeate for Mixture (2) as a function of membrane area (p_p= 0.05 bar).

3.4 High/vacuum pressure process

The aim of this part of the report is to explore the possibility of obtaining higher H_2 recovery by pressurizing the feed without violating the flammability limitation. Identical feed conditions (P=1bar, T=60°C and F=1kmol/hr) as in the previous section will be utilized. As a last step in this section, different process layouts will be investigated to explore the possibility of increasing the recovery rate.

3.4.1 Improved membrane model

Thermodynamics changes and effects may occur during the gas permeation through the membrane especially if the Δp is very high. Therefore, it is very crucial to observe the temperature change along and across the membrane through the energy balance. The new membrane model used in this investigation is based on the work done by Marco Scholz [126]. The new model will utilize the same material equations as before (Section 3.3.1), which will be coupled with new set of equations to describe the energy balance as illustrated in Figure 3.11. Similar assumptions and membrane properties will be used.

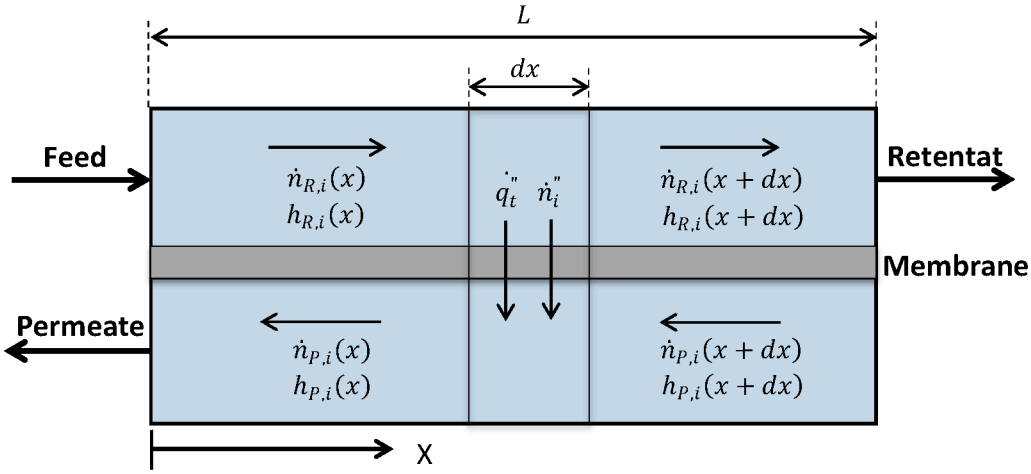

Figure 3.11: Illustration of the membrane model used in section 3.4.

Three different phenomena are included in the energy balance, namely: enthalpy change along the membrane, heat transfer through the membrane due to temperature difference and finally the enthalpy transferred by permeation. The energy balance equations are:

$$\frac{d\dot{H}_P}{dx} = -\dot{n_i}'' \, W \, h_m - \dot{q_t}'' \, W \tag{3.6}$$

$$\frac{d\dot{H}_R}{dx} = -\dot{n_i}'' \, W \, h_m - \dot{q_t}'' \, W \tag{3.7}$$

where $\dot{H}_P$ and $\dot{H}_R$ are the gas enthalpy in the permeate and retentate respectively (W), h_m is the molar enthalpy inside the membrane (J/mol) and $\dot{q_t}''$ is the heat flux through the membrane (W/m^2), which can be calculated using the following equation:

$$\dot{q_t}'' = k\,(T_R - T_P) \tag{3.8}$$

where k is the membrane heat transfer coefficient (W/m^2.K), T_R and T_P are the retentate and permeate temperature (K). The assumed value for k is 7 W/m^{2}K [127]. The required boundary conditions are:

$$\frac{d^2T_P}{dx^2}(x = L) = 0 \tag{3.9}$$

$$T_R(x = 0) = T_F \tag{3.10}$$

3.4.2 Results

Mixture (1) results:

In the previous section, there was a clear advantage in terms of both H_2 recovery and

purity rate when the permeate pressure is operated at 0.05bar instead of 0.1bar. For that reason, the remaining investigation will focus on the permeate pressure of 0.05bar in order to achieve better results.

Before representing the results, the temperature variation across and along the membrane due to gas permeation should be discussed. For all results obtained for both mixtures and at different feed pressure, there was almost no change in the temperatures of the permeate or the retentate ($\pm 0.1^{\circ}$C). This can be explained by the following reasons:

- Low values of Joule Thomson coefficients of all three components even at high and low pressure ranges (Table 3.4).
- The molar heat capacity for these components is very similar (Table 3.4).
- No external heat source that may lead to temperature change.

Therefore, it is acceptable to assume that the temperature is constant and the energy balance can be ignored for simplicity reason in the optimization step.

Table 3.4: Joule Thomson coefficient and heat capacity values for the investigated gases [128].

Component	J-T coefficient (K/bar)		Heat capacity (J/mol K)	
	60°C & 0.05bar	60°C & 4.0bar	60°C & 0.05bar	60°C & 4.0bar
H_2	- 0.036	- 0.036	29.027	29.045
N_2	0.167	0.164	29.151	29.290
O_2	0.215	0.213	29.579	29.730

As anticipated from the previous section, H_2 recovery and O_2 concentration are in much better ranges when the feed is pressurized. Using only one membrane unit, Figure 3.12 provide a clear overview of the advantages of high pressure feed. For instance with a membrane area of 60 m^2, the recovery rate jumps from 30% for 1 bar feed to 95.4% for 4 bar pressure feed. However, it must be noted that the O_2 concentration increases more rapidly with the membrane area for high pressure, which will increase the risk of the explosion.

Focusing on the 4 bar pressure feed and using two membrane units, the maximum recovery obtained for Mixture (1) is 95.2% at 60 m^2 and 6 m^2 for the first and second membrane units, respectively (Figure 3.13). The previous results for the 1 bar feed were 76.7% H_2 recovery at 250 m^2 and 22 m^2 for the first and second membrane units, respectively. Not only higher recovery was achieved but also much less membrane area in both units was required. These advantages come with an exchange for extra energy consumption to pressurize the feed.

It must be noted that increasing the membrane area for the 2^{nd} stage beyond 6 m^2, will only leads to less H_2 purity and higher O_2 concentration in the permeate with no significant increase in the recovery. For that reason, an accurate process design is required to minimize energy and membrane area usage while maximizing the recovery under safe operating conditions, which justify the latest step "the economical optimization of the process".

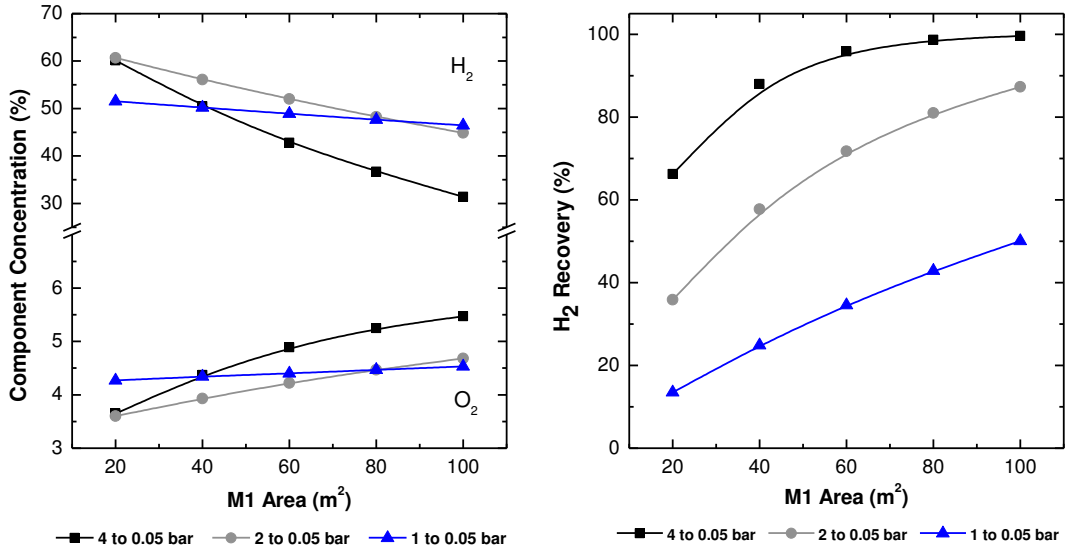

Figure 3.12: Recovery and components concentration for Mixture (1) at different membrane area and pressure ($p_P = 0.05$bar).

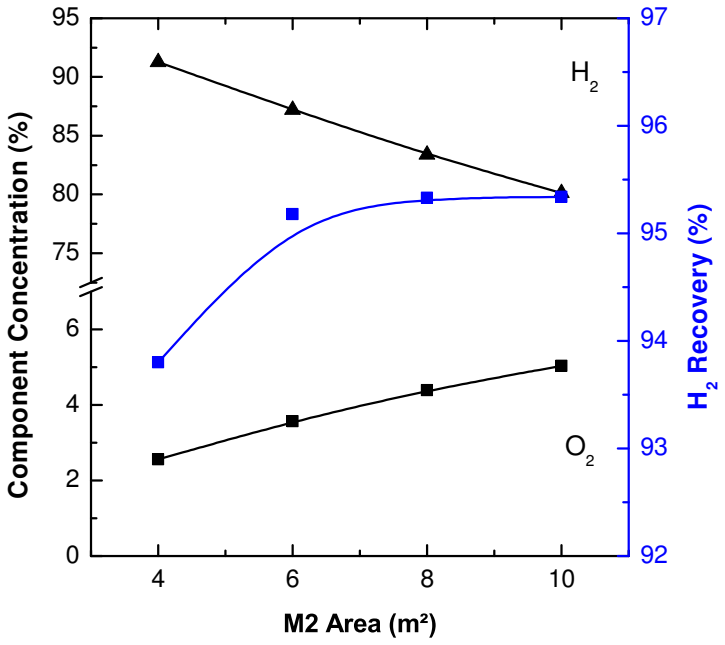

Figure 3.13: Recovery and components concentration for Mixture (1) as a function of M2 area ($p_P = 0.05$bar).

Mixture (2) results:

In Section 3.3.2, all considered membrane operating parameters applied to Mixture (2) did not satisfy the flammability constraint in the permeate. To overcome this problem, lower membrane areas and higher feed pressure were applied for Mixture (2). Using only one membrane unit, it can be seen that there are some area ranges that operate below 5% O_2 concentration for 1 bar pressure feed but the recovery is very low (about 35%) as shown in Figure 3.14.

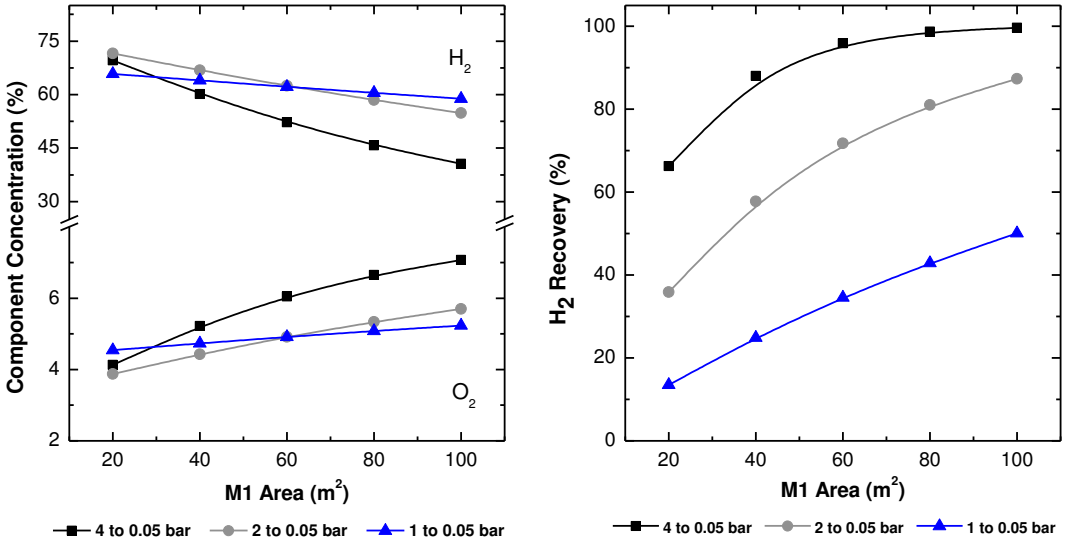

Figure 3.14: Recovery and components concentration for Mixture (2) at different membrane area and pressure ($p_P = 0.05$bar).

For 4 bar pressure feed, the system must operate at below 40 m^2 to prevent the O_2 concentration to exceed the 5% limit which limits the recovery to below 85% from the first unit. Pressurizing the permeate to 4 bar and passing it to the 2^{nd} membrane unit yields the results shown in Figure 3.15. Same behavior as Mixture (1) is obtained but with much lower H_2 recovery (below 84%).

The following remarks can represent the findings from this section:

- For Mixture (1), pressurizing the feed to 4 bar leads to an increase of H_2 recovery from 76% to 95%.
- The maximum recovery for Mixture (2) is around 83.8%, which much lower than the Mixture (1) due to higher O_2 content in the feed.
- Optimum values of the membrane areas should be determined in order to prevent additional separation cost while justifying recovery and safety constraints.

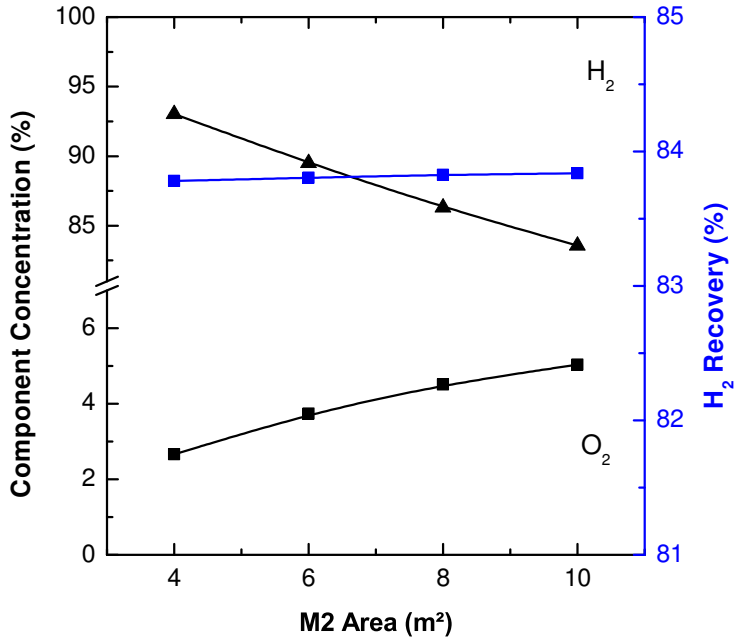

Figure 3.15: Recovery and components concentration for Mixture (2) as a function of M2 area ($p_P = 0.05$bar).

Evaluation of different process layouts:

Due to the presences of O_2 in a tertiary components system, H_2 recovery will not be limited only by process economic but also with the safety constraints. This fact can be seen clearly from the previous section where switching from Mixture (1) to Mixture (2) will drop the recovery from 95% to 83.8%. To obtain high recovery and purity for membrane based gas separation, the process should be designed with several stages. More than three stages cascade design is usually not economically feasible as the compression cost of the feed and the permeate streams increase dramatically [129].

So far, only two membrane units design is chosen to carry out the separation in order to reduce the process cost. After eliminating unreasonable connections (e.g. connecting of permeate, retentate and feed of the same membrane unit), Figure 3.16 shows all possible connections and recycles that can be formed using two units.

Mainly four possible configurations can be investigated:

1. Double pass with no recycle streams
2. Passing retentate streams into membrane units
3. Recycling the second retentate stream to the main feed
4. Recycling the second permeate stream to the main feed

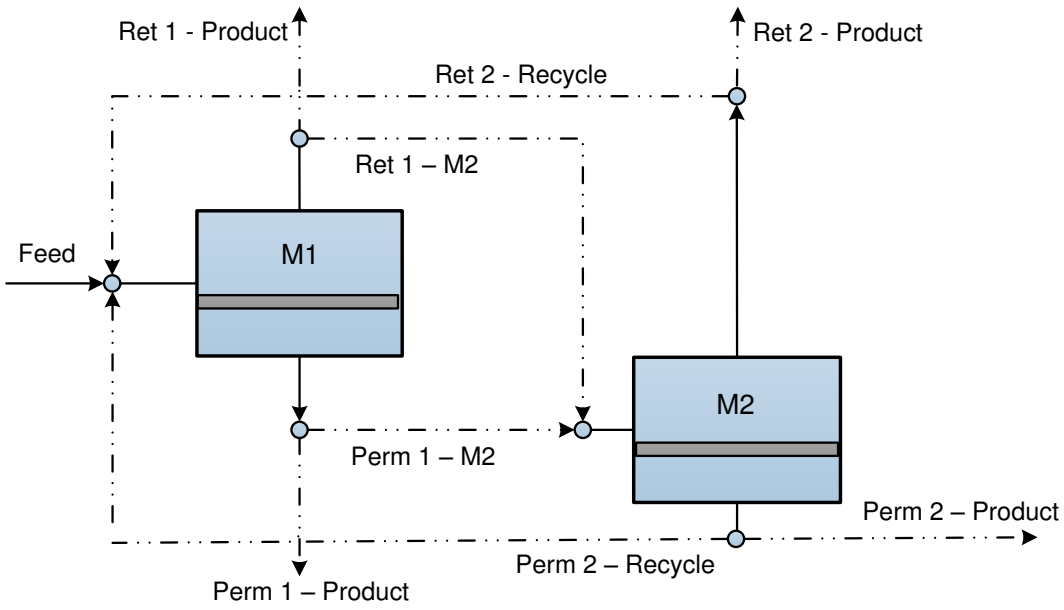

Figure 3.16: All possible connections for two membrane units design.

So far, all previous investigations and results were carried using the the double pass configuration. Limited H_2 recovery was noticed in both mixtures. The second configuration showed no benefit (as shown in Section 3.3.2) as H_2 to O_2 ratio is much lower in this case than in the main feed, which leads to more recovery restrictions.

The benefit of recycling retentat streams over permeate ones is that to prevent the energy consumption required to pressurize the recycle stream to the feed pressure range. In the third configuration, the same Aspen Custom Modular (ACM) model was switched from steady state mode to optimization mode with the following variables and constraints:

- Pressure range for both membrane feeds: 1 to 4 bar
- Pressure range for permeate: 0.05 to 2 bar
- First membrane area range: 1 to 500 m^2
- Second membrane area range: 1 to 100 m^2
- Upper limit for O_2 concentration in both permeate: $\leqslant$ 4.5%mol
- Optimization objective: maximize recovery

The only possible solution for Mixture (1) that was obtained with this configuration is to operate the system with high flow and H_2 purity recycle as shown in Figure 3.17. By using this approach, the system will eliminate the O_2 build up in the system and increase the driving force for H_2 in the membrane permeation. The H_2 recovery value will vary with the amount of the recycle stream. For example, 99.8% recovery can be achieved when the recycle stream is at 7.52 kmol/hr. However, this will results in a huge cost of the separation process as the feed size will be increased by a factor of 8, which will results in high energy consumption for compression and membrane area requirement.

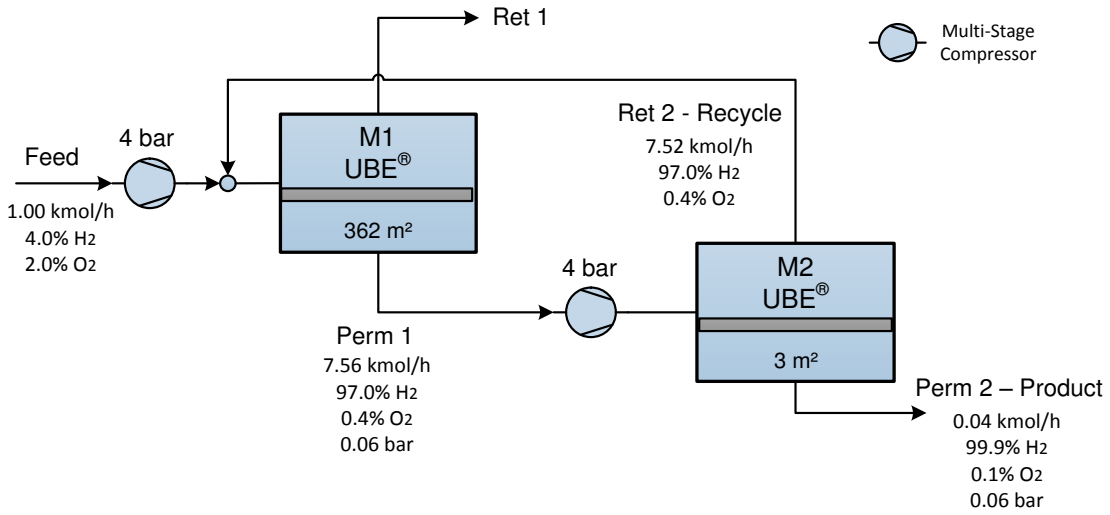

Figure 3.17: Maximizing H_2 recovery by recycling M2 retentate for Mixture (1).

Lower O_2 concentration and high driving force for H_2 can be obtained when the feed is mixed with high purity H_2 stream. This can be achieved by recycling the permeate product (fourth configuration). In order to obtain an accurate design and optimum membrane parameters for the separation, both configurations 1&4 will be considered in the optimization step.

3.5 Optimization

In this section, we will investigate the application of UBE® hollow fiber membrane to recover the diluted H_2 from the water splitting process. Additionally, we will explore the potential of novel and high performance membrane materials (not commercialized) on the process economic and design. The design will maintain a safe operating condition throughout the system by applying the flammability constraints on all streams. Nonlinear programming (NLP) will be used to optimize the recovery process by manipulating the decision variables, namely: recycling rates, feed / permeate pressures and membrane areas. The objective is to reduce the Present Value (PV) of all outgoing cash flows (no income) of the separation process including investment cost, operating cost, loss of product and depreciation.

3.5.1 Optimization approach

The process and all unit operations models will be implemented in the General Algebraic Modeling System (GAMS). GAMS is a high level modeling system utilized to optimize complex, large-scale modeling applications. NLP models consist of an objective function

that should be minimized or maximized under consideration of specified constraints. The optimization problem is formulated as follow:

$$min\, f(x) \tag{3.11}$$

subject to:

$$h(x) = 0 \tag{3.12}$$
$$g(x) \geq 0 \tag{3.13}$$
$$x \in X \tag{3.14}$$

where $f(x)$ is the objective function, $h(x)$ are the model equations, $g(x)$ is the set of constraints that define the feasible space of operation such as the pressure range or product purity, x is the vector of the optimization variables, e.g. the system pressure, the membrane area for each stage [130]. Table 3.5 shows the NLP model for the investigated process. Considering the product loses in the PV will push the optimization to aim for higher recovery rates.

Different solvers can be utilized to solve the NLP model. After carrying out trials tests with different solvers, ANTIGONE (Algorithms for coNTinuous / Integer Global Optimization of Nonlinear Equations) was chosen for this study. The solver performed and solved most of the trials in fewer time frame as mentioned in the literature [131]. As this type of solver is global, there is no need to provide initial values for the decision variables and the outcome value of the objective function is guarantee to be the global optimum.

Table 3.5: NLP model for $H_2/O_2/N_2$ separation process

Equation	Definition	Values
Objective function: f(x)	PV of all outgoing cash flows (no income) including: investment cost, operating cost, loss of product and depreciation for 15 years.	minimize
Constraints g(x)⩾0	Sets of linear and nonlinear process constraints including:	
	- H_2 recovery	e.g. ⩾90%
	- H_2 purity	e.g. ⩾95%
	- O_2 limits in permeates	⩽4.5%
	- H_2 limits in retentates	⩽4.0%
	- Max. feed pressure	⩽4 bar
	- Min. permeate pressure	⩾0.05 bar
Model equations:h(x)=0	Sets of the equipment equations required to calculate the performance and economics	-

3.5.1.1 Process model

Two membrane units will be utilized in order to achieve the required recovery and purity of the H_2 in a double pass configuration, Figure 3.18. Part of the permeate stream leaving the second membrane can be recycled back to the main feed represented by a ratio factor R. Using this approach, lower O_2 concentrations and a higher driving force for H_2 permeation can be achieved. This approach may require additional costs for extra compression and membrane area. With a 100 kmol/hr H_2 feed basis, two different flow rates for the two mixtures were investigated.

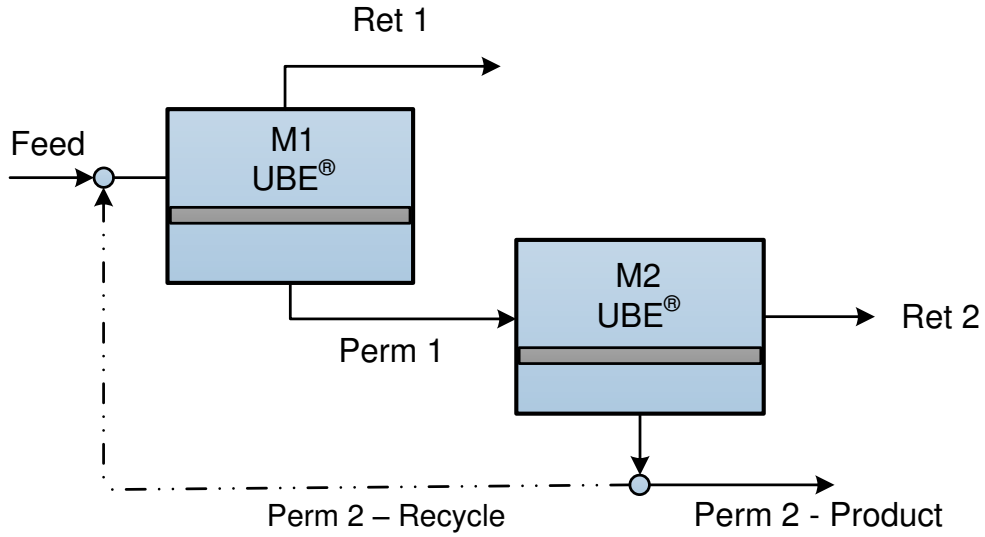

Figure 3.18: Two membrane units in double pass configuration with a recycle stream from the final product.

3.5.1.2 Unit operations

Membrane Module

For this study, a simple membrane short-cut model was utilized with the same assumptions listed in Section 3.3.1. The model will be discretized in 10 elements (j) where the following set of equations describe the gas transport through each element in counter-current flow for each species i as shown in Figure 3.19 [132]:

$$\dot{n}_{R,i,j} = \dot{n}_{i,j} + \dot{n}_{R,i,j+1} \tag{3.15}$$

$$\dot{n}_{P,i,j} = \dot{n}_{i,j} + \dot{n}_{P,i,j+1} \tag{3.16}$$

$$\dot{n}_{i,j} = Q_i \cdot (x_{i,j} \cdot p_f - y_{i,j} \cdot p_P) \cdot A_m \tag{3.17}$$

$$x_{i,j} = \frac{\dot{n}_{R,i,j}}{\sum_i \dot{n}_{R,i,j}} \tag{3.18}$$

$$y_{i,j} = \frac{\dot{n}_{P,i,j}}{\sum_i \dot{n}_{P,i,j}} \tag{3.19}$$

where $\dot{n}_{R,i,j}$ and $\dot{n}_{P,i,j}$ are the molar flow of component i, element j in the retentate and permeate (mol/s), respectively, $\dot{n}_{i,j}$ is the transferred molar flow of component i in element j (mol/s), $x_{i,j}$ and $y_{i,j}$ are the mole fraction of component i, element j in the retentate and the permeate, respectively and Am is the membrane area (m^2).

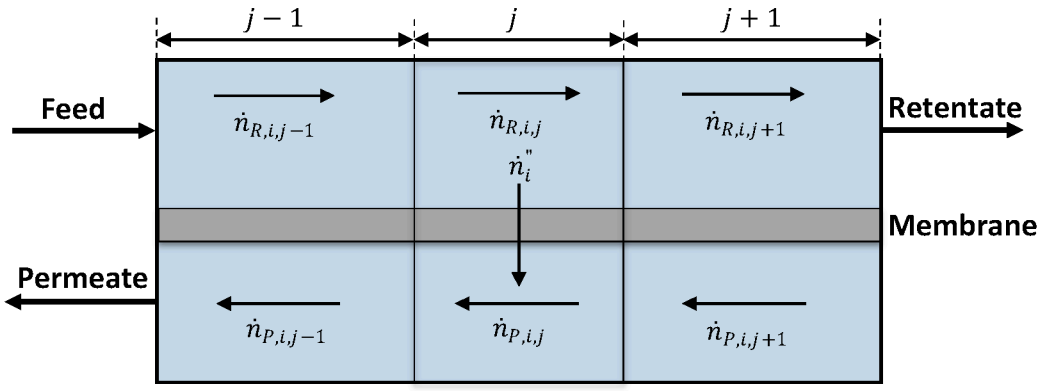

Figure 3.19: Illustration of the hollow fiber membrane model used in the optimization step.

The main study will focus on the use of the commercial polyimide membrane from UBE® (Japan). We will also investigate a new experimental polymer, TPIM-1, in order to show the impact of high performance polymers on our process. Table 3.6 shows the UBE® and TPIM-1 permeation properties used in this study [73, 82]. The reported permeability values were measured at 60°C for UBE® and 35°C for TPIM-1.

Compressors and vacuum pumps

Both centrifugal compressors and vacuum pumps can be modeled with the same set equations [132]. For simplicity, only one stage (without interstage cooling) will be used to obtain the required pressure ratio for both units. Assuming ideality (isentropic and adiabatic compression), the following equations are used to calculate the power and the

Table 3.6: Gas permeation properties for UBE® and TPIM-1 membranes [73, 82].

Component	UBE®		TPIM-1	
	Permeance (GPU)	Selectivity (Q_{H_2}/Q_i)	Permeance (GPU)	Selectivity (Q_{H_2}/Q_i)
H_2	140.0	-	3095.2	-
O_2	8.4	16.7	170.9	18.1
N_2	1.7	82.4	19.9	155.5

outlet temperatures for these units [132, 133]:

$$Power = \dot{n} \cdot c_{p,air} \cdot (T_{real} - T_{in}) \tag{3.20}$$

$$\epsilon = \frac{T_{out} - T_{in}}{T_{real} - T_{in}} \tag{3.21}$$

$$T_{out} = T_{in} \cdot (\frac{P_{out}}{P_{in}})^{(\frac{\kappa-1}{\kappa})} \tag{3.22}$$

where $Power$ is the compressor duty (kW), $\dot{n}$ is the equipment inlet stream molar flow rate (mol/s), $c_{p,air}$ is the molar heat capacity of air (kJ/mol K), T_{real} is the actual outlet temperature (K), T_{in} & T_{out} are the inlet and outlet temperatures (K), respectively, ϵ is the compressor efficiency, and κ is the isentropic exponent for air.

Computational efforts and time can be reduced significantly by reducing the number of equations or by linearizing them. Looking at Equation 3.20, the only missing value is T_{real} which can be calculated using Equations 3.21 and 3.22. After inserting all known values and combining these two equations, a single linear equation for the compressor can be found and another exponential equation for vacuum pumps. These equations are fitted to certain operational ranges, which are of interest in this work:

For UBE® membrane process:

$$T_{real,Comp} = 50.59 \cdot (P_{out,Comp}) + 333.15 \tag{3.23}$$

$$T_{real,Vac} = 333.15 \cdot (P_{in,Vac})^{-0.45} \tag{3.24}$$

For TPIM-1 membrane process:

$$T_{real,Comp} = 46.80 \cdot (P_{out,Comp}) + 308.15 \tag{3.25}$$

$$T_{real,Vac} = 308.15 \cdot (P_{in,Vac})^{-0.45} \tag{3.26}$$

where sub-index Comp & Vac refers to compressor and vacuum pumps respectively.

These equations are obtained by plotting the dependent variable (T_{real}) as function of the independent variables ($P_{out,Comp}$ and $P_{in,Vac}$). The value of the independent variable is ultimately determined by the required H_2 recovery and purity of the process. Detailed information about the development of these equations can be found in Appendix 3.7.1.

Heat exchangers

The outlet streams of the compressors and vacuum pumps must be cooled down in order to reduce the explosion risk. For this study, shell and tube heat exchangers, with process feed flowing in the tube side, are used. Furthermore, a floating head type design comprised of carbon steel material is used. Seawater is utilized as the cooling media with fixed inlet and outlet temperatures in a counter-current configuration. The following set of equations are used to calculate the required heat exchanger area (capital cost) and the seawater flow rate (operating cost) [133]:

$$Q = \dot{n} \cdot c_{p,air} \cdot (T_{real} - T_{in}) \tag{3.27}$$

$$Q = \dot{m}_{water} \cdot c_{p,water} \cdot (T_{water,out} - T_{water,in}) \tag{3.28}$$

$$Q = U \cdot A_{HX} \cdot \Delta T_{lm} \tag{3.29}$$

where Q is the heat exchanger duty (kW), $\dot{m}_{water}$ is the seawater mass flow rate (kg/s), $c_{p,water}$ is the specific heat capacity of water (kJ/kg.K), $T_{water,in}$ & $T_{water,out}$ are the inlet and outlet seawater temperature (K), respectively, U is the heat transfer coefficient (kW/m2 K), A_{HX} is the heat exchanger area and ΔT_{lm} is the counter-current log mean temperature (K).

3.5.1.3 Economics

As mentioned before, the aim of the GAMS code is to minimize the objective function f(x), which is the PV of the separation process which includes:

- Capital Cost (CC): includes compressors, vacuum pumps, heat exchangers and membrane units.
- Operational Cost (OC): includes energy consumption, water consumption, loss of product and membrane replacement on a yearly basis.

Since the operation cost is assumed to be constant over time, the following formula can be used to calculate the PV [134]:

$$PV_{i,T} = CC + R_t \cdot \frac{(i+1)^T - 1}{(i+1)^T \cdot i} \tag{3.30}$$

where $PV_{i,T}$ is the plant present value ($) with interest rate i (%) and lifetime T (year), CC is the capital cost ($), and R_t is the net cash flow in year t ($).

The results obtained for each mixture will be compared in terms of the H_2 specific cost, which is calculated by diving the Equivalent Annual Cost (EAC) ($/year) over the annual H_2 production (kg/year). The following formual was used to calculate the EAC:

$$EAC = \frac{PV}{A_{T,i}} \tag{3.31}$$

$$A_{T,i} = \frac{1 - \frac{1}{(1+i)^T}}{i} \tag{3.32}$$

where $A_{T,i}$ is the present value of annuity factor (year).

For membranes, 55€/m^2 was used as the purchase price (cartridge cost) and the installation cost is 30% of the total membrane purchase price. We assumed that the membrane is replaced every four years with a cost equivalent to the total initial cartridge cost. The capital cost of the other equipment can be estimated using Guthrie's method [135]. This method is based on a power law expression to account for the nonlinear increase of cost with equipment size, which is known as the economy of scale. This method has an error of ± 25% to estimate the investment cost [133]. In general, all equipment costs can be

estimated using the bare module cost (BC) equation:

$$BC = C_0 \cdot (\frac{S}{S_0})^{\alpha} \tag{3.33}$$

This equation estimates the cost of new equipment with size (S) comparing to the size (S_0) and cost (C_0) of the reference equipment with a specific exponent (α). After that, the calculated cost has to be updated with three different factors to estimate the present-day costs. These factors are as follows:

- Update Factor (UF) is used to account for inflation
- Material and Pressure Factor (MPF) is used to account for different material selection
- Module Factor (MF) is used to account for installation, shipping and supervision

It must be noted that a factor of 2 was added to MF to more realistically represent the equipment cost in today's economy [132]. These values vary depending on the equipment size and the operating conditions. They can be estimated using tables and figures provided [133, 135]. The final Capital Cost (CC) is calculated as follow:

$$CC = UF \cdot BC \cdot (MPF + MF - 1) \tag{3.34}$$

For compressors and vacuum pumps, the equipment size is based on the required duty, while for heat exchangers are based on the calculated area. The operating cost is calculated based on both electricity and cooling water consumption. Table 3.7 shows the process and equipment parameters of the process, while all required economic parameters are listed in Table 3.8.

Table 3.7: Process parameters for $H_2/O_2/N_2$ separation process.

Parameter	Value	Unit
Feed flow rate:		
a) Mixture (1)	2500.0	kmol/hr
b) Mixture (2)	1666.7	kmol/hr
ϵ_{Comp}	0.80	-
ϵ_{Vac}	0.50	-
κ	1.40	-
$T_{in(UBE)}$	333.15	K
$T_{in(TPIM-1)}$	308.15	K
$P_{in,Comp}$	1	bar
$P_{out,Vac}$	1	bar
U_{Comp} (high pressure) [133]	220.00	$W/m^2.K$
U_{Vac} (ambient pressure) [133]	100.00	$W/m^2.K$
$T_{water,in}$	298.15	K
$T_{water,out}$	308.15	K

Table 3.8: Economic parameters for $H_2/O_2/N_2$ separation process.

Parameter	Value	Unit
Annual Operating hours	8000	hr
Plant Lifetime (T)	15	years
Interest Rate (i)	9	%
Hydrogen Price [136]	2	\$/kg
Currency Exchange	1.2	€ to \$
Electricity Price - 2014 [137]	0.084	€/kWh
Water Price	0.080	€/m^3
Compressor reference cost (C_0)	23,000	\$
Compressor reference size (S_0)	74.60	kW
Exponent α_{Comp}	0.77	-
UF*	5.03	-
MPF_{Comp}	1.15	-
MF_{Comp}	5.01	-
Heat exchanger reference cost (C_0)	5,000	\$
Heat exchanger reference size (S_0)	37.1	m^2
Exponent α_{HX}	0.65	-
MPF_{HX}	1.00	-
MF_{HX}	5.29	-

* Obtained from Chemical Engineering magazine (Nov. 2014)

3.5.2 Results

For each set of data obtained from the optimization, the H_2 recovery and/or the purity must be specified. Detailed analysis will be provided for Mixture (1) with full process diagram showing the layout and operating conditions. Main results with major differences will be highlighted for Mixture (2). Finally as a last effort to reduce the cost, we will explore the benefits of utilizing a high performance membrane material on the process.

3.5.2.1 Mixture (1) optimization results

The first results for Mixture (1) were obtained by specifying the H_2 recovery, while the purity will be a variable determined by the optimization. Figure 3.20 demonstrates the layout of the process with the major results obtained from the optimization for an 86% recovery rate, as an example. The process consists of one compressor and one vacuum pump for each membrane unit and four heat exchangers in total. It must be noticed that the high value of membrane area required for the first unit was expected as the investigated mixture is diluted and more membrane area is required to process the stream. Moreover, both retentate streams contain very low H_2 concentration (<1%mol) with high O_2 ratio.

So it is not economically beneficial to consider recycling these streams and it may also leads to higher explosion risk as shown in Section 3.4.2.

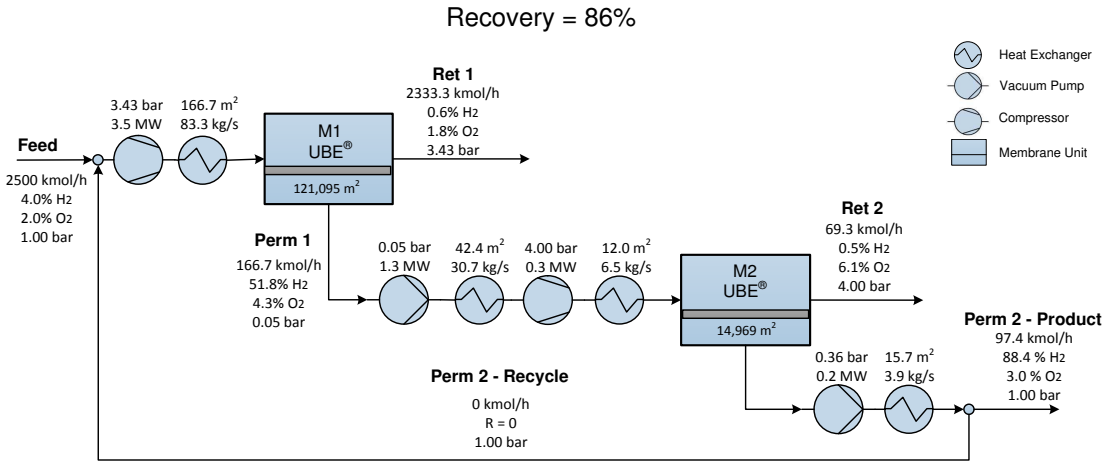

Figure 3.20: Mixture (1) process layout for 86% recovery rate.

Figure 3.21 represents the results for Mixture (1) for specified recovery up to 98%. The O_2 concentration in the permeate and feed streams is processed at $\leqslant 4.5\%$ in which the remaining 0.5% is a safety margin.

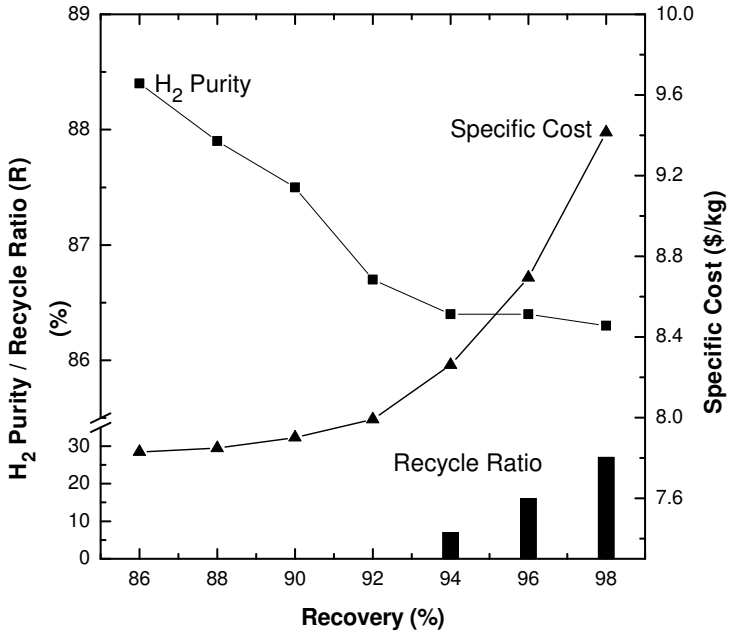

Figure 3.21: Specific cost for Mixture (1) for specified H_2 recovery.

A tradeoff between the recovery and the purity of the H_2 can be observed up to 92%. As the recycle stream starts to be utilized, the purity decreases slightly as the recovery approaches 98%. However, this leads to an exponential increase in the total and the specific costs. In general, the specific cost of separating the H_2 from this diluted mixture is tremendously high especially at >92% recovery rates. The cost is even higher than the estimated production price of H_2 at \$2/kg [136].

Analyzing the capital cost of the lowest and the highest recovery rates shows that an increase of 42% of the capital cost is required to level up the recovery as shown in Table 3.9. For both recovery rates, compressors have the highest cost between all four operation units. Combined, the pressure equipment (compressors and vacuum pumps) accounts for 60% of the total capital cost in both cases, while heat exchangers account for less than 2%. About 34% increase in the operational costs is required to level up the recovery from 86% to 98%. It is obvious that increasing the recovery will lower the losses of product. However, this cost is on par with the cooling water cost at the lower recovery rate. As expected, the energy cost has the major lead with more than 58% of the total operational cost with the membrane replacement coming in second with 30% of the total cost.

If both H_2 recovery and purity are specified, different results are obtained. In Figure 3.22, different purity values were chosen for the same recovery to carry out the optimization. It is clear that targeting purity higher than 92.5% will cause an exponential increase in the separation costs. This can be explained by the high value of the recycle ratio (R), where more of the final stream is sent back for further separation and polishing to achieve a higher purity.

Table 3.9: Mixture (1) capital and operating cost analysis for lowest and highest recovery rate.

	86% Recovery	98% Recovery
Capital Cost (CC)		
Compressors	45.2%	38.8%
Vacuum Pumps	17.5%	21.1%
Membranes	35.4%	38.5%
Heat Exchangers	1.9%	1.6%
Total	27.50 Mio.€	39.14 Mio.€
Operating Cost (OC)		
Energy	58.9%	59.9%
Membrane Replacement	29.8%	34.6%
Loss of Product	6.4%	0.6%
Cooling Water	4.9%	4.9%
Total	5.96 Mio.€	7.97 Mio.€

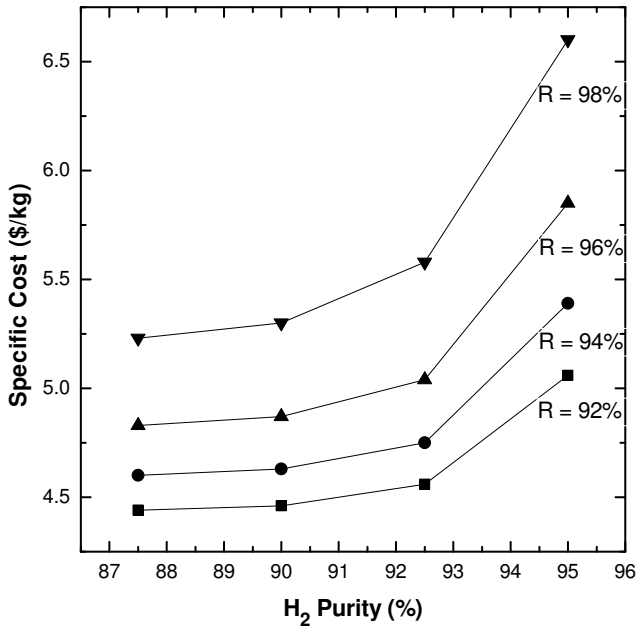

Figure 3.22: Specific cost for Mixture (1) for specified H_2 recovery and purity.

Table 3.10 shows the capital cost analysis for the lowest and highest purity at 92% recovery rate. The major equipment that has an increase of more than 55% in terms of cost is the vacuum pumps with a minimal cost increase for the other equipment. This indicates that more H_2 purity can be achieved in a tertiary system by operating the permeate at the lowest pressure possible.

Table 3.10: Mixture (1) capital cost analysis for lowest and highest purity for 92% recovery rate.

	87.5% Purity	95.0% Purity
Compressors	46.0%	42.3%
Vacuum Pumps	18.2%	24.8%
Membranes	34.0%	31.1%
Heat Exchangers	1.8%	1.8%
Total	30.57 Mio.€	34.84 Mio.€

3.5.2.2 Mixture (2) optimization results

The same procedures were followed for Mixture (2). Looking at Figure 3.23 and comparing to Mixture (1), we can see that H_2 can be recovered at a much lower cost in general. The use of the recycled stream from early value of recovery is associated with the higher content of O_2 in the feed for Mixture (2). The reduction in cost can be seen more clearly from Figure 3.24. For example, we can achieve 28% reduction in cost when targeting 90%

recovery rate with 95% purity if we switch from Mixture (1) to Mixture (2). The reduction is the results of the lower feed flow rates for Mixture (2) with higher H_2 concentration. These two factors play a major role in reducing the required membrane area and the compression power. Another key difference is that the exponential increase of the cost starts from a higher purity value, around 95% instead of 92.5% for Mixture (1).

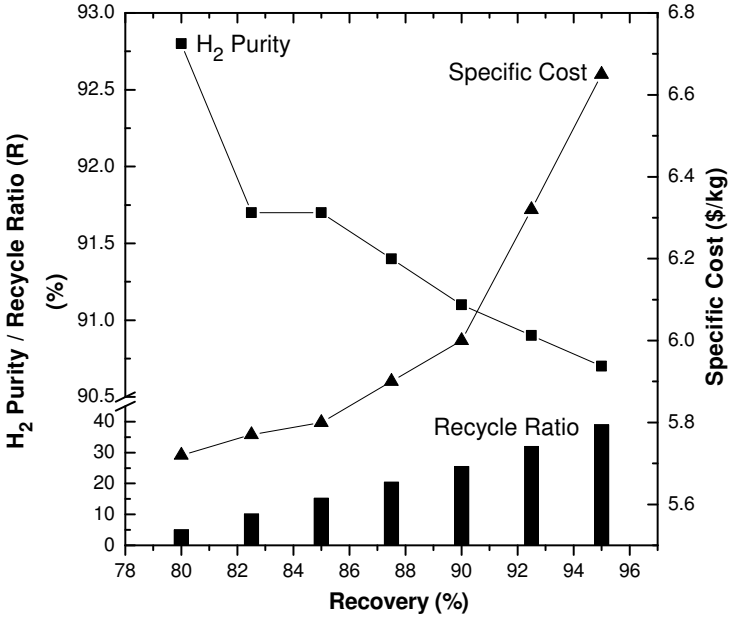

Figure 3.23: Specific cost for Mixture (2) for specified H_2 recovery.

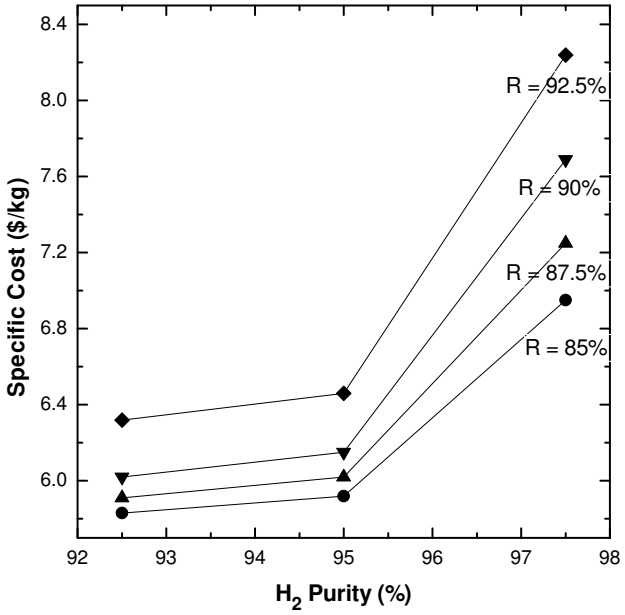

Figure 3.24: Specific cost for Mixture (2) for specified H_2 recovery and purity.

The following remarks summarize the findings from investigating both mixtures:

- With partial recycling of the final product, further H_2 recovery can be achieved. However, this increases investment and operational costs.
- Capital and operational costs of pressure equipment account for 60% of the cost.
- Higher H_2 purity can be achieved at lower permeate pressure.
- The H_2 recovery and purity for Mixture (1) are limited to 92% and 92.5%, respectively. Beyond these values, the specific cost of H_2 increases dramatically. However, these values are limited to 90% and 95%, respectively, for Mixture (2) (see Figure 3.25).
- Cost reduction of 25% can be noticed when comparing the above recommended values for Mixture (1) and (2).
- The final product stream of Mixture (1) contains around 3-4 %mol O_2, depending on the H_2 purity and recovery, while Mixture (2) contains around 1-2 %mol O_2.
- In general, the specific cost of H_2 separation is still higher than the estimated production price for both mixtures.

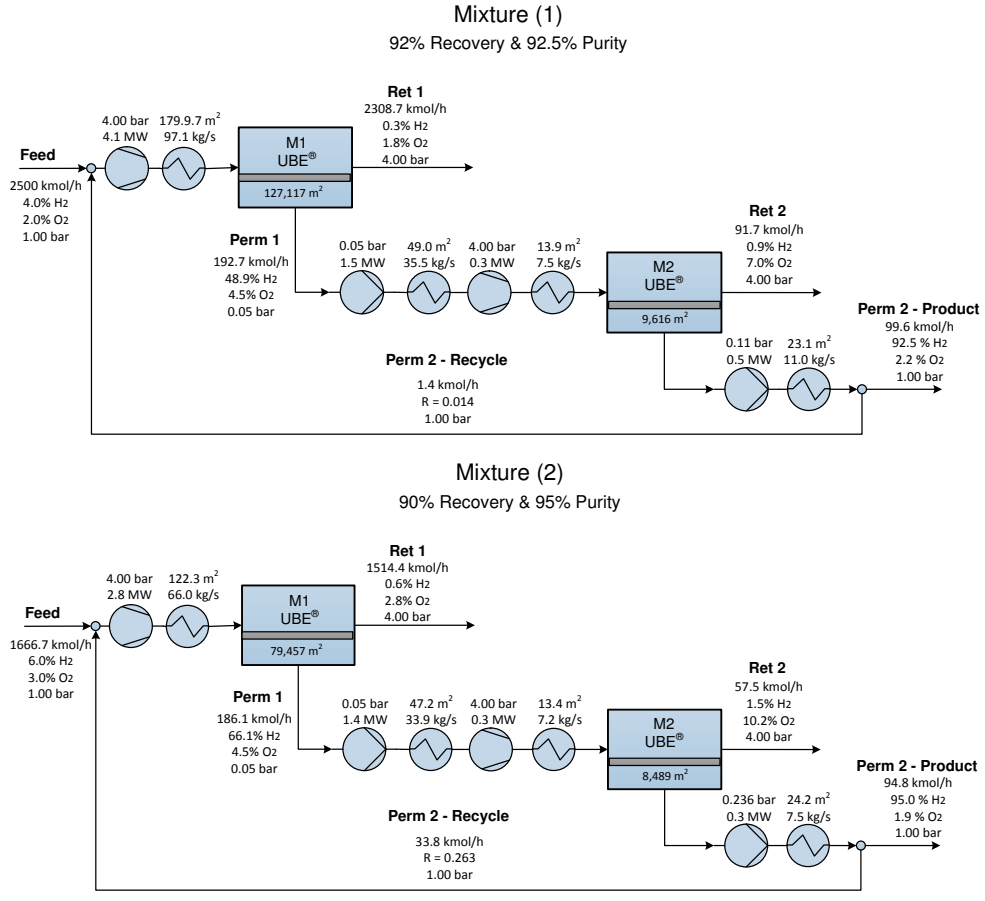

Figure 3.25: Process layout for H_2 recovery and purity limited values for Mixture (1) and Mixture (2).

3.5.2.3 Impact of a High Performance Polymer

As development research continue to grow in the field of membrane material, it is interesting to investigate the impact of high performance polymers in our process. A new experimental polymer, TPIM-1, demonstrates the highest H_2 selectivity and permeability in recent publications [73]. Comparing the permeability values listed in Table 3.6 with the UBE® membrane, we see a slight increase in H_2/O_2 selectivity and a very high increase in the H_2/N_2 selectivity. However, it must be noted that there is an increase of O_2 to N_2 selectivity from 5 for UBE® to 8.6 for TPIM-1. This may increase the challenge of controlling the flammability limits.

The optimization study was carried out for both mixtures at three different recovery rates and compared to the UBE® membrane results assuming that the membrane cost and thickness for TPIM-1 are the same. Furthermore, the process temperature used in TPIM-1 process was lowered to 35°C in order to match the permeability data available in the literature. This temperature variation will only affect the total cost by 5% by reducing the cost of the pressure equipment.

Analyzing the results in Table 3.11 shows that higher H_2 purity is obtained for the two mixtures at all three recovery rates. This is the result of the high H_2 selectivity of TPIM-1. Moreover, the specific cost of H_2 separation is lower comparing to UBE® for two reasons: (1) reduction of membrane area due to high permeability values, (2) reduction in compressor duties because the required feed pressure is lower. The recycled stream with high purity H_2 increases the driving force for permeation by increasing the molar concentration. However, a very high recycle rate with high H_2 purity is required for the TPIM-1 membrane. This is the result of the high O_2 selectivity over N_2. The higher O_2 permeability causes the permeate to reach the explosive limit much faster and at lower recovery rates than on UBE®. To mitigate this challenge, more recycle stream is needed to lower the O_2 concentration in the feed.

Table 3.11: Summary of the performance and economic results comparing UBE® and TPIM-1 membranes for both mixtures.

		UBE®			TPIM-1		
	Recovery (%)	H_2 Purity (%)	Recycle (%)	Specific Cost ($/kg)	H_2 Purity (%)	Recycle (%)	Specific Cost ($/kg)
Mixture (1)	90.0	87.5	0.0	7.90	88.0	52.0	4.54
	92.5	86.4	1.0	8.05	91.1	54.0	4.61
	95.0	86.4	12.0	8.46	91.2	57.0	4.73
Mixture (2)	90.0	91.0	26.0	6.08	92.9	54.0	3.64
	92.5	90.9	32.0	6.30	95.6	56.0	3.98
	95.0	90.7	39.0	6.64	94.6	58.0	3.98

Since TPIM-1 is an experimental material, we can anticipate a higher cost per square meter. We repeated the simulations using two times and three times the baseline cost (55€/m^2) to investigate the influence of the membrane cost on the optimization. Respective

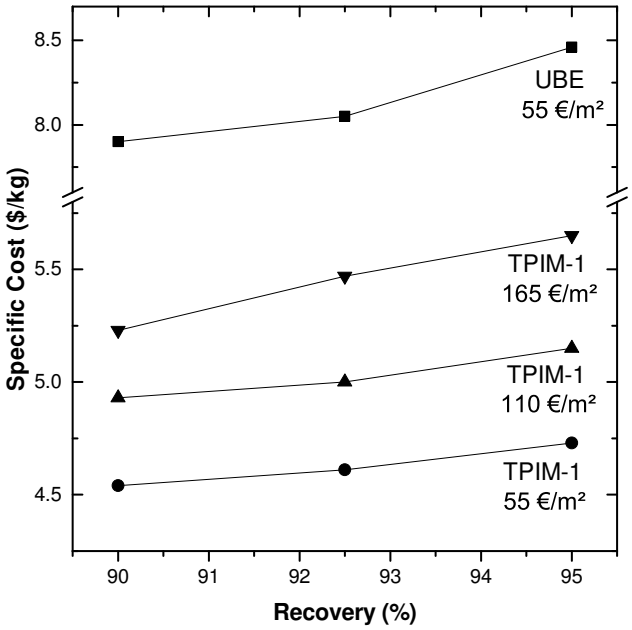

(a) Mixture (1)

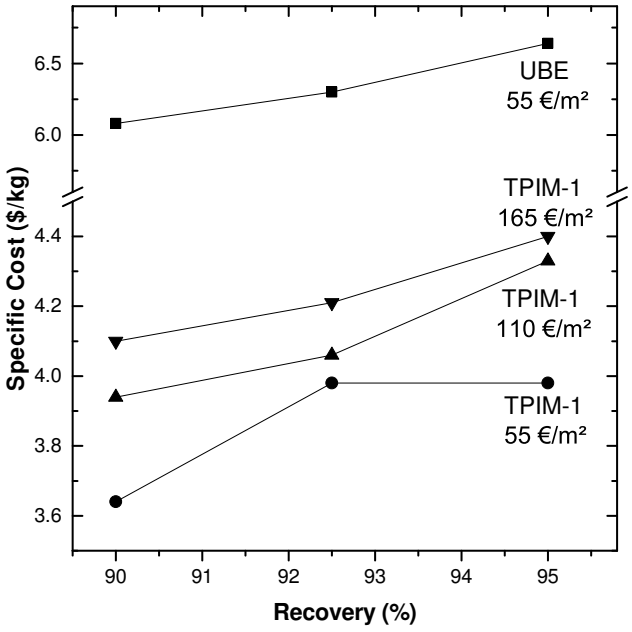

(b) Mixture (2)

Figure 3.26: TPIM-1 membrane price influence on H_2 specific cost

trends for these difficult pricing structures are shown in Figure 3.26. As expected, the specific cost does increase, but the change is minimal less than 20%, and in all scenarios the specific cost remains lower than the baselines for the UBE® system. Detailed results of this investigation can be found in Appendix 3.7.2.

3.6 Conclusion

In this chapter, we investigated our first effort to recover H_2 from photocatalytic water splitting. We assumed the reactor products (H_2 & O_2) are diluted with N_2 for safer operation. Mixture (1) with 4%mol and Mixture (2) with 6%mol H_2 concentration were investigated thoroughly in three steps to recover the H_2 using commercial membrane material UBE®. All flammability constraints, essential assumptions and modelling equations were listed to insure accurate results.

The first step aimed to recover the H_2 between ambient and vacuum pressure range. For the considered operating conditions, the maximum recovery for Mixture (1) was 76.7% with no results that can satisfy the constraints for Mixture (2). The second steps revealed the advantages of pressurizing the feed to higher pressure range. Not only higher recovery rates were achieved but also much less membrane area was required for both mixtures. The maximum recovery obtained was 95% and 83% for Mixture (1) and Mixture (2), respectively. The last part of the second step also showed the possibility of increasing the recovery by partial recycling of the product stream.

As a final step, we explored process optimization to economically recover the diluted H_2 while applying recovery and flammability constraints. This optimization problem was formulated in a NLP model and GAMS was used to resolve and obtain the results with an objective function of minimizing the PV. Both mixtures showed high specific separation costs with a limited recovery and purity. Beyond these minimum values, the cost increases dramatically. For instance, a 92% recovery and 92.5% purity is possible for Mixture (1), but the specific recovery cost is \$8.20/kg. For Mixture (2), 90% recovery and 95% purity was achievable with a specific recovery cost of \$6.15/kg. Comparing these two mixtures at this step showed a reduction of 25% in the recovery cost when the feed is switched from 4 mol% H_2 to 6 mol%. In a final effort to reduce costs, we explored the benefits of using a higher performance experimental polymer for the membrane. The results showed lower separation costs in general, but with a high recycle rate. It was concluded that while high H_2/O_2 and H_2/N_2 selectivities are attractive, a lower O_2/N_2 selectivity is needed to minimize the flammability of the permeate.

3.7 Appendix

3.7.1 Development of T_{real} equations (Eq.3.23 to 3.26)

As stated in the Section 3.5.1.2, the equations to calculate the T_{real} for both compressors and vacuum pumps can be simplified to reduce the computational time and efforts. Combaining Eq.3.21 and Eq.3.22 and solving for T_{real} leads to:

$$T_{real} = T_{in} + \frac{T_{in}}{\epsilon}\left[\left(\frac{P_{out}}{P_{in}}\right)^{\frac{\kappa-1}{\kappa}} - 1\right] \tag{3.35}$$

This new equation will be applied for the four cases we have, which are the T_{real} for

compressors and vacuum pumps for UBE® and TPIM-1.

for UBE® compressors:

- The known values are:

  T_{in}= 333.15 K, $\epsilon = 0.8$, P_{in}= 1 bar, $\kappa = 1.4$

- After inserting known values, Eq. 3.35 will become:

  $T_{real,Comp} = 416.4(P_{out,Comp})^{0.286} - 83.3$

- This equation will be linearized using the following formula:

  $T_{real,Comp} = X(P_{out,Comp}) + T_{in}$

- The intersection must be equal to the process temperature (in this case it is for UBE® = 60°C) and the value of X will be modified to fit the curve.

- The original equation and the fitted one are plotted and R2 is calculated.

- This fitting is valid between $2.5 \leq P_{out,Comp} \leq 4.5$ bar which is within the operating range of the optimization (see Figure 3.27).

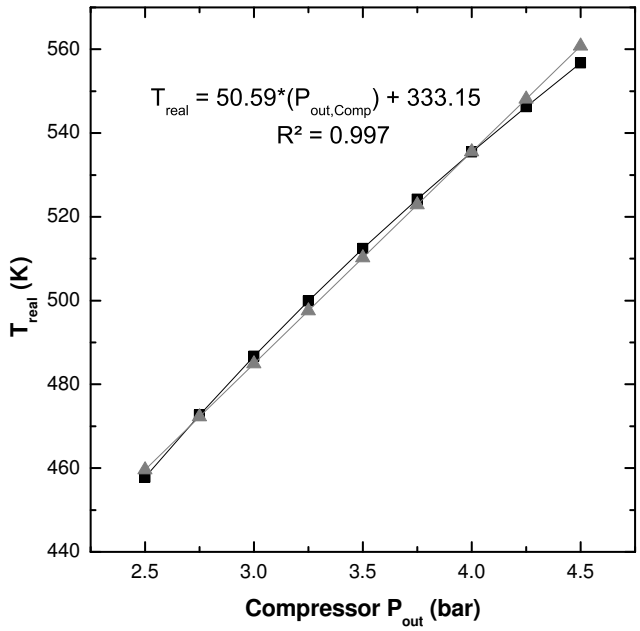

Figure 3.27: Linearized equation calculating T_{real} as a function of P_{out} for UBE® compressor.

for UBE® vacuum pumps:

- The known values are:

  T_{in}= 333.15 K, $\epsilon = 0.5$, P_{out}= 1 bar, $\kappa = 1.4$

- After inserting known values, Eq. 3.35 will become:

  $T_{real,Vac} = 666.3(P_{in,Vac})^{-0.286} - 333.15$

- This equation will be fitted using the following formula:

  $T_{real,Vac} = T_{in}(P_{in,Vac})^{X}$

- The intersection must be equal to the process temperature (in this case it is for UBE® = 60°C) and the value of X will be modified to fit the curve.
- The original equation and the fitted one are plotted and R2 is calculated.
- This fitting is valid between $0.05 \leq P_{in,Vac} \leq 1.0$ bar which is within the operating range of the optimization (see Figure 3.28).

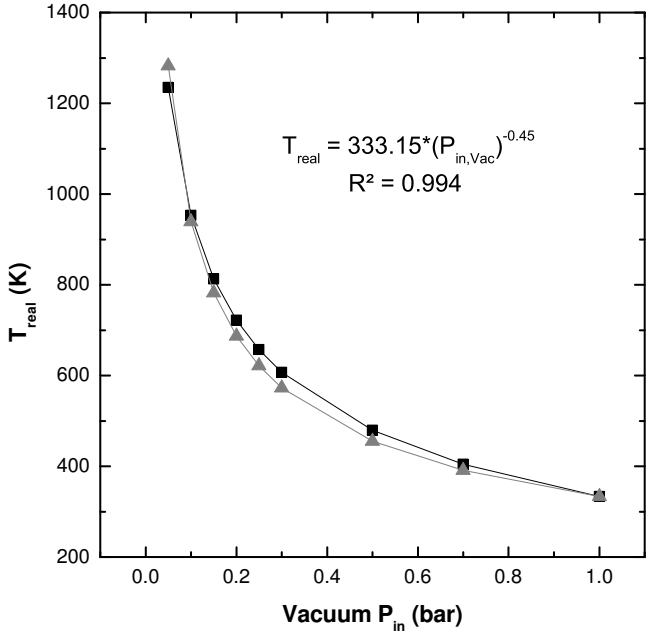

Figure 3.28: Exponential equation calculating T_{real} as a function of P_{in} for UBE® vacuum pump.

for TPIM-1 compressors:

- Same procedures were followed as in UBE® compressors but with $T_{in} = 308.15K$
- This fitting is valid between $2.5 \leq P_{out,Comp} \leq 4.5$ bar which is within the operating range of the optimization (see Figure 3.29).

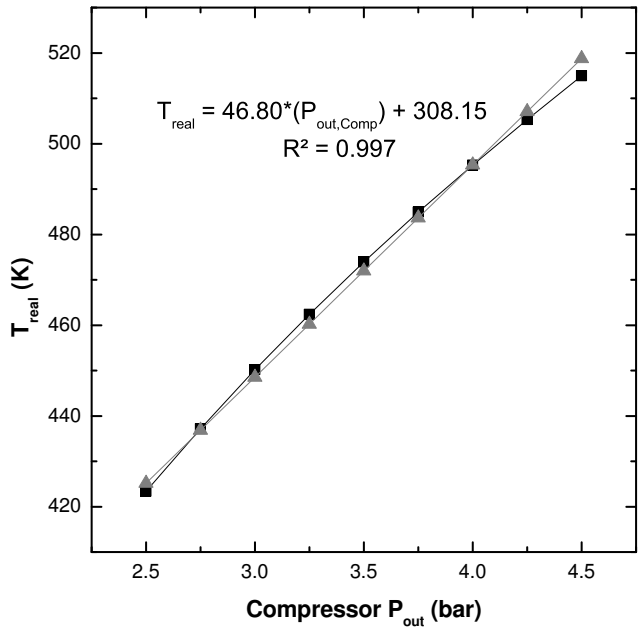

Figure 3.29: Linearized equation calculating T_{real} as a function of P_{out} for TPIM-1 compressor.

for TPIM-1 vacuum pump:

- Same procedures were followed as in UBE® vacuum pumps but with $T_{in} = 308.15K$
- This fitting is valid between $0.05 \leq P_{in,Vac} \leq 1.0$ bar (see Figure 3.30).

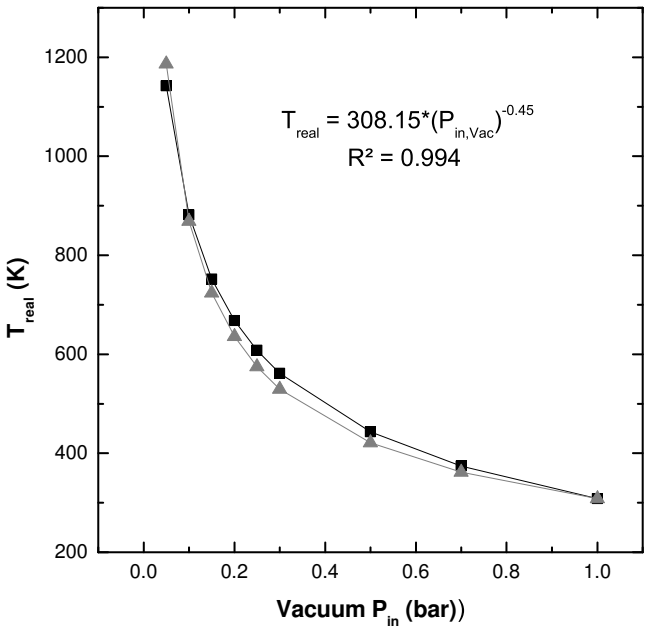

Figure 3.30: Exponential equation for T_{real} as a function of P_{in} for TPIM-1 vacuum pump.

3.7.2 Higher membrane price for TPIM-1 investigation

Table 3.12: Detailed results for the influence of higher membrane price for TPIM-1 on the process economic.

		TPIM-1 (110€/m^2)			TPIM-1 (165€/m^2)		
	Recovery (%)	H_2 Purity (%)	Recycle (%)	Specific Cost ($/kg)	H_2 Purity (%)	Recycle (%)	Specific Cost ($/kg)
Mixture (1)	90.0	91.2	49.0	4.93	91.5	46.0	5.23
	92.5	91.3	51.0	5.00	93.5	49.0	5.47
	95.0	91.4	55.0	5.15	93.5	53.0	5.65
Mixture (2)	90.0	94.6	52.0	3.94	94.6	50.0	4.10
	92.5	94.6	54.0	4.06	94.6	53.0	4.21
	95.0	95.7	58.0	4.33	94.6	57.0	4.40

CHAPTER 4

H_2 Recovery using CO_2 Diluent

This chapter has been published:
S. Alsayegh, J. Johnson, X. Wei, B. Ohs, J. Lohaus, M. Wessling *CO_2 aided H_2 recovery from water splitting processes*, International Journal of Hydrogen Energy (2017), DOI: 10.1016/j.ijhydene.2017.07.023

4.1 Introduction

In the previous chapter, we investigated the use of N_2 as an inert due to of its availability and lower cost compared to other diluents. The results showed a very high specific cost for the separation process due to high feed flow rates containing highly diluted H_2. The flammability range of H_2 in O_2 or air mixture is very wide and the operational area is narrow, which makes the design of the separation process more difficult, risky and costly. Utilizing CO_2 as suppressant for H_2 flammability proves to be more effective than N_2 [138–140]. Due to its higher heat capacity, the laminar burning velocity is decreased and the flammability range is reduced; allowing for greater operational area in the flammability diagrams. The extinction effects of CO_2 occur at a value greater than 73%mol [122, 139]. Using this value along with the Lower Flammability Limits (LFL) and the Upper Flammability Limits (UFL) of H_2, we can construct the theoretical flammability diagrams of a $H_2/O_2/CO_2$ mixture as shown in Figure 4.1. This will enable processing increased H_2 content in the feed, which in turn decreases the total feed flow rate and provides a higher driving force for H_2 separation.

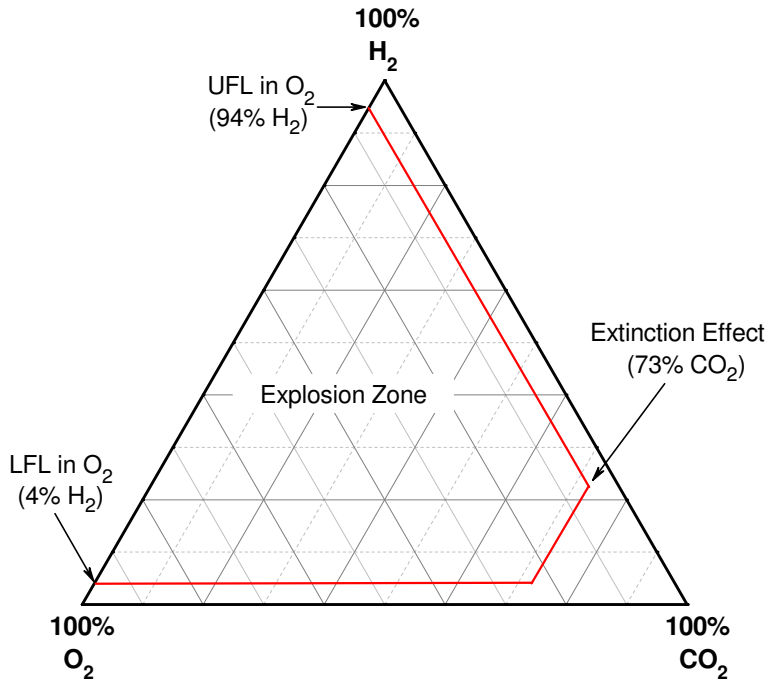

Figure 4.1: H_2 flammability diagram in $H_2/O_2/CO_2$ mixture under normal operating conditions.

In this chapter, we investigate the application of composite polymer membrane commercially available from Membrane Technology and Research, Inc. (MTR) to recover H_2 from a water splitting process aided by CO_2 as a flammability suppressant. Both H_2-selective (Proteus^{TM}) and CO_2-selective (Polaris^{TM}) spiral wound membranes are utilized in this investigation. The process designs maintain the flammability constraints on all streams in order to insure safe operating conditions. Based on the expected flammability envelope for this ternary mixture, we have chosen the molar composition for the feed stream shown

Table 4.1: Feed compositions for the investigated process.

Gas	Concentration
Carbon Dioxide (CO_2)	76%mol
Hydrogen (H_2)	16%mol
Oxygen (O_2)	8%mol

in Table 4.1. The design problem is formulated as a nonlinear programming (NLP) to minimize the objective function, which is the Present Value (PV) of all outgoing cash flows (no income) of the separation process. The selected decision variables, namely: recycle rates, feed / permeate pressures and membrane areas, will be manipulated to achieve the results. The results will be compared to previous chapter in order to show the advantages of using CO_2 as a diluent. We conclude the study with a comparative cost analysis between the operation of spiral wound and hollow fiber membrane architectures. Hypothetical hollow fibers based on the MTR materials were used in this investigation. Figure 4.2 shows a graphical abstract for the process.

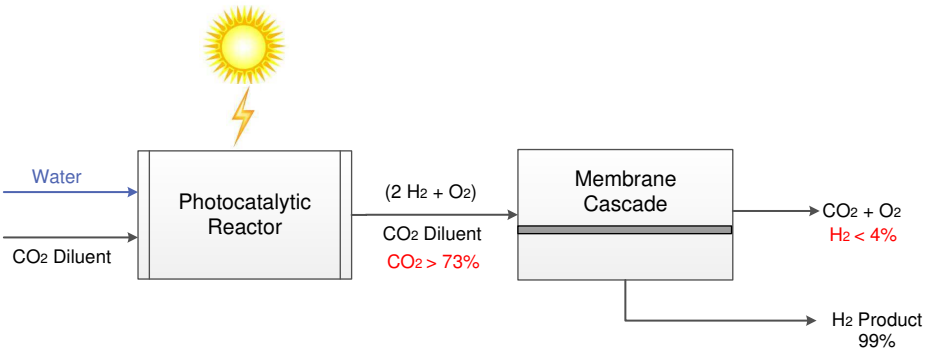

Figure 4.2: Graphical abstract for the investigated process.

4.2 Optimization Approach

General Algebraic Modeling System (GAMS) was utilized to solve the NLP model for the investigated process. A global optimizer is needed to guarantee the optimum solution for the objective function. The Branch-AND-Reduce Optimization Navigator (BARON) was chosen for this task. This computational system implement a special type of branch-and-bound algorithm to improve the performance and reduce the computational time required [141, 142]. Table 4.2 shows the full description of optimization equations for the investigated process.

Table 4.2: NLP model for $H_2/O_2/CO_2$ separation process.

Equation	Definition	Values
Objective function: f(x)	PV of all outgoing cash flows (no income) including: investment cost, operating cost, loss of product and depreciation for 15 years.	minimize
Constraints g(x)$\geqslant$0	Sets of linear and nonlinear process constraints including:	
	- H_2 recovery	$\geqslant$70%
	- H_2 purity	$\geqslant$99%
	- O_2 limits in permeates	$\leqslant$5.0%
	- H_2 limits in retentates	$\leqslant$4.0%
	- Max. streams pressure (absolute)	$\leqslant$30 bar
	- Min. permeate pressure (absolute)	$\geqslant$0.3 bar
	- Max. trans-membrane pressure [91]	$\leqslant$12 bar
Model equations:h(x)=0	Sets of the equipment equations required to calculate the performance and economics	-

4.2.1 Process Model

Contrary to the N_2 diluent study, three membrane units are needed to achieve desired product purity of 99%. In general, the H_2/CO_2 selectivity for most polymeric membrane materials is much lower when compared to H_2/N_2 selectivity. This can be explained by the high diffusivity of H_2 and the high solubility of CO_2. As mentioned before, both Proteus^{TM} and Polaris^{TM} membranes will be utilized within the membrane unit. Figure 4.3 shows the three different layouts that were explored in this study.

The first unit of all three layouts is the H_2-selective membrane. Also, compressors. vacuum pumps and heat exchangers are used between the membrane units in order to match the requisite operational parameters for the respective membrane systems.

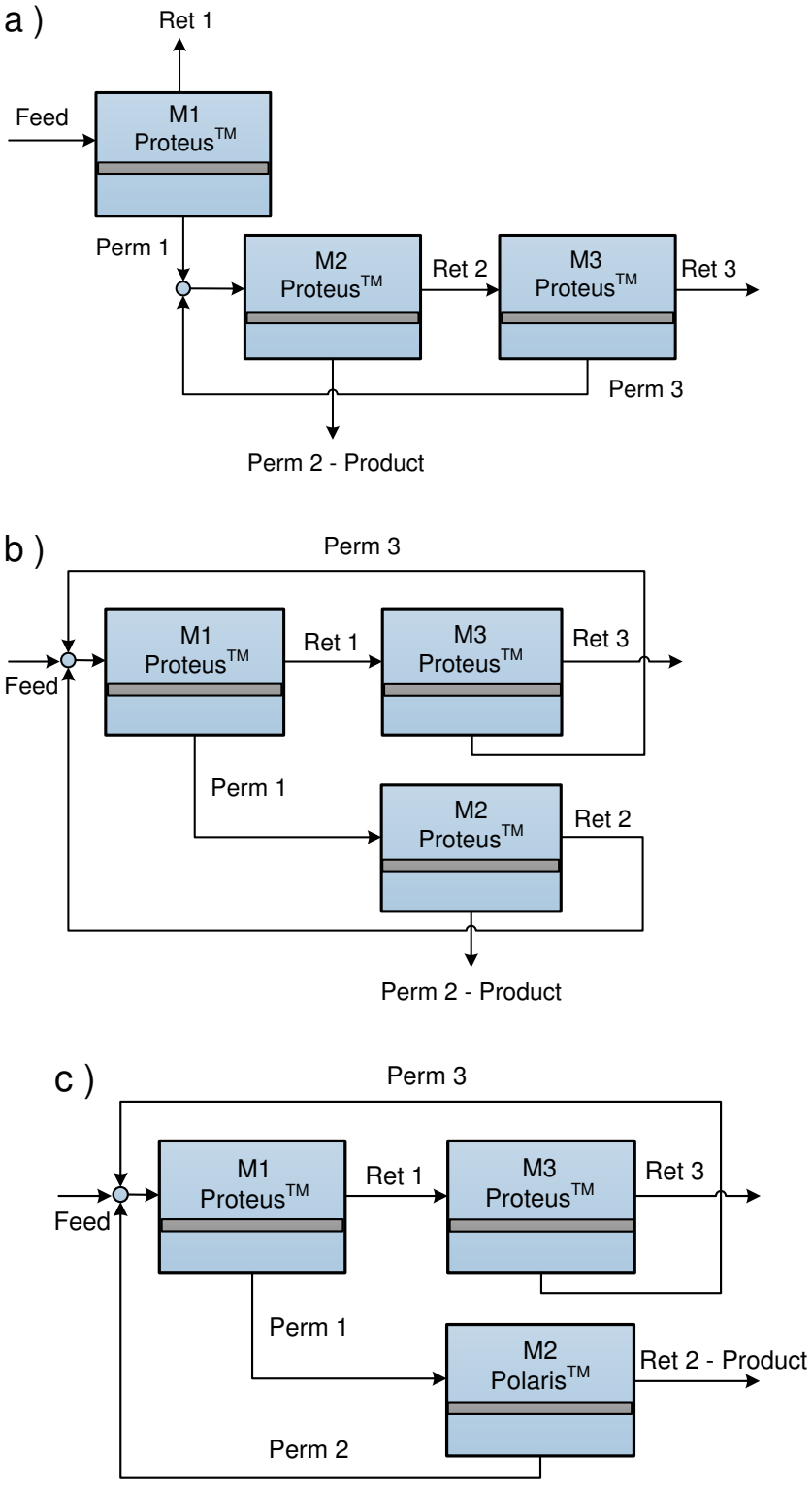

Figure 4.3: Three layouts for the investigated process.

4.2.2 Unit Operations

Membrane Module

A simple membrane short-cut model for both configuration (spiral wound and hollow fiber) was utilized for this investigation with the following assumptions:

- The system is in steady state
- No temperature and pressure drop along and across the membrane
- No interactions between the components were considered (no flux coupling)
- Constant selectivity and permeability along the membrane
- Concentration polarization is negligible
- Spiral wound configuration is considered as cross flow with unhindered permeate withdrawal with 10 elements of discretization (Figure 4.4)
- Hollow fiber configuration is considered as counter-current flow with 10 elements of discretization (Figure 3.19)

The numbers of discretized elements (j) were chosen to balance the outcome precision and computational time. Meanwhile, the following sets of equations are used to describe the transport through each element for every species (i) for the spiral wound configuration [134]:

$$\dot{n}_{R,i,j} = \dot{n}_{i,j} + \dot{n}_{R,i,j+1} \tag{4.1}$$

$$\dot{n}_{P,i} = \sum_0^j \dot{n}_{i,j} \tag{4.2}$$

$$\dot{n}_{i,j} = Q_i \cdot (x_{i,j} \cdot p_f - y_i \cdot p_P) \cdot A_m \tag{4.3}$$

$$x_{i,j} = \frac{\dot{n}_{R,i,j}}{\sum_i \dot{n}_{R,i,j}} \tag{4.4}$$

$$y_i = \frac{\dot{n}_{P,i}}{\sum_i \dot{n}_{P,i}} \tag{4.5}$$

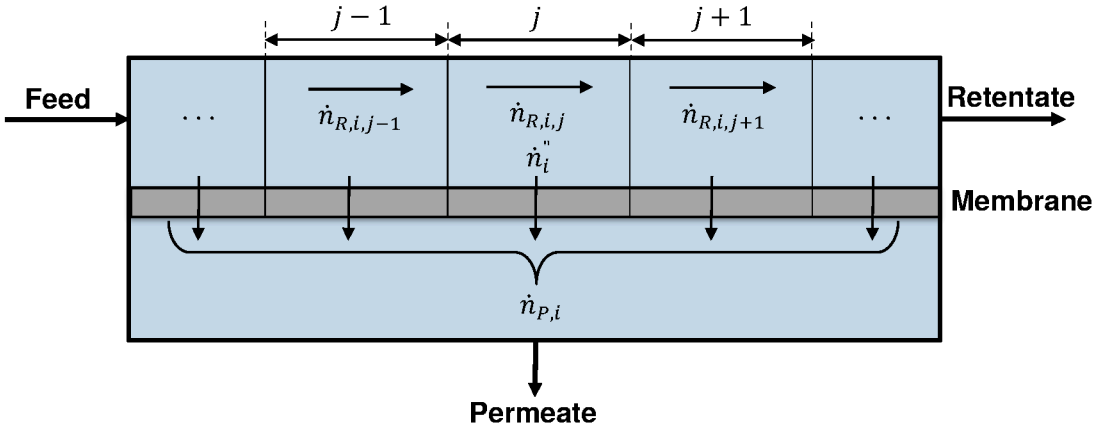

Figure 4.4: Illustration of the spiral wound membrane model used.

The same equations in Section 3.5.1.2 where utilized to describe the hollow fiber configurations. Table 2.4 shows the permeation data for the selected membrane materials. Permeabilities were measured at 150°C for Proteus^{TM} and 30°C for Polaris^{TM}. For the sake of direct comparison, these values are used in both spiral wound and hollow fiber membrane configurations.

Other process units

All three process layouts shown in Figure 4.3 include necessary compressors, vacuum pumps and heat exchangers. Details of these process units were discussed in detail in Chapter 3. When compared to the N_2 diluent investigated process, this separation system is more complex and required additional computational efforts due to the implementation of a three-stage membrane cascade with two different materials. Consequently, most of the equations used to calculated unit performance have been linearized. Detailed information about the development of these equations can be found in Appendix 4.5.

4.2.3 Economics

In order to represent the advantages of using a CO_2 diluent system over N_2, we applied the same economical basis (Section 3.5.1.3) to calculate the Present Value (PV) in this work. For MTR membranes, a price of \$500/m^2 was used for the cost of a complete, installed skid for both materials. The annual cost for replacing the membrane modules is estimated at \$100/m^2 [85, 91]. As in the previous chapter, capital costs (CC) of the auxiliary equipment can be estimated using Guthrie's method. Table 4.3 shows the process parameters for all equipment used in this chapter, while the corresponding economic parameters are the same as in Table 3.8.

Table 4.3: Process parameters for $H_2/O_2/CO_2$ separation process.

Parameter	Value	Unit
H_2 feed flow rate	100.0	kmol/hr
ϵ_{Comp}	0.80	-
ϵ_{Vac}	0.50	-
κ	1.35	-
T_{Feed}	318.15	K
T_{in}	303.15	K
$T_{in,Proteus}$	423.15	K
$T_{in,Polaris}$	303.15	K
$P_{out,Vac}$	1.0	bar
U_{Comp} (high pressure) [133]	220.00	W/m^2.K
U_{Vac} (ambient pressure) [133]	100.00	W/m^2.K
$T_{water,in}$	298.15	K
$T_{water,out}$	308.15	K

4.3 Results

Optimization calculations were set to achieve a minimum of 99% purity of the H_2 product while maintaining a recovery rate of at least 70%. For each process configuration, an optimal recovery rate exists which represents a balance between operation costs and product loss. The primary focus of this study was built around an MTR membrane in the spiral wound form.

4.3.1 Optimal Process Layout

The first set of results for the three layouts, as determined through our optimization calculations, are shown in Table 4.4. It is clear that when the flammability limits are applied to the process, the specific cost of the separation process increases. The increased costs varies between the three process layouts; there is 27% increase for layout (c). The violation of the flammability limits occurred in the retentate stream of the first membrane unit (Ret 1) for both layout (b) and (c). This can be explained by the recycling of two streams with different molar concentration than the feed which alters the flammability limitation of the mixed stream, from CO_2 extinction effect ($\geqslant$73%) to O_2 limits ($\leqslant$5%).

In terms of performance with flammability limits, process layout (a) shows the lowest specific cost of \$5.97/kg, but with a relatively low recovery rate of 73.7%. Even though layout (c) shows the highest recovery rate, the specific cost and O_2 concentration in the product are the highest among the three layouts. Moreover, despite having the final product stream in layout (c) at high pressure, the cost of pressurizing the recycle stream is greater than the product stream as the flow rate of the recycle stream is usually higher. A complete flow diagram with corresponding operational values is provided in Figure 4.5 for each process design.

Table 4.4: Optimization results for the investigated process layouts with and without flammability limits.

Parameter	Layout (a)		Layout (b)		Layout (c)	
	with limits	without limits	with limits	without limits	with limits	without limits
Specific cost (\$/kg)	5.97	5.97	6.49	6.24	7.64	5.99
Recovery (%)	73.7	73.7	86.1	86.4	86.9	89.7
Product H_2 (%)	99.0	99.0	99.0	99.0	99.0	99.0
Product O_2 (%)	81 ppm	81 ppm	80 ppm	80 ppm	0.3	1.0
Violation	-	-	-	Ret1 at 5.7% O_2	-	Ret1 at 7.6% O_2

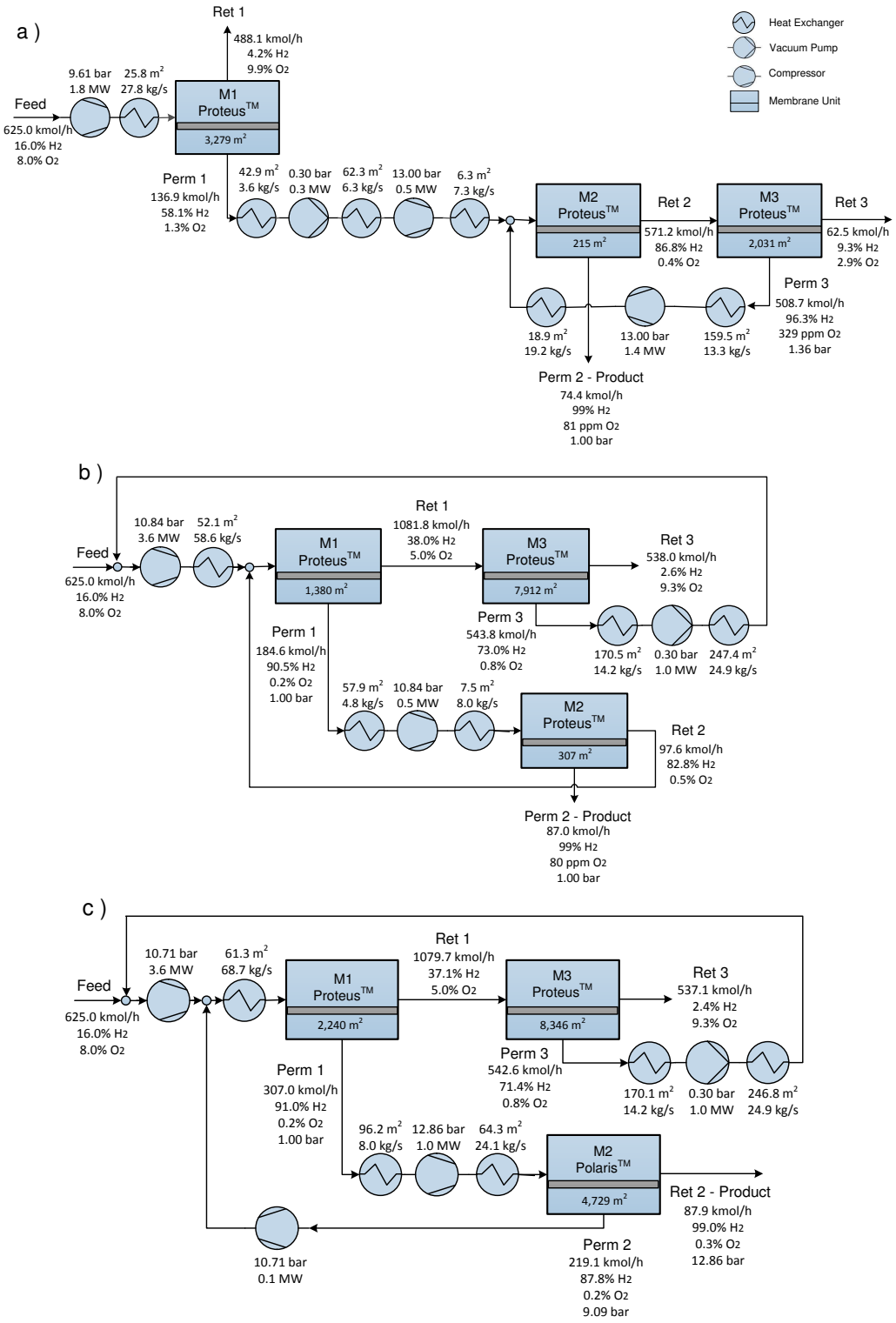

Figure 4.5: Optimization results for the three process layouts with flammability limits (Stream pressures are in bara).

Analyzing the capital cost and the operational cost of these layouts shows that a majority of the cost is derived from the pressure equipment, which accounts for more than 70% of the capital cost and 65% of the operational cost. A breakdown of the CC and OC for the corresponding process units is provided in Table 4.5. Furthermore, there is an increase in the total membrane area required for both layout (b) and (c), which affect both CC and OC. This increase is associated with the utilization of two recycle streams in these two layouts. Layout (c) has even higher membrane costs due to the particularly large recycle stream (20% higher comparatively). This excessive recycle flows are mandatory to satisfy the product purity and flammability constraints and also to compensate for the low selectivity of Polaris^{TM} compared to Proteus^{TM} membranes.

Table 4.5: Capital and operating cost of the investigated process layouts.

	Layout (a)	Layout (b)	Layout (c)
Capital Cost (CC)			
Compressors	71.2%	57.4%	55.7%
Vacuum pumps	7.5%	18.9%	15.7%
Membranes	13.5%	17.7%	23.5%
Heat exchangers	7.8%	6.0%	5.1%
Total	\$20.52 MM	\$27.06 MM	\$32.65 MM
Operating Cost (OC)			
Energy	65.7%	70.8%	66.3%
Membrane replacement	11.7%	16.3%	22.1%
Loss of product	18.2%	7.7%	6.1%
Utility	4.4%	5.2%	5.5%
Total	\$4.73 MM/year	\$5.89 MM/year	\$6.94 MM/year
Specific Cost	\$5.97/kg	\$6.49/kg	\$7.64/kg

Analyzing the recovery profiles of the three layouts provide further insight on how the system behaves with respect to the decision variables that are optimized in order to satisfy the product constraints. Four different profiles are illustrated in Figure 4.6 for specific costs, total membrane area, energy consumption and recycle flow rates. Figure 4.6a shows that layout (a) has better performance and lower specific costs over the whole range of the recovery rate specially at a recovery rate lower than 82.5%. This process layout shows a drastic increase in recycle flow rate above this recovery rate (Figure 4.6b), which reflects the increase in the membrane area required (Figure 4.6c) and the specific cost. The energy consumption profiles demonstrate normal increase with the recovery value as shown in Figure 4.6d. Between 85% and 90% recovery rates, both layouts (a) and (b) are very comparable in terms of cost and energy consumption. Finally, both layouts (b) and (c) exhibit similar behaviors in all profiles with layout (b) showing lower values and cost.

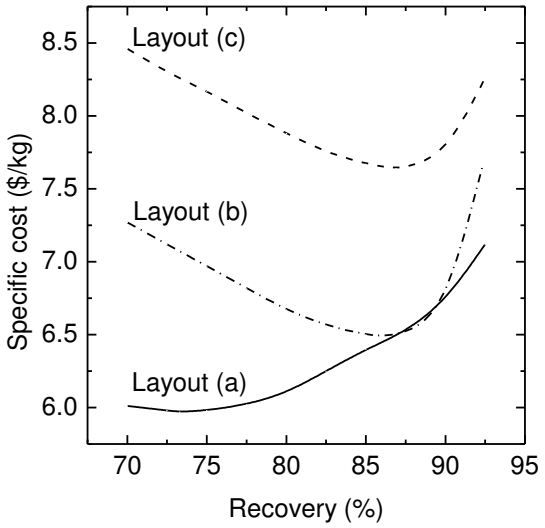

(a) Specific cost recovery profile

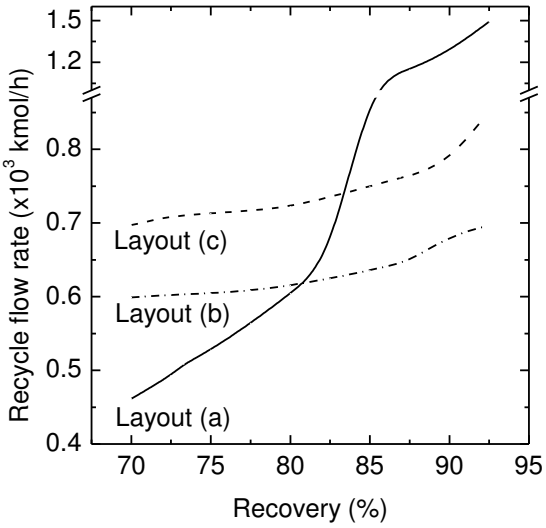

(b) Recycle flow rate recovery profile

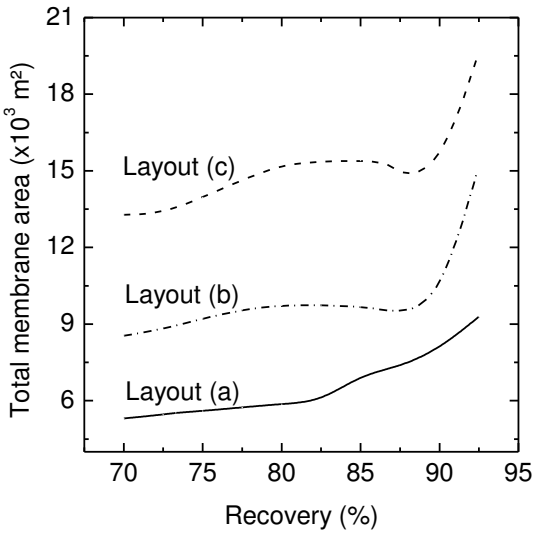

(c) Total membrane area recovery profile

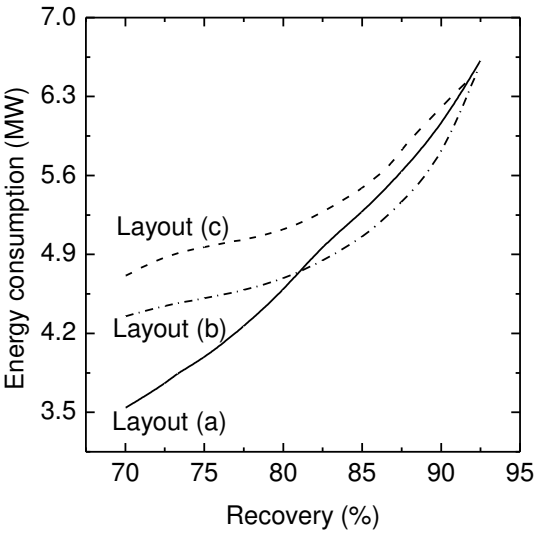

(d) Energy consumption recovery profile

Figure 4.6: Recovery profiles for the investigated process layouts.

Comparing these results with our previous N_2 diluent study, the following remarks can be highlighted:

- A more complex process design is needed to recover H_2 from the CO_2 diluent due to lower H_2/CO_2 selectivity compared to H_2/N_2 selectivity.
- Higher purity product with lower specific cost can be achieved with a CO_2 diluent system but with slight decrease in recovery rate.
- Lower O_2 concentration in the product streams are achievable for the CO_2 diluent system.
- Table 4.6 shows the optimal results obtained from both systems at 85% recovery rate with 99% purity. Using a CO_2 diluent will decrease the specific cost by 50% comparatively with less O_2 impurity.

Table 4.6: Optimal results obtained from CO_2 and N_2 diluent systems.

Parameters	N_2 diluent system Mixture (2)	CO_2 diluent system Layout (a)
Specific Cost ($/kg)	12.88	6.40
Recovery (%)	85.0	85.0
Product H_2 (%)	99.0	99.0
Product O_2 (%)	0.4	0.1

4.3.2 Spiral Wound and Hollow Fiber Configurations

Membrane configuration and flow pattern play major roles in the membrane separation performance. Hollow fiber membrane modules with counter-current flow have the advantages of lower production cost due to the high packing density (membrane area / module volume). However, hollow fibers can suffer from performance obstacles, such as permeate pressure drop, flow distribution and concentration polarization [80, 143, 144]. Regardless, it is interesting to examine the results of our study and compare the two membrane architectures in terms of their theoretical performance without considering their respective industrial limitations.

Assuming the same membrane performance metrics (Table 2.4) for the hollow fiber configuration along with the assumptions listed in Section 4.2.2, the recovery profiles for layouts (a) and (b) were calculated. A comparison of recovery profiles is provided in Figure 4.7.

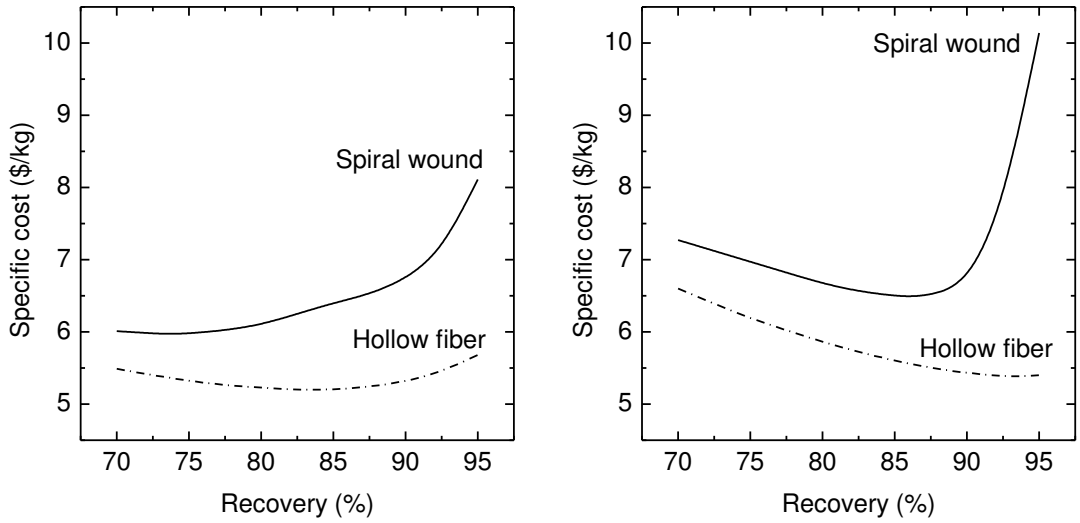

(a) Layout (a) (b) Layout (b)

Figure 4.7: Recovery profiles for spiral wound and hollow fiber membrane configurations.

For both layouts, it is obvious that hollow fibers have significantly improved cost performance and optimum recovery rate. The product purity and recovery can be achieved using lower pressure values for the membrane feed, which reflect the reduction in the specific costs. As we highlighted in Table 4.5, pressure equipment/operation accounts for a significant portion of the overall CC and OC. Figure 4.8 shows the local driving force (the partial pressure difference between feed and permeate) in the first membrane unit in layout (a), which is required to achieve the same results (85% product recovery and 99% purity). In general, layout (a) shows lower specific cost than layout (b) over the entire recovery range. Techno-economic analyses comparing spiral wound versus hollow fiber membranes wherein 85% product recovery and 99% purity are achieved is provided in Table 4.7. From these values we can achieve a reduction of 18% and 13% in specific costs for layouts (a) and (b), respectively.

Table 4.7: Optimization results for the layout (a) and (b) for hollow fiber and spiral wound configurations at 85% recovery and 99% purity.

Parameter	Layout (a)		Layout (b)	
	spiral wound	hollow fiber	spiral wound	hollow fiber
Specific cost ($/kg)	6.40	5.20	6.50	5.60
Energy consumption (MW)	5.27	3.85	5.05	4.01

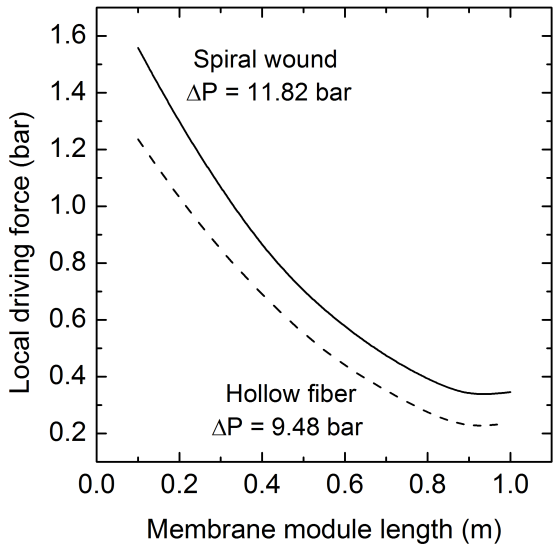

Figure 4.8: Localized driving force for first membrane unit in layout (a) for spiral wound and hollow fiber configurations (85% product recovery and 99% purity).

4.4 Conclusion

In this investigation, we showed the advantages of using CO_2 as a flammability suppressant over N_2 where the thermodynamic nature of CO_2 permits higher H_2 contents in the original feed. The study listed all flammability constraints, essential assumptions and modelling equations to ensure accurate results. We explored process optimization to economically recover the diluted H_2 and achieve 99% product purity. This optimization problem was formulated in a NLP model and GAMS was used to resolve and obtain the results with an objective function of minimizing the PV.

In order to design the separation process, two membrane materials from MTR were selected to design three process layouts. The optimum layout was comprised of three H_2-selective membrane units and a single recycle stream, which consequently proved to be the optimum layout over the whole range of the recovery profile. Layout (b), which comprised of the H_2-selective membrane with two recycle streams. A second configuration with H_2-selective membranes and two recycle streams showed comparable performance when 85-90% recovery was achieved. Our third configuration, which used both H_2- and CO_2-selective membranes, was the least favourable solution due to the exceptionally high recycle flow rates. Overall, layout (a) showed the best economic at 85% recovery rate with 99% product purity at a cost of \$6.40/kg. Unfortunately this value is higher than the assumed production cost of H_2 (\$2/kg). We further compared our results with the previous chapter based on a N_2 diluent system. Using CO_2 as a diluent yields higher purities, lower separation costs, and reduced O_2 content in the product stream.

We concluded this study with a comparison between the commercially available MTR spiral wound membrane and a hypothetical hollow fiber module with matching permeability

performance. Lower specific costs were obtained for all process layouts and recovery ranges for the hollow fiber configuration due to its enhanced separation performance in this process over spiral wound.

4.5 Appendix

The development of the T_{real} equations follows the same procedures that we utilize in the previous chapter (Section 3.7). However, both compressors and vacuum pumps pressure ranges are different as indicated in Table 4.2. The final equation for T_{real} is:

$$T_{real} = T_{in} + \frac{T_{in}}{\epsilon}\left[(\frac{P_{out}}{P_{in}})^{\frac{\kappa-1}{\kappa}} - 1\right] \tag{4.6}$$

This equation is applied for the Feed Compressor, Permeate Vacuum Pump, Mid/Recycle Compressors (high and low Pressure ratio).

Feed Compressor:

- The known values are: T_{in}= 318.15 K, $\epsilon = 0.8$, P_{in}= 1 bar, $\kappa = 1.35$
- After inserting known values, Eq. 4.6 will become:

  $T_{real,Comp} = 397.7(P_{out,Comp})^{0.259} - 79.5$
- The original equation was plotted between the range $4.0 \leq P_{out,Comp} \leq 13.5$ bar, which is within the operating range of the optimization
- The fitted linear equation was created and the corresponding value of R^2 was calculated. See Figure 4.9 for fitted trend and representative equation.

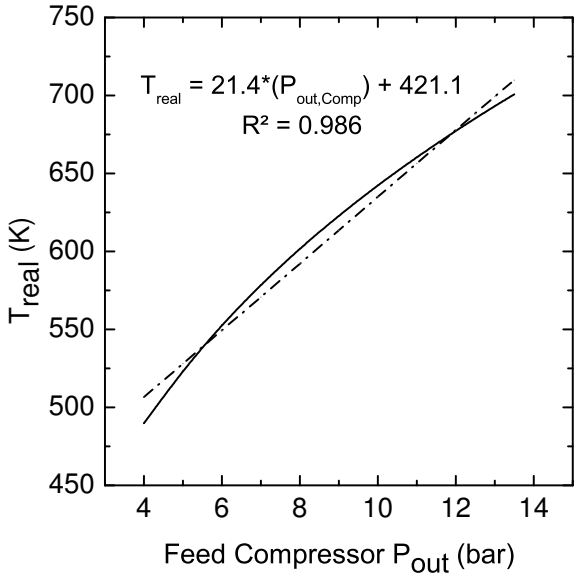

Figure 4.9: Linearized equation calculating T_{real} as a function of P_{out} for the feed compressor.

Permeate Vacuum Pump:

- The known values are: T_{in}= 303.15 K, $\epsilon = 0.5$, P_{out}= 1 bar, $\kappa = 1.35$
- After inserting known values, Eq. 4.6 will become:

  $T_{real,Vac} = 606.3(P_{in,Vac})^{-0.259} - 303.15$
- The original equation was plotted between the range $0.3 \leq P_{in,Vac} \leq 0.7$ bar, which is within the operating range of the optimization
- The fitted linear equation was created and the corresponding value of R^2 was calculated. See Figure 4.10 for fitted trend and representative equation.

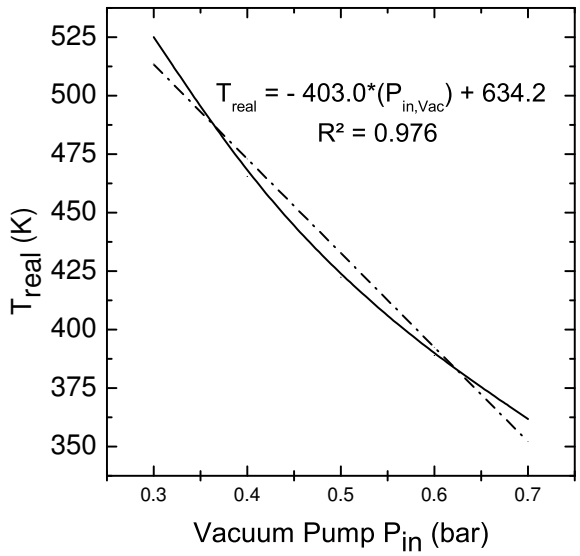

Figure 4.10: Linearized equation calculating T_{real} as a function of P_{in} for vacuum pump.

Mid/Recycle Compressor (High-Pressure Ratio):

- The known values are: T_{in}= 303.15 K, $\epsilon = 0.8$, $\kappa = 1.35$
- After inserting known values, Eq. 4.6 will become:

  $T_{real,Comp} = 378.9(\frac{P_{out}}{P_{in}})^{0.259} - 75.8$
- The original equation was plotted between the range $4.0 \leq P_{out,Comp} \leq 13.5$ bar, which is within the operating range of the optimization
- The fitted linear equation was created and the corresponding value of R^2 was calculated. See Figure 4.11 for fitted trend and representative equation.

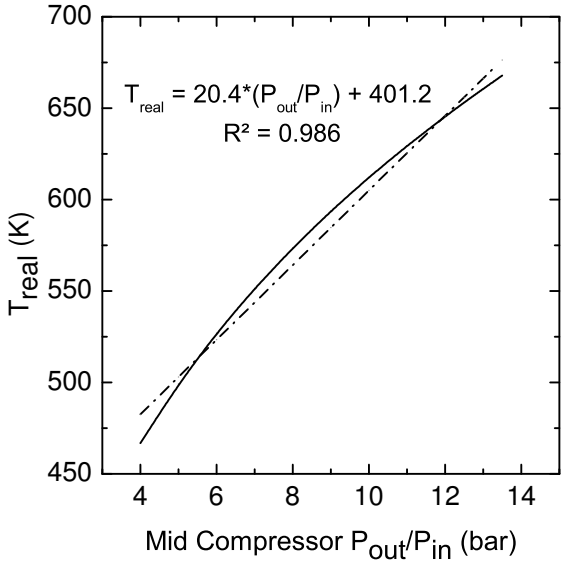

Figure 4.11: Linearized equation calculating T_{real} as a function of $(\frac{P_{out}}{P_{in}})$ for compressor (high-pressure ratio.

Mid/Recycle Compressor (Low-Pressure Ratio):

- The known values are: T_{in}= 303.15 K, $\epsilon = 0.8$, $\kappa = 1.35$
- After inserting known values, Eq. 4.6 will become: $T_{real,Comp} = 378.9(\frac{P_{out}}{P_{in}})^{0.259} - 75.8$
- The original equation was plotted between the range $1.0 \leq P_{out,Comp} \leq 2.8$ bar.
- The fitted linear equation was created and the corresponding value of R^2 was calculated. See Figure 4.12 for fitted trend and representative equation.

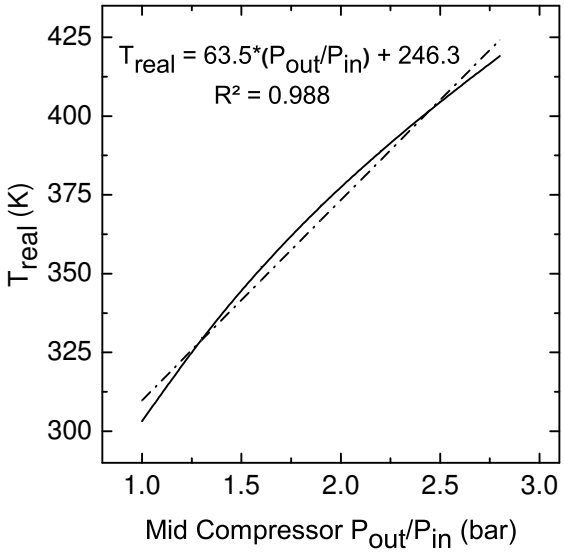

Figure 4.12: Linearized equation calculating T_{real} as a function of $(\frac{P_{out}}{P_{in}})$ for compressor (low-pressure ratio.

CHAPTER 5

Methanol Production from Water Splitting Process

This chapter has been submitted:
S. Alsayegh, J. Johnson, B. Ohs, M. Wessling *Methanol production via direct carbon dioxide hydrogenation using hydrogen from photocatalytic water splitting: process development and techno-economic analysis*, Journal of Cleaner Production (2018).

5.1 Introduction

As highlighted in Chapter 1, the global increase in energy demand will lead to higher CO_2 emission via additional consumption of fossil fuels to satisfy this demand. One approach to mitigate this problem is to utilize Carbon dioxide Capture and Reuse (CCR) processes for fuels and value-added chemical production (e.g. methanol production), which can partially close the carbon cycle in the atmosphere [116, 145]. Besides the reduction of CO_2 emissions, this approach would also generate economic benefits and positive social-political images [107].

Building upon the CO_2 utilization and renewable H_2 production from water splitting, we have identified an opportunity to utilize H_2 from water splitting coupled with CCR to create a novel process for methanol production as shown in Figure 5.1. Leveraging the flexibility of membrane separations, we have designed a process scheme that enables on-purpose production of the necessary ratio of CO_2 and H_2 that can be utilized in a conceptual CO_2 hydrogenation reactor. A CO_2 capture unit (Plant 1) will supply pure CO_2, as a raw material and diluent, to the photocatalytic reactor (Plant 2) which safely transfers the reaction products. The resulting ternary mixture is sent to a membrane separation plant (Plant 3) to recover both H_2 and CO_2 with a preferred stoichiometric ratio of 3:1 (H_2:CO_2). Residual CO_2 from Plant 3 is recovered to minimize costs and energetic footprint. The H_2/CO_2 mixture is compressed and fed to the methanol loop in Plant 4 (included product recovery units). To demonstrate the potential impact of this process, we focused on minimizing the Present Value (PV) of all outgoing cash flows of Plant 3 as this is the core innovation for the process. Stringent flammability constraints were applied during the optimization process to ensure safe operating conditions. Optimum or ideal case studies regarding Plants 1, 2, and 4 were extracted from the literature and were assimilated into the overall economic and energetic analyses. To the best of our knowledge, this is the first fundamental process design for methanol synthesis using H_2 from water splitting and captured CO_2 as both a diluent and a raw material.

5.2 Process description and economics

The process design aims to utilize a renewable source and method of H_2 production from photocatalytic water splitting (as estimated in the study of US DOE [27]) while mitigating the flammability risks inherent to the simultaneous production of H_2 and O_2. Moreover, the separation plant (Plant 3) is designed to recover H_2 with lower purities that what was designed in Chapter 4, which will result in a cost reduction for the proposed process, comparatively. These design elements are combined with ideal scenarios reported for the other plants in the overall process concept.

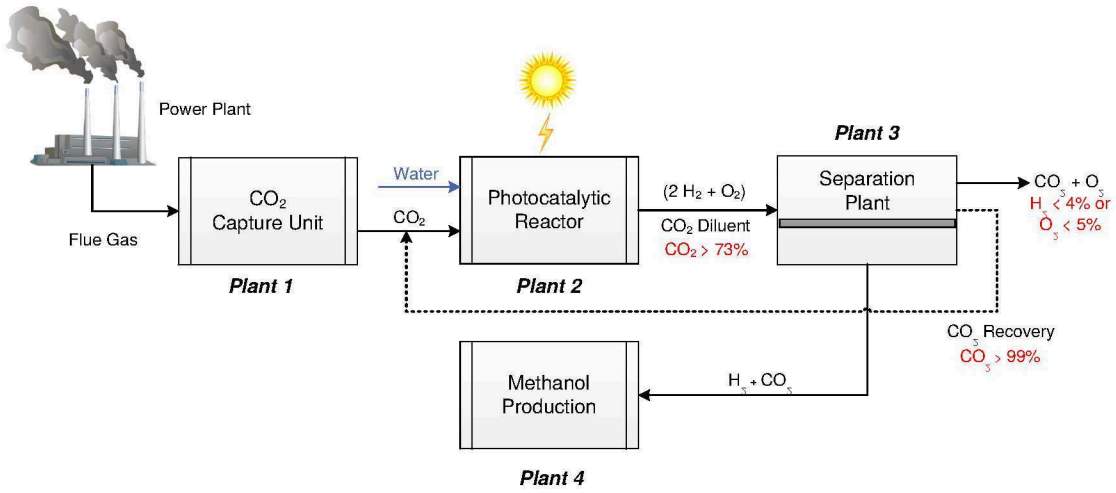

Figure 5.1: General layout of the proposed methanol synthesis from photocatalytic water splitting and captured CO_2.

The following general assumptions concerning the four plants were taken into consideration in this investigation:

- Each plant will be designed individually with no heat integration.
- The process will be designed based on a H_2 production rate of 1000 kmol/h from Plant 2.
- The cost of feed from Plants 1 and 2 will be treated as purchasing raw materials.
- A pure CO_2 stream will be supplied by Plant 1.
- In Plant 3, the targeted purity of CO_2 recovery is 99 mol%, which will be recycled back to Plant 2 with no additional treatment.
- Trace amounts of O_2 leaving Plant 3 will be converted to H_2O using a stoichiometric reactor (O_2 removal unit) in Plant 4. The minor cost of this unit will be neglected in this study.

In the following subsections, we will provide a brief description of Plants 1 and 2 along with the primary parameters used for both economic and energy analysis. The separation plant (Plant 3) will be based on the previous Chapter 4. However, new membrane layouts design along with updated economic parameters and constraints (for CO_2 recovery) will be implemented in the optimization problem. Finally, Plant 4 will be adopted from the work of Van-Dal and Bouallou [112] but with an alternate feed stream composition based on the surrogate raw materials sources. The process economics will be calculated using Guthrie's method [133, 135]. Moreover, sensitivity analysis on both economic and energy parameters of the process will be carried out, namely:

- CO_2 capture price ($\$/kg_{CO_2 produced}$)
- Electricity price ($\$/kWh$)

- Plant lifetime (yr)
- Energy requirement for CO_2 capture ($kWh/kg_{CO_2 processed}$)
- Solar-to-Hydrogen (STH) efficiency (%)

5.2.1 Plant 1: CO_2 capture

Both cost and energy consumption for CO_2 capture from power plants are strongly dependent on the fossil fuel type (e.g., oil, coal, natural gas, biomass) and the technology used to produce the electricity or heat [7]. Some examples of power plant technologies include: Supercritical Pulverized Coal (SCPC), Natural Gas Combined Cycle (NGCC), and Integrated Gasification Combined Cycle (IGCC) [146]. There are numerous proposed technologies for large scale CO_2 capture, such as: liquid amine-based absorption, solid-state adsorbents (pressure or thermal swing) [147], membranes [148], and hybrid concepts [149]. Amine based solvents, however, are the most prevalent and mature solution for CO_2 capture [150]. Carbon dioxide capture technologies are integrated within fossil fuel power plants via one of three primary designs [7, 146, 151, 152]:

- *Post-combustion Capture:* CO_2 is removed from the flue gas after complete combustion of fossil fuels with air. The low-pressure flue gas contains around 16 mol% of CO_2.
- *Pre-combustion Capture:* CO_2 is removed before the combustion of H_2, which is produced via steam reforming of the fossil fuel to produce syngas. The potential stream for CO_2 capture contains around 38 mol% CO_2 at elevated pressures ($\approx 30 bar$).
- *Oxyfuel Combustion:* Concentrated O_2 is utilized instead of air to burn the fossil fuel. Doing so removes the necessity to separate diluted CO_2 from N_2 [153]. A high-quality CO_2 stream is generated after removing water vapor.

For this investigation, the base case will use standard parameters to calculate the cost of CO_2 as a raw material along with energy consumption. These parameters and the respective values used in this chapter are provided in Table 5.1.

Table 5.1: Process and economic parameters for the proposed process

	Parameter	Value	Unit
	Base Case		
Process	CO_2 capture efficiency [2, 153]	90.0	%
Parameters	CO_2 energy requirement [2]	0.30	kWh/$kg_{CO_2 processed}$
	STH efficiency [27]	10.0	%
	Catalyst density[112]	1775	kg_{cat}/m^3_{cat}
	fixed bed porosity[112]	0.4	-
	Catalyst lifetime [154]	2	yr
	catalyst wt. to CO_2 feed	0.50	$kg_{cat}/(kg_{CO_2}/h)$
Economic	CO_2 capture price [2, 146]	0.035	\$/$kg_{CO_2 produced}$
Parameters	H_2 production price[27, 28]	0.65	\$/$kg_{H_2 produced}$
	Annual operating hours	8000	h
	Plant lifetime (T)	15	yr
	Interest rate (i)	9.0	%
	Currency exchange - 2016 [155]	1.1	€ to \$
	Electricity price - 2016 [137]	0.087	\$/kWh
	Water price [113]	0.033	\$/m^3
	Membrane price [85]	500.0	\$/m^2
	Membrane replacement [85]	100.0	\$/$m^2.yr$
	Update Factor*	4.75	-
	Catalyst price [156]	100.0	€/kg_{cat}
	Sensitivity Analysis		
Energy	CO_2 energy requirement	0.15-0.45	kWh/$kg_{CO_2 processed}$
Parameters	STH efficiency	5.0-15.0	%
Economic	CO_2 capture price [2, 146]	0.020-0.035	\$/$kg_{CO_2 produced}$
Parameters	Plant lifetime (T)	15-30	yr
	Electricity price	0.060-0.087	\$/kWh

** Chemical Engineering Plant Cost Index (Nov. 2016)*

5.2.2 Plant 2: Photocatalytic reactor

Photoelectrochemical water splitting is initiated when solar photons are absorbed by a semiconductor material. Hence, a transparent slurry reactor, made of high-density polyethylene (HDPE), is used to allow sun light to enter the reactor. The semiconductor nano-sized catalysts are suspended in a potassium hydroxide (KOH) electrolyte solution. An example catalyst is 40 nm iron oxide (Fe_2O_3) with a 5nm shell layer of TiO_2 [28]. Upon reacting with sunlight, the catalysts produce electron-hole pairs that react with water to drive both the H_2 and O_2 evolution reactions. The benchmark value of solar-to-hydrogen (STH) efficiency is 10% [27]. Produced gases from this reactor are sent to a product recovery facility (Plant 3) to yield H_2. Previous reports describe the use of a pressure swing adsorption (PSA) design to recover H_2 [27]. Upon further evaluation of the cost of the production analysis [27, 28], we see that more than 60% of the capital cost and a majority of the operating costs are associated with gas compression and purification. The separation step was estimated under the assumption of no explosion limitation between H_2 and O_2 even though the produced stoichiometric gas composition (66.7 mol% H_2 and 33.3 mol% O_2) is obviously within the explosive region as shown in Figure 5.2.

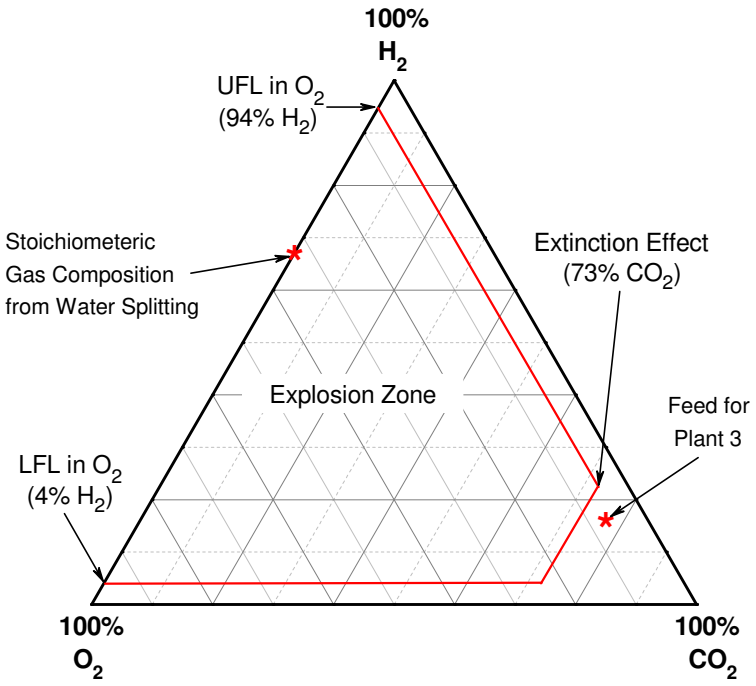

Figure 5.2: H_2 flammability diagrams in $H_2/O_2/CO_2$ mixture under normal operating conditions.

In our investigation, CO_2 received from Plant 1 will be utilized to dilute and sweep the produced stoichiometric gas to a membrane-based separation facility (Plant 3). The composition of the diluted stream entering Plant 3 is similar to the feed composition in Chapter 4 (Table 4.1). Base case parameters for Plant 2 are shown in Table 5.1 including the updated estimated production price of H_2 (60% lower than previous reports [27]). Additionally, a range of parameter values for the corresponding sensitivity analysis are also listed in Table 5.1.

5.2.3 Plant 3: Separation plant

Membranes have the potential to compete with other conventional separation processes (e.g. PSA) to separate the tertiary mixture of $H_2/O_2/CO_2$ leaving Plant 2. Figure 5.3 shows two membrane process layouts, which will be optimized to recover both H_2 and CO_2, at a ratio of 3:1, while minimizing the O_2 concentration in the outlet stream entering the methanol synthesis facility (Plant 4). Both Proteus^{TM} and Polaris^{TM} membranes from MTR will be utilized within the membrane units (Table 2.4). Layout (a) has no recycle stream; however, it utilizes two vacuum pumps in membrane units M1 and M2 on the permeate. Layout (b), on the other hand, requires only one vacuum pump for the M1 permeate. The retentate from M2 is recycled back to the first membrane unit (M1), which increases the driving force and enhances the process recovery. In both configurations, the M3 membrane unit is comprised of a CO_2-selective membrane (Polaris^{TM}) to purify and recover residual CO_2 to 99 mol%, which will be sent back to the Plant 2 sweep stream thereby minimizing the release of additional CO_2.

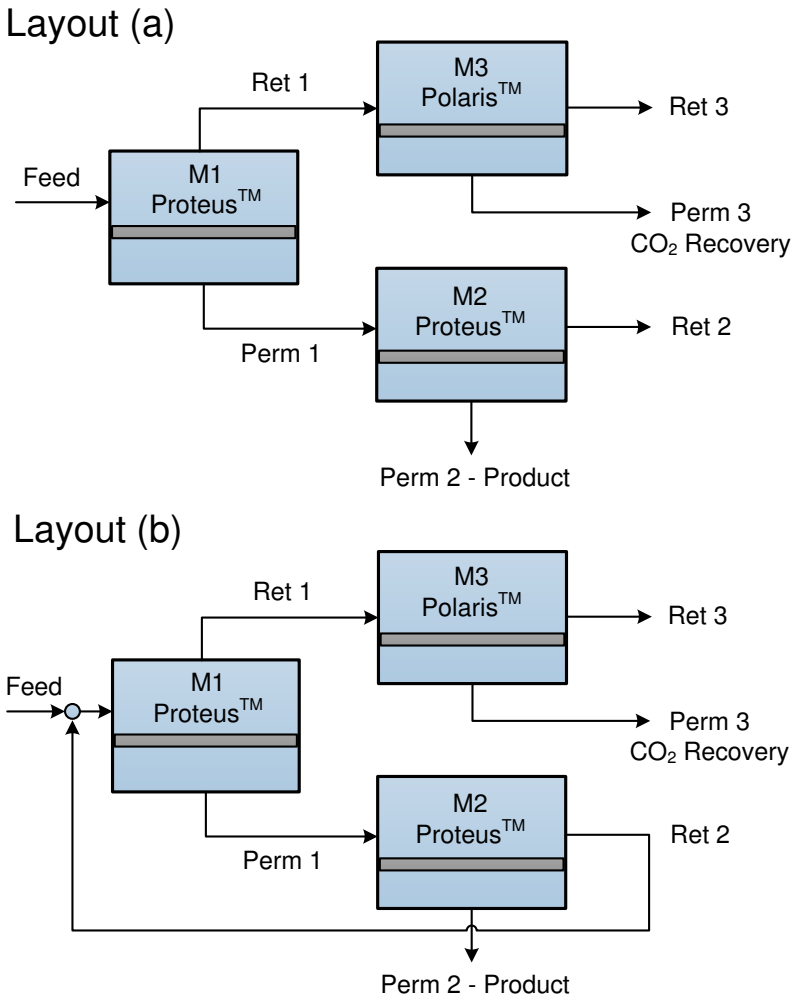

Figure 5.3: Two membrane proces layouts for Plant 3.

Table 5.2: NLP model for Plant 3.

Equation	Definition	Values
Objective function: f(x)	PV of all outgoing cash flows (no income) including: investment cost, operating cost, loss of product and depreciation for n years.	minimize
Constraints g(x)$\geqslant$0	Sets of linear and nonlinear process constraints including:	
	- H_2 recovery	$\geqslant$80%
	- H_2 purity in Perm 2 stream	=75%
	- CO_2 purity in Perm 3 stream	$\geqslant$99.9%
	- O_2 limits in permeates	$\leqslant$5.0%
	- Max. streams pressure (absolute)	$\leqslant$30 bar
	- Min. permeate pressure (absolute)	$\geqslant$0.5 bar
	- Max. trans-membrane pressure [91]	$\leqslant$12 bar
Model equations:h(x)=0	Sets of the equipment equations required to calculate the performance and economics	-

The optimization problem is solved by nonlinear programming (NLP) to minimize the objective function which is the Present Value (PV) of all outgoing (negative) cash flows including the cost of raw materials (CO_2 from Plant 1 and H_2 from Plant 2). Using this approach will achieve the optimization objectives along with minimizing the loss of raw materials. General Algebraic Modeling System (GAMS) is used to solve the NLP based on a global optimization solver (BARON). Table 5.2 shows the optimization equations for the proposed separation plant (Plant 3).

Although not shown, both process layouts illustrated in Figure5.3 include the necessary compressors, vacuum pumps and heat exchangers to manipulate the decision variables, namely: recycle rates, membrane area, and feed/permeate pressure in order to achieve the results. All details of these process units, including the membrane units, were described in Chapter 4. Table 5.1 shows the updated economic parameters used to calculate the PV and the sensitivity analysis.

5.2.4 Plant 4: Methanol production

The conversion of CO_2 into renewable methanol can be achieved via two different approaches. A one-step approach, also known as direct CO_2 hydrogenation, utilizes a renewable H_2 source and captured CO_2 to directly form methanol over a Cu-based catalyst [107, 112]. The two-step approach requires the formation of syngas from CO_2 (via renewable energy source), which is then converted to methanol through a conventional process [112]. In this investigation, the one-step approach to produce methanol was employed.

Early investigations were carried on the use of Cu-based catalysts for the conversion of CO_2 to methanol [152, 157–159]. More specifically, a commercially available catalyst

($Cu/ZnO/Al_2O_3$) can be used according to the following two reactions:

$$CO_2 + 3\,H_2 \longrightarrow CH_3OH + H_2O$$

$$CO_2 + H_2 \longleftrightarrow CO + H_2O$$

Reaction kinetics were adopted from the work of Van-Dal and Bouallou [112] which are suitable for direct implementation into Aspen Plus using the LHHW (Langmuir-Hinshelwood-Hougen-Watson) reaction model. The reactions will be carried out in an adiabatic packed bed reactor using the parameters listed in Table 5.1. A detailed process flow sheet is described in Section 5.3.2.1.

5.2.5 Overall process economic and energy analysis

As stated before, the economic calculations for the Capital Cost (CC) will be estimated using Guthrie's method as in the previous two chapters. Since there are new process units involved in this investigation (e.g. reactor, flash drums and distillation columns), all equipment specifications and parameters will be summarized in Appendix 5.5.1. After the CC and Operating Cost (OC) calculations, the PV and the NPV can be calculated as follows [134]:

$$PV_{i,T} = CC + OC \cdot \frac{(i+1)^T - 1}{(i+1)^T \cdot i} \tag{5.1}$$

$$NPV_{i,T} = R_t \cdot \frac{(i+1)^T - 1}{(i+1)^T \cdot i} - CC \tag{5.2}$$

where NPV is the net cash flow (\$), R_t is the net cash flow resulting from the annual difference between the methanol sales and operating cost of the proposed process. The total NPV will be calculated using the current methanol price of \$0.38/kg_{MeOH} [118] and the base case parameters listed in Table 5.1.

The Specific Cost (SC) can be calculated as described in Section 3.5.1.3. All four plants will be compared through the cash flow required to process the base case flow rate of 1000 kmol/h from Plant 2. For this purpose, the following specific costs are calculated:

- *SC(1)* = CO_2 capture price ($\$/kg_{CO_2 \text{produced}}$)
- *SC(2)* = H_2 production price ($\$/kg_{H_2 \text{produced}}$)
- *SC(3)* = Specific cost of Plant 3 ($\$/kg_{H_2 \text{recovered}}$)
- *SC(1-3)* = Specific cost of Plant 3 including raw materials ($\$/kg_{H_2 \text{recovered}}$)
- *SC(4)* = Specific cost of Plant 4 ($\$/kg_{\text{MeOH produced}}$)

Two energy efficiencies will be utilized to compare with other solar energy based methanol production [115]:

$$Net\ Energy\ Efficiency = \frac{MeOH\ chemical\ energy}{\mathrm{H_2}\ chemical\ energy\ +\ Utilities}$$

$$Gross\ Energy\ Efficiency = \frac{MeOH\ chemical\ energy}{Total\ solar\ energy\ +\ Utilities}$$

The net energy efficiency is the ratio of the chemical energy of the produced methanol over the chemical energy of the produced H_2 from Plant 2 via sunlight (solar energy) and the utilities. The gross energy efficiency accounts for the total solar energy required for H_2 production from Plant 2. The chemical energy for methanol and H_2 will be calculated using the Higher Heating Value (HHV) of 726 MJ/kmol$_{MeOH}$, and 286 MJ/kmol$_{H_2}$ respectively.

5.3 Results and discussions

As mentioned in the process assumption, the derivative costs from Plants 1 & 2 will be estimated using the prices of CO_2 capture and H_2 production. To obtain the mixture compositions listed in Table 4.1 for the base case, an initial supply of 4750 kmol/h for CO_2 from Plant 1 is required for plant start-up. However, the net amount of CO_2 consumption will be determined after the optimization study of Plant 3 is completed in order to estimate the CO_2 recovery.

5.3.1 Plant 3: Separation plant

5.3.1.1 Optimization results

The optimization aims at a H_2 purity of 75 mol% with a minimum recovery of 80%. Optimizing the process to minimize the separation costs without considering raw materials cost led to misleading results by ignoring the CO_2 recovery membrane unit (M3). Thus, it was essential to optimize the process to minimize SC (1-3) instead of SC (3) for both layouts. The optimization problem for layout (a) could not be solved when all constraints listed in Table 5.2 were implemented. This was resolved by reducing the CO_2 purity in Perm 3 stream to 98.8% for this layout only. Moreover, layout (a) suffered from a limited recovery rate of 93% for H_2. This design limit is related to the maximum trans-membrane pressure (TMP_{max}) of 12 bar as shown in Figure 5.4.

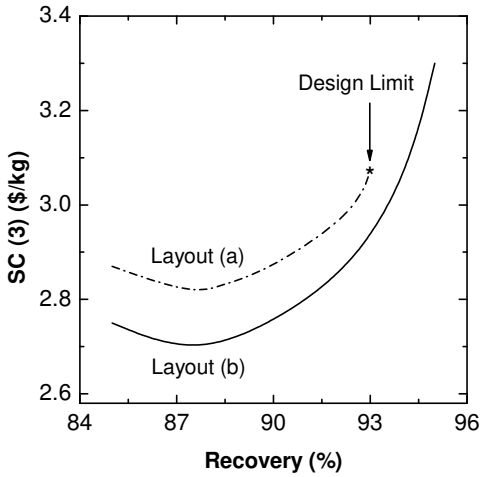

(a) Separation specific cost SC (3) profile

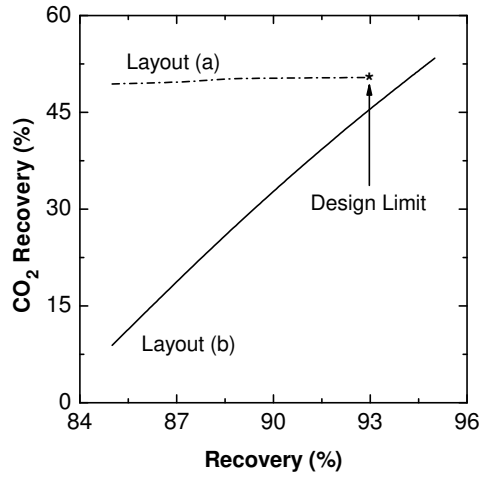

(b) CO_2 recovery rate profile

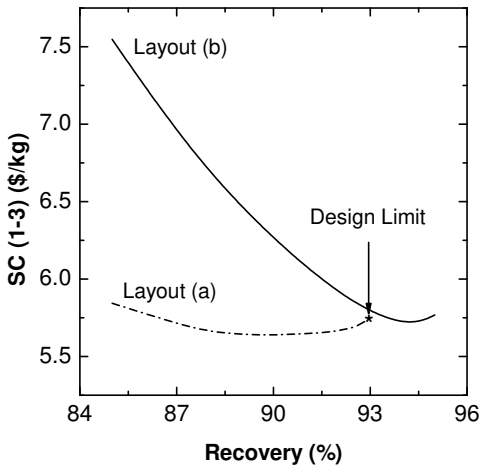

(c) Separation specific cost SC (1-3) profile

Figure 5.4: Optimization results for Plant 3.

Figure 5.4a shows clearly the lower cost of operating layout (b) over layout (a), even with all constraints implemented. The optimum recovery for the separation process should be around 87.5% based on the SC (3) analysis. However, there is a trade-off. At 87.5% H_2 recovery, the CO_2 recovery is limited (< 15%), as shown in Figure 5.4b, which drives the overall specific costs (SC 1-3) higher when raw materials are considered. Based on Figure 5.4c, both layouts exhibit similar cost at high H_2 recovery rate with a distinct advantage for layout (b) for having higher CO_2 purity in the recovery stream and higher H_2 recovery rates. Layout (a) would be attractive if lower H_2 recovery rates were acceptable, but that is unlikely due to the intrinsic economic value of H_2. Figure 5.5 and Table 5.3 show the optimum results for layout (b), which will be used as the basis of the complete investigation for this proposed methanol production route.

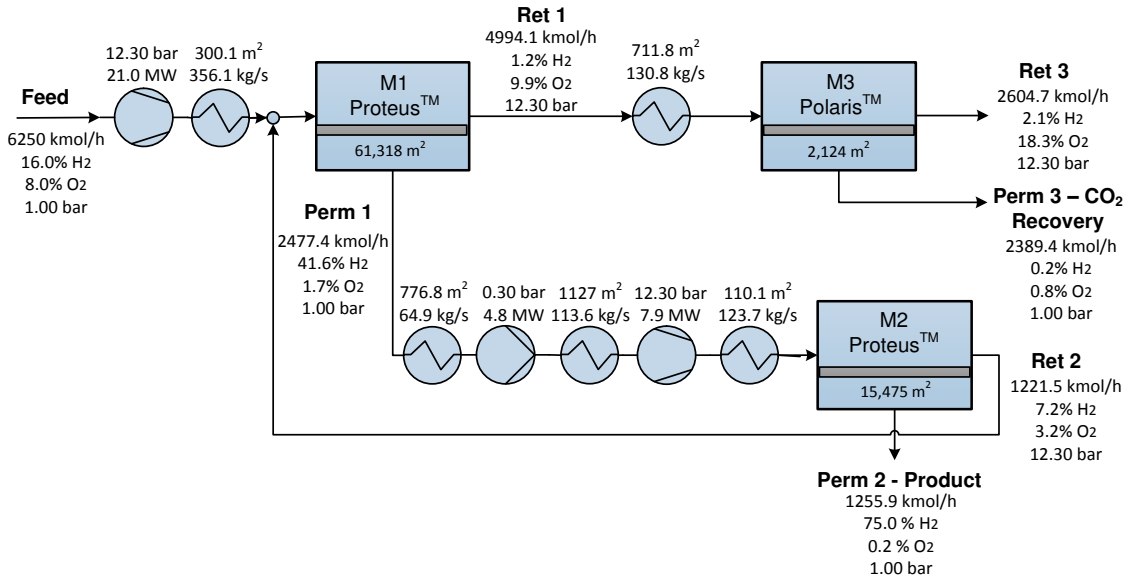

Figure 5.5: Optimum process layout for Plant 3.

Table 5.3: Optimum process and economic results for Plant 3 (base case).

Parameter	Value	Unit
H_2 recovery (Perm 2)	94.2	%
CO_2 recovery (Perm 3)	50.3	%
O_2 (Perm 2)	2480	ppm
Capital Cost (CC)	119.72	Million $
Operating Cost (OC)	32.05	Million $/yr
Raw materials cost	39.57	Million $/yr
SC (3)	3.08	$\$/kg_{\mathrm{H_2recovered}}$
SC (1-3)	5.69	$\$/kg_{\mathrm{H_2recovered}}$

As shown in Table 5.3, there are trace amounts (ppm) of O_2 in the product stream entering the methanol reactor (Plant 4). There are no reports in the open literature describing the effects of O_2 on the commercial methanol process or catalyst; which is logical as the conventional syngas composition does not contain O_2 [160, 161]. Rather than ignore the residual O_2, we considered three different scenarios to address this challenge:

- *Scenario (1)*: Treat O_2 as an inert gas in Plant 4
- *Scenario (2)*: O_2 reaction with H_2 to form water in the methanol reactor (Plant 4)
- *Scenario (3)*: O_2 removal unit with negligible cost

Scenario (1) was not considered since O_2 is likely to be very active on the copper based catalysts. Additionally, the Aspen Plus simulation showed a slight increase in product loss in Plant 4 due to requisite increase in the flare flow rate to prevent O_2 build up in the reaction loop. The challenge for Scenario (2) was to find reaction kinetics (LHHW) that were suitable for Aspen Plus to combine with direct CO_2 hydrogenation kinetics (none have been reported to date). Therefore, Scenario (3) was selected for this study. Some processes were described in the literature concerning the removal of residual O_2 in other gas H_2 containing mixtures similar to our study [162, 163] and there are even commercially available technologies (e.g. $X{-}O_2{}^{TM}$ from Newpoint Gas, Ltd.).

5.3.1.2 Sensitivity analysis

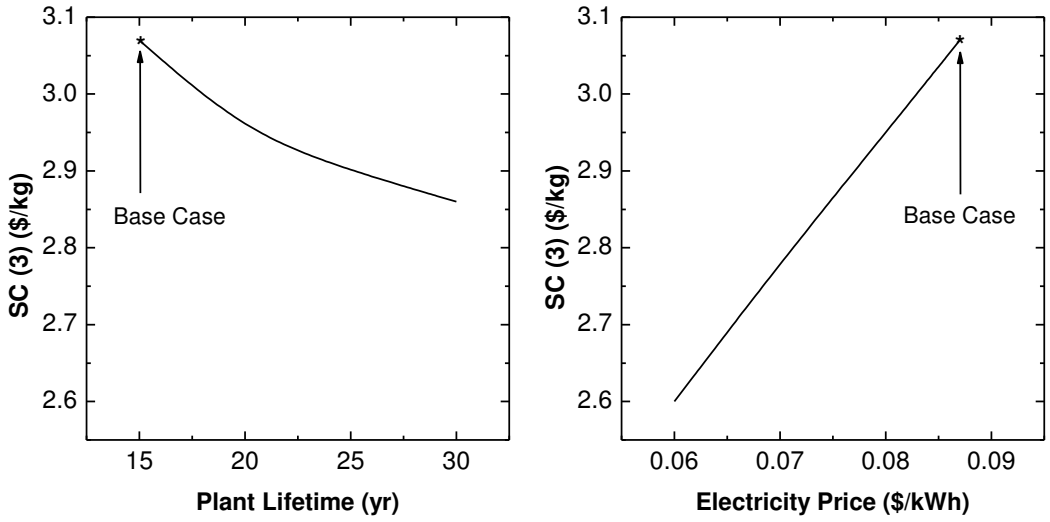

(a) Plant lifetime influence on SC (3) (b) Electricity price influence on SC (3)

Figure 5.6: Sensitivity analysis for Plant 3.

The results shown in Table 5.3 are obtained using the base case parameters. Two of these parameters were chosen to be part of the sensitivity analysis affecting Plant (3) cost, namely: plant lifetime and electricity price. Figure 5.6 summarizes the findings where specific cost SC (3) is reduced by 6.8% when the plant lifetime increases from 15 to 30 years

of operation. More influence can be noticed when the electricity price decreases from 0.087 to 0.06 $/kWh, where the specific cost drops linearly by 15.3%. This reduction is a direct result from the findings of Chapter 4 where the electricity cost accounts for approximately 70% of the total operating costs to run the membrane separation plant.

5.3.2 Plant 4: Methanol production

5.3.2.1 Flowsheet description

The process flowsheet for the methanol synthesis loop is shown in Figure5.7 and was adopted from the work of Van-Dal and Bouallou [112]. Fresh feed is delivered to the gate from Plant 3 and is comprised of H_2, CO_2, and trace amounts of O_2. The O_2 is converted to water using a catalytic conversion reactor with the following reaction stoichiometry:

$$2\,H_2 + O_2 \longrightarrow 2\,H_2O$$

This conversion results in a minor loss of H_2, about 0.66%, from the main feed entering Plant 4. Four adiabatic compressors (isotropic efficiency of 0.80) with intermediate cooling (cooling water) are utilized to compress the feed to 75bar. The compressed feed (Stream 9) is mixed with the recycle stream (Stream 22) from the reactor and preheated (HX-5) to 210°C using a fraction (60%) of the reactor outlet (Stream 13). The preheated feed (Stream 11) enters a fixed bed adiabatic reactor filled with 6840 kg of $Cu/ZnO/Al_2O_3$ catalyst. The calculated reactor volume is 6.33 m^3. The reactor products are divided into two streams (Streams 13 & 14) at an elevated temperature of 284°C. Stream 14 is used as an integrated heat source for the reboiler in the distillation column (D-1) and preheater (HX-7). The divided streams are recombined and cooled via HX-6 to 35°C. The first knock-out drum (Drum-1) separates the unreacted gases (Stream 19) from methanol/water liquid products (Stream 20). A fraction (1%) of Stream 19 is purged to prevent the accumulation of by-products. The remaining unreacted gasses (Stream 22) are recycled and combined with Stream 9 before returning to the reactor.

Liquid Stream 20, also known as crude methanol, is expanded to 1.2 bar (VLV-1), which separates most of the unreacted gasses from the liquid product in the second flash drum (Drum-2). The liquid stream leaving the second drum is preheated (HX-7) to 80°C before entering the distillation column (D-1). The column is operated with a reflux ratio of 1.1 over 33 trays. The bottom stream (102°C and 1.1 bar) is water with 171 wt-ppb of methanol. The distillate stream (64°C and 1.0 bar) contains the purified methanol along with 58 wt-ppm of water and some unreacted gases. This stream (Stream 27) is compressed and cooled to 40°C as a final polishing step to remove the unreacted gases in the third flash drum (Drum-3). Detailed stream information is available in Appendix 5.5.2.

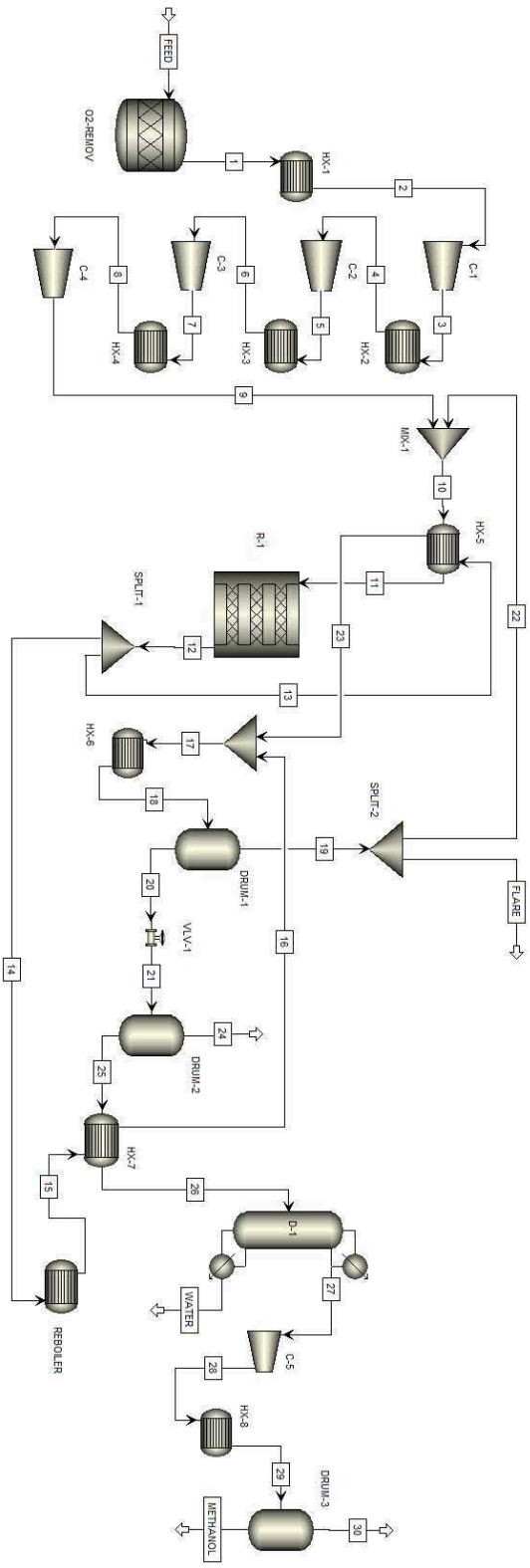

Figure 5.7: Process flowsheet for Plant 4.,

5.3.2.2 Economic results

Plant 4 capacity is designed for a production rate of 73,056 t_{MeOH}/yr (≈ 73 kta) delivering a methanol purity of 99.37 wt%. Table 5.4 summarizes the process and economic results for Plant 4 based on the base case parameters. Analysis of the capital and operating costs shows that a majority of the costs (75.8% and 84.1%, respectively) are related to investment and operation cost of the compressors (similar to Plant 3).

Table 5.4: Process and Economic results for Plant 4 (base case)

Parameter	Value	Unit
Methanol production	9132.0	kg/h
Methanol yields	0.67	kg_{MeOH} / kg_{CO_2}
Methanol purity	99.37	%wt
Capital Cost (CC)	28.29	Million $
- Heat exchangers	20.6	%
- Compressors	75.8	%
- Flash drums	0.9	%
- Distillation column	2.2	%
- Reactor	0.5	%
Operating Cost (OC)	4.82	Million $/yr
- Cooling water	8.1	%
- Electricity	84.1	%
- Catalyst replacement	7.8	%
SC (4)	0.114	$\$/kg_{\text{MeOH produced}}$

5.3.3 Overall process

5.3.3.1 Economic and energy analysis

Looking at the overall process economics, the total capital cost required for Plants 3&4 is $148 million with an annual operating cost of 76.44 million $/yr (including the raw materials from Plants 1&2). Using the current methanol price of $0.38/$kg_{MeOH}$, our proposed process results in a negative NPV of $540.40 million over a 15-year plant lifetime. A methanol price of $1.30/$kg_{MeOH}$ is the required value for the break-even point in our base case; which is more than three times higher than the current methanol price.

Building on the base case parameters and the 1000 kmol/h H_2 production from Plant 2, Figure5.8 represents the negative cash flow required for each plant. These values were calculated given the purchase price of CO_2 and H_2 from Plants 1&2, respectively, and the calculated specific cost for the separation (SC 3) and methanol (SC 4) plants. Around

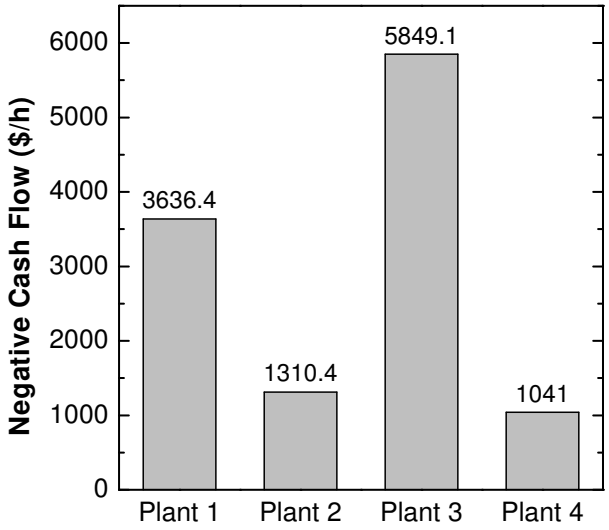

Figure 5.8: Negative cash flow analysis for the overall process economic (base case).

49% of the overall operating cost is associated with Plant 3 which is directly linked to the recovery of diluted H_2 at a high feed flow rate. The process constraints and requirements result in a high demand for membrane area and energy to deliver the desired product. Purchasing the CO_2 comes in second with more than 30% of the cost.

The energy analysis calculation is summarized in Table 5.5 and detailed calculations are provided in Appendix 5.5.3. Non-solar energy required for the photocatalytic reactor (Plant 2) was neglected since the gas processing part of the DOE study was replaced by Plant 3 in our work. The low value of the gross energy efficiency (6.25%) was expected as the efficiency of solar-to-hydrogen (STH) for water splitting is relatively low compared to other techniques, like photovoltaic cells. Both efficiencies could be improved by optimizing the heat integration between the four plants and utilizing higher performance membrane materials in Plant 3, which will reduce the compressor duties due to lower recycle rates.

Table 5.5: Energy analysis for the overall process (base case)

Energy consumption	MWh/t_{MeOH}	$MMBtu/t_{MeOH}$
MeOH chemical energy	6.29	21.46
H_2 chemical energy	8.70	29.69
Total solar energy	87.00	296.86
Plant 1 energy	3.79	12.93
Plant 2 utility	Negligible	Negligible
Plant 3 utility	7.32	24.98
Plant 4 utility	2.51	8.54
Net Energy Efficiency	28.18 %	
Gross Energy Efficiency	6.25 %	

5.3.3.2 Sensitivity analysis

The process sensitivity with respect to the primary economic parameters (plant lifetime, electricity price, and CO_2 capture cost) is represented by calculating the break-even value for the methanol price as shown in Figure 5.9. Plant lifetime has the weakest influence since it only shows a 6.2% reduction in the break-even value. The cost of the CO_2 raw materials has the greatest impact (13.1% reduction) when the capture price drops from 0.035 to 0.020 $\$/kg_{CO_2}$. The best case scenario, where the plant is operated for 30 years with \$0.060/kWh electricity price and $\$0.020/kg_{CO_2}$, has a break-even value for methanol at $\$0.96/kg_{MeOH}$, which is around 26.5% reduction from the base case result, but still 2.5 times more than the current price of fossil fuel derived methanol.

The energy required for the CO_2 capture in Plant 1 was varied to highlight its influence on the process energy efficiency. Surprisingly, it has a minor influence on the net energy efficiency (±2.5%) and negligible influence on the gross energy efficiency (±0.1%) as shown in Table 5.6. The gross energy is dominated by the total energy required for the hydrogen production, which was manipulated by different values of STH. The efficiency value increases by 2.5% when the STH value reaches 15%.

Table 5.6: Energy sensitivity analysis for the overall process

Parameter	CO_2 capture energy (kWh/kg)			STH (%)		
	0.15	0.30	0.45	5	10	15
Net Energy Efficiency (%)	30.80	28.15	25.98	Not applicable		
Gross Energy Efficiency (%)	6.37	6.25	6.14	3.35	6.25	8.78

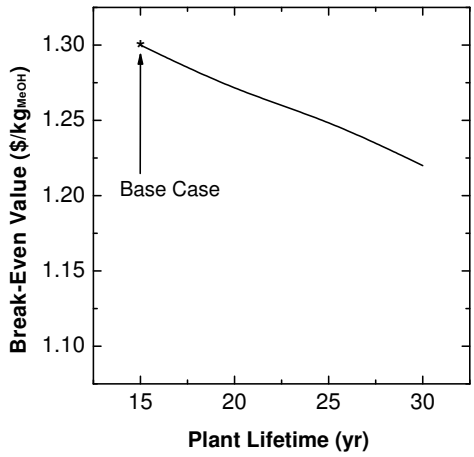

(a) Plant lifetime influence

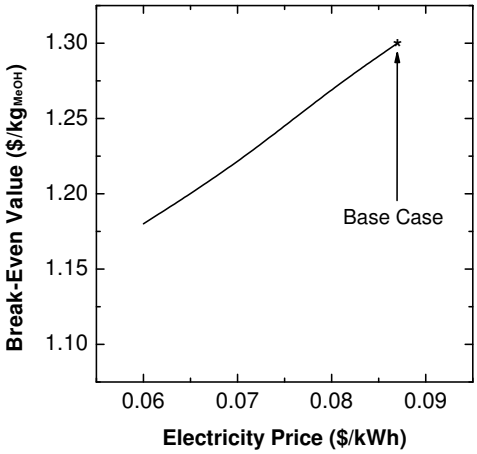

(b) Electricity price influence

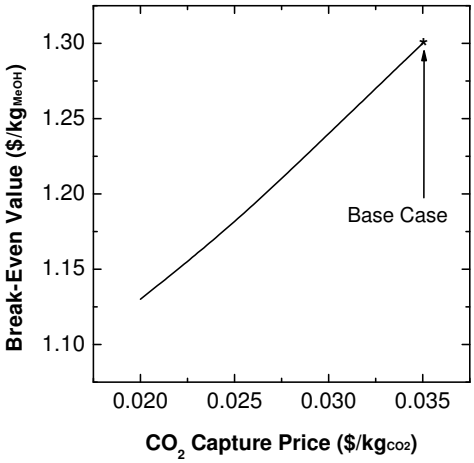

(c) CO_2 capture price influence

Figure 5.9: Process economic parameters influence on break-even value of methanol.

5.3.3.3 Comparison with other alternative processes

As explained previously, solar energy can be utilized in different ways to produce methanol using captured CO_2. Kim and coworkers built an exemplary case study for such process based on a solar conversion technology to produce CO (and H_2 via WGS) from CO_2 and H_2O [115]. We have compared our findings with their work. As a special case for this comparison, we recalculated our results using similar economic parameters as shown in Table 5.7.

The thermochemical approach utilizes more CO_2, converted to CO, to produce the same amount of methanol. Obviously, an extraordinary amount of CO is required to carry out both water gas shift (to produce H_2) and conventional methanol synthesis. Whereas, the direct hydrogenation process proposed in our study required less CO_2 as a raw material feed. Regarding the total process energy, both studies promote similar net energy efficiencies, with CO_2 hydrogenation having a 16% edge. The thermochemical approach, on the other hand, is more efficient (65%) in terms of gross energy. The Solar-to-Chemical efficiency is at 20% for the thermochemical approach, which is two times higher than what is assumed for the STH in our work. Finally, the break-even value is markedly lower (26%) in our study compared to the thermochemical approach, which will be a considerable controlling variable in technology commercialization.

Table 5.7: Comparison between this study and methanol production via thermochemical conversion proposed by Kim, *et al.* [115]

	This Study	Kim and Coworkers
Technology used	Direct CO_2 hydrogenation using H_2 from photocatalytic water splitting	Methanol from CO_2 and water using thermochemical conversion of CO_2 to CO
Raw materials	Purchased CO_2 and H_2	Purchased CO_2 and de-ionized water
Economic Parameters		
- Project lifetime (T)	30 years	30 years
- Interest rate (i)	8%	8%
- CO_2 price	\$0.035/kg	\$0.035/kg
- Electricity Price	\$0.06/kWh	\$0.06/kWh
Results		
- Methanol yields	0.67 kg_{MeOH} / kg_{CO_2}	0.75 kg_{MeOH} / kg_{CO_2}
- Methanol purity	99.37%wt	99.06%wt
- Break-even value	\$0.94/kg_{MeOH}	\$1.22/kg_{MeOH}
- Net energy efficiency	28.18%	24.30%
- Gross energy efficiency	6.25%	10.40%

5.4 Conclusion

Photocatalytic water splitting is a low-cost H_2 source, but the simultaneous production of H_2 and O_2 in a closed environment introduces significant explosion hazards. In this chapter, we presented a novel process that utilized captured CO_2 as a diluent to recover the H_2 safely from the photocatalytic reactor and as a raw material to produce methanol. The process consisted of four plants, namely: a CO_2 capture unit (Plant 1), photocatalytic reactor (Plant 2), membrane separation plant (Plant 3), and methanol synthesis loop based on direct CO_2 hydrogenation (Plant 4). Plants 1&2 were not simulated in this investigation, but rather their associated costs were presented as purchasing raw materials. Process development and techno-economic analyses were carried on the separation and synthesis plants.

Two membrane layouts were optimized to recover both H_2 and CO_2 at a ratio of 3:1 while maintaining both safety and process constraints. A membrane cascade configuration (Layout (b)) comprised of three membrane units and one recycle stream, showed the lowest specific cost for H_2 recovery ($\$3.08/kg_{\mathrm{H_2 recovered}}$). The product stream from this plant was fed to the methanol plant. A reaction scheme based on a $Cu/ZnO/Al_2O_3$ catalyst was used to convert H_2 and CO_2 directly to methanol. The overall economics of the process revealed a high production cost compared to the conventional methanol production from natural gas. Given the base case parameters, a break-even value of methanol of $\$1.30/\mathrm{kg_{MeOH}}$ is needed to become economically attractive. Among the four plants, the separation plant has the highest negative cash flow effect with more than 49% of the total operating cost. Economic sensitivity analyses were carried for three parameters, namely: plant lifetime, electricity price and CO_2 capture price. The cost of the CO_2 raw materials has the highest impact. A 13.1% reduction on the break-even value was achieved when the capture price drop from 0.035 to 0.020 $\$/\mathrm{kg_{CO_2}}$. Moreover, the best case scenario, where the plant is operated for 30 years with \$0.060/kWh electricity price and $\$0.020/\mathrm{kg_{CO_2}}$, showed a 26.5% reduction in cost ($\$0.96/\mathrm{kg_{MeOH}}$) compared to the base case. As for the energy efficiency, the proposed process demonstrated a 28.18% net energy efficiency. However, this value dropped to 6.25% for the gross energy efficiency when the total solar energy is accounted for (given an STH of 10%).

5.5 Appendix

5.5.1 Capital cost (CC) estimation

As described in Section 3.5.1.2, the capital cost (CC) was calculated using Guthrie's method using the following equations:

$$BC = C_0 \cdot (\frac{S}{S_0})^{\alpha} \tag{5.3}$$

$$CC = UF \cdot BC \cdot (MPF + MF - 1) \tag{5.4}$$

The MPF value is calculated using further parameters that differ based on equipment type, construction materials, pressure and temperature values. In this appendix, we will provide full details for each equipment.

Heat exchanger

Shell and tube heat exchangers are used in the simulation of Plant 4 utilizing seawater as a cooling media. The value of MPF can be calculated using the following equation:

$$MPF = F_m(F_p + F_d) \tag{5.5}$$

where F_m is the material factor, F_p is the pressure factor and F_d is the design factor.

All required specifications and parametric values for Eq.(5.3) to Eq.(5.5) are listed in Table 5.8. For all equipment, the maximum pressure specification available for F_p is 70.0 bar. We assumed this F_p value is applicable for the simulation of Plant 4, which operates at 75.0 bar.

Table 5.8: Heat exchanger specifications and parameters.

Parameter / Specification	Value	Unit
Design type (Floating Head)	F_d=1	-
Material (Carbon Steel)	F_m=1	-
Pressure factor:		
1.0 bar $\leqslant$ P $\leqslant$ 11.3 bar	F_p=0.00	-
11.3 bar $\leqslant$ P $\leqslant$ 21.7 bar	F_p=0.10	-
28.6 bar $\leqslant$ P $\leqslant$ 56.2 bar	F_p=0.52	-
56.2 bar $\leqslant$ P $\leqslant$ 70.0 bar	F_p=0.55	-
Reference cost (C_0)	5,000	\$
Reference size (S_0)	37.1	m^2
Exponent α	0.65	-
Module factor	MF=5.29	-
Update factor	UF=4.75	-

Compressors

Centrifugal compressors were used in Plant 4 and the MPF value is only a function of the design type as shown in Eq.(5.6):

$$MPF = F_d \tag{5.6}$$

Table 5.9 shows all the parameters required for CC calculation.

Table 5.9: Compressor specifications and parameters.

Parameter / Specification	Value	Unit
Design type (Centrifugal / motor)	F_d=1	-
Reference cost (C_0)	23,000	$
Reference size (S_0)	74.57	kW
Exponent α	0.77	-
Module factor	MF=5.01	-
Update factor	UF=4.75	-

Vessels (Flash Drums)

The sizing of vertical flash drums is based on a five-minute liquid hold up with length over diameter (L/D) ratio of 4. As cylindrical vessels require two factor (length and diameter) for sizing, Eq.(5.7) is used instead of Eq.(5.3) along with the MPF Eq.(5.8):

$$BC = C_0(\frac{L}{L_0})^{\alpha} \cdot (\frac{D}{D_0})^{\beta} \tag{5.7}$$

$$MPF = F_m F_p \tag{5.8}$$

Table 5.10 shows all the parameters required for CC calculation:

Table 5.10: Flash drum specifications and parameters.

Parameter / Specification	Value	Unit
Material (Carbon Steel)	F_m=1	-
Pressure factor:		
1.0 bar $\leqslant$ P $\leqslant$ 4.4 bar	F_p=1.0	-
63.1 bar $\leqslant$ P $\leqslant$ 70.0 bar	F_p=2.5	-
Reference cost (C_0)	1,000	$
Reference size (L_0)	1.22	m
Reference size (D_0)	0.91	m
Exponent α	0.81	-
Exponent β	1.05	-
Module factor	MF=4.23	-
Update factor	UF=4.75	-

Distillation Column

The cost calculation for distillation columns is divided into three parts:

- Reboiler and condenser, which are calculated as heat exchangers.
- The column, which is calculated as a pressure vessel.
- Tray stack, which required a new calculation using the Eq.(5.9) and Eq.(5.7)

$$MPF = F_m + F_s + F_t \tag{5.9}$$

where: F_s is the tray spacing factor and F_t is the tray type.

Table 5.11 shows all the parameters required for the tray stack calculation:

Table 5.11: Flash drum specifications and parameters.

Parameter / Specification	Value	Unit
Material (Carbon Steel)	F_m=0	-
Tray spacing (24")	F_s=1.0	-
Tray type (valve)	F_t=0.4	-
Reference cost (C_0)	180	$
Reference size (L_0)	3.05	m
Reference size (D_0)	0.61	m
Exponent α	0.97	-
Exponent β	1.45	-
Module factor	MF=1.0	-
Update factor	UF=4.75	-

Reactor

The cost of the reactor in Plant 4 is treated as a pressure vessel. The reactor dimensions are calculated using the information provided in Table 5.1.

5.5.2 Detailed streams information for Plant 4

In this section, we will provide full stream information for Plant 4 as shown in Table 5.12.

Table 5.12: Detailed stream information for Plant 4.

Stream	FEED	1	2	3	4	5
Mole Fraction (%)						
H_2	0.750	0.747	0.747	0.747	0.747	0.747
CO_2	0.248	0.248	0.248	0.248	0.248	0.248
H_2O	0.000	0.005	0.005	0.005	0.005	0.005
CO	0.000	0.000	0.000	0.000	0.000	0.000
CH_3OH	0.000	0.000	0.000	0.000	0.000	0.000
O_2	0.002	0.000	0.000	0.000	0.000	0.000
Total Flow (kmol/h)	1255.82	1252.71	1252.71	1252.71	1252.71	1252.71
Total Flow (kg/h)	15678.43	15678.43	15678.43	15678.43	15678.43	15678.43
Temperature (°C)	150.00	150.00	35.00	194.48	50.00	190.11
Pressure (bar)	1.00	1.00	1.00	3.80	3.80	12.00

Stream	6	7	8	9	10	11
Mole Fraction (%)						
H_2	0.747	0.747	0.747	0.747	0.839	0.839
CO_2	0.248	0.248	0.248	0.248	0.126	0.126
H_2O	0.005	0.005	0.005	0.005	0.001	0.001
CO	0.000	0.000	0.000	0.000	0.031	0.031
CH_3OH	0.000	0.000	0.000	0.000	0.003	0.003
O_2	0.000	0.000	0.000	0.000	0.000	0.000
Total Flow (kmol/h)	1252.71	1252.71	1252.71	1252.71	7394.75	7394.75
Total Flow (kg/h)	15678.43	15678.43	15678.43	15678.43	60612.92	60612.92
Temperature (°C)	50.00	158.99	50.00	159.12	57.48	210.00
Pressure (bar)	12.00	30.00	30.00	75.00	75.00	75.00

Stream	12	13	14	15	16	17
Mole Fraction (%)						
H_2	0.783	0.783	0.783	0.783	0.783	0.783
CO_2	0.094	0.094	0.094	0.094	0.094	0.094
H_2O	0.044	0.044	0.044	0.044	0.044	0.044
CO	0.034	0.034	0.034	0.034	0.034	0.034
CH_3OH	0.045	0.045	0.045	0.045	0.045	0.045
O_2	0.000	0.000	0.000	0.000	0.000	0.000
Total Flow (kmol/h)	6821.59	4088.74	2728.64	2728.64	2728.64	6815.90
Total Flow (kg/h)	60612.92	36394.44	24245.17	24245.17	24245.17	60678.55
Temperature (°C)	284.34	284.34	284.34	128.94	80.21	85.18
Pressure (bar)	75.00	75.00	75.00	75.00	75.00	75.00

Stream	18	19	20	21	22	FLARE
Mole Fraction (%)						
H_2	0.783	0.858	0.020	0.020	0.858	0.858
CO_2	0.094	0.101	0.028	0.028	0.101	0.101
H_2O	0.044	0.001	0.483	0.483	0.001	0.001
CO	0.034	0.038	0.001	0.001	0.038	0.038
CH_3OH	0.045	0.003	0.468	0.468	0.003	0.003
O_2	0.000	0.000	0.000	0.000	0.000	0.000
Total Flow (kmol/h)	6815.90	6204.08	611.82	611.82	6142.04	62.04
Total Flow (kg/h)	60678.55	45388.37	15290.19	15290.19	44934.48	453.88
Temperature (°C)	35.00	35.00	35.00	29.12	35.00	35.00
Pressure (bar)	75.00	75.00	75.00	1.20	75.00	75.00

Stream	23	24	25	26	WATER
Mole Fraction (%)					
H_2	0.783	0.389	0.000	0.000	0.000
CO_2	0.094	0.480	0.003	0.003	0.000
H_2O	0.044	0.019	0.508	0.508	1.000
CO	0.034	0.022	0.000	0.000	0.000
CH_3OH	0.045	0.091	0.489	0.489	0.000
O_2	0.000	0.000	0.000	0.000	0.000
Total Flow (kmol/h)	4088.74	31.41	580.40	580.40	294.86
Total Flow (kg/h)	36394.44	809.38	14480.81	14480.81	5312.07
Temperature (°C)	88.37	28.00	28.00	80.00	102.27
Pressure (bar)	75.00	1.20	1.20	1.20	1.10

Stream	27	28	29	30	METHANOL
Mole Fraction (%)					
H_2	0.000	0.000	0.000	0.075	0.000
CO_2	0.007	0.007	0.007	0.565	0.005
H_2O	0.000	0.000	0.000	0.000	0.000
CO	0.000	0.000	0.000	0.006	0.000
CH_3OH	0.993	0.993	0.993	0.355	0.995
O_2	0.000	0.000	0.000	0.000	0.000
Total Flow (kmol/h)	285.54	285.54	285.54	1.01	284.53
Total Flow (kg/h)	9168.74	9168.74	9168.74	36.75	9131.99
Temperature (°C)	64.05	77.96	40.00	40.00	40.00
Pressure (bar)	1.00	1.20	1.20	1.00	1.00

5.5.3 Calculation of the overall process energy analysis

a) MeOH $chemical\,energy = 726\,\frac{MJ}{kmol} * \frac{1}{32.04}\,\frac{kmol}{kg} * 1000\,\frac{kg}{t} * \frac{1}{3600}\,\frac{MWh}{MJ} = 6.29\,\frac{MWh}{t_{MeOH}}$

b) H_2 $chemical\,energy = \frac{high\,heating\,value\,of\,H_2\,produced}{methanol\,production\,rate}$

$$= \frac{1000\,\frac{kmol}{h} * 286\,\frac{MJ}{kmol}}{9.132\,\frac{t}{h}} * \frac{1}{3600}\,\frac{MWh}{MJ} = 8.70\,\frac{MWh}{t_{MeOH}}$$

c) $Total\,solar\,energy = \frac{H_2\,chemical\,energy}{STH\,efficiency} = \frac{8.70\,\frac{MWh}{t}}{0.1} = 87.0\,\frac{MWh}{t_{MeOH}}$

d) $Plant\,1\,energy = \frac{Required\,CO_2\,flowrate * CO_2\,capture\,energy\,requirement}{methanol\,production\,rate * CO_2\,capture\,efficiency}$

$$= \frac{2360.75\,\frac{kmol}{h} * 44.01\,\frac{kg}{kmol} * 0.3\,\frac{kWh}{kg_{CO_2}} * \frac{1}{1000}\,\frac{MWh}{kWh}}{9.132\,\frac{t}{h} * 0.9} = 3.79\,\frac{MWh}{t_{MeOH}}$$

e) $Plant\,2\,utility = Negligible$

f) $Plant\,3\,utility = \frac{Energy\,for\,Heat\,Exchangers + Compressors}{methanol\,production\,rate} = \frac{66.81\,MW}{9.132\,\frac{t}{h}} = 7.32\,\frac{MWh}{t_{MeOH}}$

g) $Plant\,4\,utility = \frac{Energy\,for\,Heat\,Exchangers + Compressors}{methanol\,production\,rate} = \frac{22.97\,MW}{9.132\,\frac{t}{h}} = 2.51\,\frac{MWh}{t_{MeOH}}$

CHAPTER 6

Conclusion

6.1 Summary

In this thesis, we have developed and investigated membrane-based processes to recover and utilize H_2 generated from photocatalytic water splitting while resolving the explosion hazard raised from the simultaneous production of H_2 and O_2. Two flammability suppressants were investigated, namely: N_2 and CO_2. Detailed information about H_2 flammability in these two diluents and the impact of the operating conditions were described in detail in order to identify the parametric range that ensures a safe separation process.

In the first approach to recover H_2 as pure product, we assumed the reactor products (H_2 & O_2) from water splitting are diluted with N_2. Two gaseous mixtures with different molar concentrations were investigated (Mixture (1) with 4%mol and Mixture (2) with 6%mol H_2 concentration) using commercial available membranes from UBE® (Japan). The preliminary studies revealed that the best membrane cascade design is the double pass configuration with partial recycle of the product stream. To economically recover the diluted H_2, optimization study was performed for the two mixtures. The optimization problem was formulated in a NLP model and GAMS was used to resolve and obtain the results with an objective function of minimizing the PV. Both mixtures showed high specific separation costs with a limited recovery and purity. Beyond these minimum values, the cost increases dramatically. For instance, a 92% recovery and 92.5% purity is possible for Mixture (1) at specific cost of \$8.20/kg. For Mixture (2), 90% recovery and 95% purity was achievable with a specific recovery cost of \$6.15/kg. Comparing these two mixtures showed a reduction of 25% in the specific cost when the feed is switched to higher molar concentration. In a final effort to reduce costs, we explored the benefits of using a higher performance experimental polymer for the membrane. The results showed lower separation costs in general up to 40%, but with a high recycle rate.

The second approach was to utilize CO_2 as a flammability suppressant over N_2. The thermodynamic nature of CO_2 permits higher H_2 contents in the feed, which was proven to beneficial to reduce the cost as shown in the first approach. The study listed the new flammability constraints, essential assumptions and modelling equations to ensure accurate results. Several membrane cascade designs were implemented to recover H_2 product (99%) while maintaining compositions outside flammability ranges. The optimization study was based on the use of commercially available membranes reported by MTR, namely: H_2-selective membrane (Proteus^{TM}) and CO_2-selective membrane (Polaris^{TM}). The optimum layout was comprised of three H_2-selective membrane units with a single recycle stream, resulting in 85% recovery rate with 99% product purity at a cost of \$6.4/kg. Unfortunately this value is higher than the assumed production cost of H_2 (\$2/kg). We further compared our results with the previous chapter based on a N_2 diluent system. Using CO_2 as a diluent resulted in higher purities, lower separation costs up to 50%, and reduced O_2 content in the product stream. We concluded this study with a comparison between the commercially available MTR spiral wound membrane and a hollow fiber module. Lower specific cost was obtained (18% reduction) for all process layouts for the hollow fiber configuration over spiral wound due to its enhanced separation performance in this process.

As a final approach to reduce the H_2 capture costs from water splitting, we have developed a conceptual process comprised of integrated facilities to produce methanol (a more value-

added chemical) from captured CO_2 and H_2. The first process unit supplied captured CO_2, which was used as a raw material and a diluent to recover H_2 safely from the photocatalytic reactors. The tertiary mixture ($H_2/O_2/CO_2$) was safely processed in a membrane-based separation plant, which was optimized to produce a 3:1 H_2 and CO_2 mixture. This binary mixture was then used as feedstock for methanol production via the direct CO_2 hydrogenation approach. Based on a detailed economic analysis, the break-even value of the methanol produced using this approach was higher than the current market price for fossil fuel derived methanol. The main drivers for the higher cost were the expenditures of the separation plant and the feed-stock costs of CO_2. An economic sensitivity analysis of the process revealed the strong influence of the CO_2 market price compared with electricity costs and depreciated plant lifetime for the selected parameters. The best-case scenario, where the lifetime is 30 years with \$0.060/kWh electricity price and \$0.020/kg_{CO_2} raw material cost, has a break-even value for methanol at \$0.96/kg_{MeOH}. Based on a target solar-to-hydrogen efficiency of 10% in the photocatalytic reactor units, the gross energy efficiency of the entire process was 6.25%. As a final element, we present a comparison of our process with alternative renewable methanol synthesis routes from the literature to highlight the differences in electrochemical (our approach) and thermochemical approaches to produce methanol.

6.2 Outlook

The investigations within this thesis revealed the potential of membrane processes in the production of renewable chemicals. As shown in Chapter 3 and Chapter 4, the membrane material performance and architecture have strong influence on the separation cost in terms of membrane area reduction and lower compressor duty. For Chapter 5, the proposed process showed promise for both production cost and energy efficiency as an alternative for renewable driven methanol production, but it is clear that further research and development is needed for both H_2 recovery and methanol production. These improvement techniques include developing higher performance membrane materials, lower CO_2 capture prices, enhanced STH efficiency of the photocatalysts, and systematic process integration between the plants to reduce energy consumption. Moreover, variable ratios of H_2 and CO_2, leaving the separation plant, should be explored in order to enhance methanol production.

These investigation studies clearly identify the potential of membranes and carbon capture to produce value-added commodity chemicals and highlights the opportunities for the scientific community to advance in this field.

References

[1] A. Sieminski *et al.*; *International energy outlook*; Energy Information Administration (EIA), 2014

[2] J. David and H. Herzog; *The cost of carbon capture*; in *fifth international conference on greenhouse gas control technologies, Cairns, Australia* (2000) pages 13–16

[3] C.-H. Huang and C.-S. Tan; *A review: CO_2 utilization*; Aerosol Air Qual. Res 14 (2014) 480–499

[4] J. Hansen, M. Sato, P. Hearty, R. Ruedy, M. Kelley, V. Masson-Delmotte, G. Russell, G. Tselioudis, J. Cao, E. Rignot *et al.*; *Ice melt, sea level rise and superstorms: evidence from paleoclimate data, climate modeling, and modern observations that 2°C global warming could be dangerous*; Atmospheric Chemistry and Physics 16 (6) (2016) 3761–3812

[5] C. B. Field, V. R. Barros, K. Mach and M. Mastrandrea; *Climate change 2014: impacts, adaptation, and vulnerability*; volume 1 (2014); Cambridge University Press Cambridge and New York

[6] S. C. Roy, O. K. Varghese, M. Paulose and C. A. Grimes; *Toward solar fuels: photocatalytic conversion of carbon dioxide to hydrocarbons*; Acs Nano 4 (3) (2010) 1259–1278

[7] M. Ramdin, T. W. de Loos and T. J. Vlugt; *State-of-the-art of CO_2 capture with ionic liquids*; Industrial & Engineering Chemistry Research 51 (24) (2012) 8149–8177

[8] M. Dresselhaus and I. Thomas; *Alternative energy technologies*; Nature 414 (6861) (2001) 332–337

[9] N. S. Lewis; *Toward cost-effective solar energy use*; science 315 (5813) (2007) 798–801

[10] C. Acar, I. Dincer and C. Zamfirescu; *A review on selected heterogeneous photocatalysts for hydrogen production*; International Journal of Energy Research 38 (15) (2014) 1903–1920

[11] K. A. Connelly and H. Idriss; *The photoreaction of TiO_2 and Au/TiO_2 single crystal and powder surfaces with organic adsorbates. Emphasis on hydrogen production from renewables*; Green Chemistry 14 (2) (2012) 260–280

[12] K. Maeda and K. Domen; *Photocatalytic water splitting: recent progress and future challenges*; The Journal of Physical Chemistry Letters 1 (18) (2010) 2655–2661

[13] S. Dutta; *A review on production, storage of hydrogen and its utilization as an energy resource*; Journal of Industrial and Engineering Chemistry 20 (4) (2014) 1148–1156

[14] M. Shalygin, S. Abramov, A. Netrusov and V. Teplyakov; *Membrane recovery of hydrogen from gaseous mixtures of biogenic and technogenic origin*; international journal of hydrogen energy 40 (8) (2015) 3438–3451

[15] A. Kudo and Y. Miseki; *Heterogeneous photocatalyst materials for water splitting*; Chemical Society Reviews 38 (1) (2009) 253–278

[16] I. Dincer and C. Acar; *Review and evaluation of hydrogen production methods for better sustainability*; International journal of hydrogen energy 40 (34) (2015) 11094–11111

[17] C. Acar, I. Dincer and G. F. Naterer; *Review of photocatalytic water-splitting methods for sustainable hydrogen production*; International Journal of Energy Research 40 (11) (2016) 1449–1473

[18] L. Ding, H. Zhou, S. Lou, J. Ding, D. Zhang, H. Zhu and T. Fan; *Butterfly wing architecture assisted CdS/Au/TiO_2 Z-scheme type photocatalytic water splitting*; international journal of hydrogen energy 38 (20) (2013) 8244–8253

[19] C.-H. Liao, C.-W. Huang and J. Wu; *Hydrogen production from semiconductor-based photocatalysis via water splitting*; Catalysts 2 (4) (2012) 490–516

[20] H. Ahmad, S. Kamarudin, L. Minggu and M. Kassim; *Hydrogen from photocatalytic water splitting process: A review*; Renewable and Sustainable Energy Reviews 43 (2015) 599–610

[21] A. Steinfeld; *Solar hydrogen production via a two-step water-splitting thermochemical cycle based on Zn/ZnO redox reactions*; International Journal of Hydrogen Energy 27 (6) (2002) 611–619

[22] J. A. Turner; *Sustainable hydrogen production*; Science 305 (5686) (2004) 972–974

[23] G. Centi and S. Perathoner; *Towards solar fuels from water and CO_2*; ChemSusChem 3 (2) (2010) 195–208

[24] S. Abanades and G. Flamant; *Thermochemical hydrogen production from a two-step solar-driven water-splitting cycle based on cerium oxides*; Solar Energy 80 (12) (2006) 1611–1623

[25] I. Akkerman, M. Janssen, J. Rocha and R. H. Wijffels; *Photobiological hydrogen production: photochemical efficiency and bioreactor design*; International journal of hydrogen energy 27 (11) (2002) 1195–1208

[26] M. L. Ghirardi, A. Dubini, J. Yu and P.-C. Maness; *Photobiological hydrogen-producing systems*; Chemical Society Reviews 38 (1) (2009) 52–61

[27] B. D. James, G. N. Baum, J. Perez and K. N. Baum; *Technoeconomic analysis of photoelectrochemical (PEC) hydrogen production*; Technical report; Directed Technologies, Inc., Arlington, VA (United States) (2009)

[28] B. A. Pinaud, J. D. Benck, L. C. Seitz, A. J. Forman, Z. Chen, T. G. Deutsch, B. D. James, K. N. Baum, G. N. Baum, S. Ardo *et al.*; *Technical and economic feasibility of centralized facilities for solar hydrogen production via photocatalysis and photoelectrochemistry*; Energy & Environmental Science 6 (7) (2013) 1983–2002

[29] M. R. Shaner, H. A. Atwater, N. S. Lewis and E. W. McFarland; *A comparative technoeconomic analysis of renewable hydrogen production using solar energy*; Energy & Environmental Science 9 (7) (2016) 2354–2371

[30] A. Fujishima and K. Honda; *Electrochemical photolysis of water at a semiconductor electrode*; nature 238 (5358) (1972) 37–38

[31] K. Maeda; *Z-scheme water splitting using two different semiconductor photocatalysts*; ACS Catalysis 3 (7) (2013) 1486–1503

[32] S.-C. Yu, C.-W. Huang, C.-H. Liao, J. C. Wu, S.-T. Chang and K.-H. Chen; *A novel membrane reactor for separating hydrogen and oxygen in photocatalytic water splitting*; Journal of membrane science 382 (1) (2011) 291–299

[33] M. Balat; *Potential importance of hydrogen as a future solution to environmental and transportation problems*; International journal of hydrogen energy 33 (15) (2008) 4013–4029

[34] N. Muradov and T. Veziroglu; *From hydrocarbon to hydrogen-carbon to hydrogen economy*; International Journal of Hydrogen Energy 30 (3) (2005) 225–237

[35] D. Rand and R. Dell; *FUELS - HYDROGEN PRODUCTION | Coal Gasification* (2009); ISBN 9780444527455

[36] T. Eggeman; *Ammonia*; John Wiley & Sons, Inc.; ISBN 9780471238966 (2010) DOI:10.1002/0471238961.0113131503262116.a01.pub3; URL: http://dx.doi.org/10.1002/0471238961.0113131503262116.a01.pub3

[37] K. Hou and R. Hughes; *The kinetics of methane steam reforming over a Ni/α-Al_2O catalyst*; Chemical Engineering Journal 82 (1) (2001) 311–328

[38] M. Azarhoosh, H. A. Ebrahim and S. Pourtarah; *Simulating and Optimizing Auto-Thermal Reforming of Methane to Synthesis Gas Using a Non-Dominated Sorting Genetic Algorithm II Method*; Chemical Engineering Communications 203 (1) (2016) 53–63

[39] J. A. Ritter and A. D. Ebner; *State-of-the-art adsorption and membrane separation processes for hydrogen production in the chemical and petrochemical industries*; Separation Science and Technology 42 (6) (2007) 1123–1193

[40] I. Ismagilov, E. Matus, V. Kuznetsov, N. Mota, R. Navarro, S. Yashnik, I. Prosvirin, M. Kerzhentsev, Z. Ismagilov and J. Fierro; *Hydrogen production by autothermal reforming of methane: Effect of promoters (Pt, Pd, Re, Mo, Sn) on the performance of Ni/La_2O_3 catalysts*; Applied Catalysis A: General 481 (2014) 104–115

[41] V. M. Shinde and G. Madras; *Catalytic performance of highly dispersed Ni/TiO_2 for dry and steam reforming of methane*; Rsc Advances 4 (10) (2014) 4817–4826

[42] E. J. Sheu and A. Mitsos; *Optimization of a hybrid solar-fossil fuel plant: Solar steam reforming of methane in a combined cycle*; Energy 51 (2013) 193–202

[43] A. P. Singh, S. Singh, S. Ganguly and A. V. Patwardhan; *Steam reforming of methane and methanol in simulated macro & micro-scale membrane reactors: Selective separation of hydrogen for optimum conversion*; Journal of Natural Gas Science and Engineering 18 (2014) 286–295

[44] A. Iulianelli, S. Liguori, J. Wilcox and A. Basile; *Advances on methane steam reforming to produce hydrogen through membrane reactors technology: A review*; Catalysis Reviews 58 (1) (2016) 1–35

[45] J. H. Gary, G. E. Handwerk and M. J. Kaiser; *Petroleum refining: technology and economics* (2007); CRC press

[46] R. M. Dessau; *Dehydrogenation, dehydrocyclization and reforming catalyst* (1991); uS Patent 5,011,805

[47] R. Ramachandran and R. K. Menon; *An overview of industrial uses of hydrogen*; International Journal of Hydrogen Energy 23 (7) (1998) 593–598

[48] NexantThinking^{TM}; *Process Evaluation / Research Planning: Methanol* (2017); URL: http://thinking.nexant.com/sites/default/files/report/field_attachment_abstract/201707/PERP2017-7_Flyer.pdf; accessed 2017-11-20

[49] K.-C. Xie; *Coal gasification*; in *Structure and Reactivity of Coal*; pages 181–241; Springer (2015)

[50] V. Spallina, M. Romano, P. Chiesa, F. Gallucci, M. van Sint Annaland and G. Lozza; *Integration of coal gasification and packed bed CLC for high efficiency and near-zero emission power generation*; International journal of greenhouse gas

control 27 (2014) 28–41

[51] Y. Man, S. Yang, D. Xiang, X. Li and Y. Qian; *Environmental impact and techno-economic analysis of the coal gasification process with/without CO_2 capture*; Journal of cleaner production 71 (2014) 59–66

[52] K. Jordal, R. Anantharaman, T. A. Peters, D. Berstad, J. Morud, P. Nekså and R. Bredesen; *High-purity H_2 production with CO_2 capture based on coal gasification*; Energy 88 (2015) 9–17

[53] R. Bhandari, C. A. Trudewind and P. Zapp; *Life cycle assessment of hydrogen production via electrolysis–a review*; Journal of cleaner production 85 (2014) 151–163

[54] J. Nowotny, C. Sorrell, L. Sheppard and T. Bak; *Solar-hydrogen: environmentally safe fuel for the future*; International journal of hydrogen energy 30 (5) (2005) 521–544

[55] I. Uehara; *Separation and purification of hydrogen*; Energy carriers and conversion systems with emphasis on hydrogen 1 (2008) 268e82

[56] S. Sircar and T. Golden; *Purification of hydrogen by pressure swing adsorption*; Separation Science and Technology 35 (5) (2000) 667–687

[57] H. Khajuria; *Model-based design, operation and control of pressure swing adsorption systems*; Ph.D. thesis; Department of Chemical Engineering and Chemical Technology, Imperial College London (2011)

[58] D. M. Ruthven, S. Farooq and K. S. Knaebel; *Pressure swing adsorption*; volume 480 (1994); VCH publishers New York

[59] M. Mofarahi and F. Gholipour; *Gas adsorption separation of CO_2/CH_4 system using zeolite 5A*; Microporous and Mesoporous Materials 200 (2014) 1–10

[60] M. Mofarahi and M. Seyyedi; *Pure and binary adsorption isotherms of nitrogen and oxygen on zeolite 5A*; Journal of Chemical & Engineering Data 54 (3) (2009) 916–921

[61] J. Yang, C.-H. Lee and J.-W. Chang; *Separation of hydrogen mixtures by a two-bed pressure swing adsorption process using zeolite 5A*; Industrial & engineering chemistry research 36 (7) (1997) 2789–2798

[62] S. Ga, H. Jang and J. H. Lee; *New performance indicators for adsorbent evaluation derived from a reduced order model of an idealized PSA process for CO_2 capture*; Computers & Chemical Engineering 102 (Supplement C) (2017) 188 – 212; ISSN 0098-1354; DOI:https://doi.org/10.1016/j.compchemeng.2016.11.021; sustainability & Energy Systems

[63] A.-M. Banu, D. Friedrich, S. Brandani and T. Düren; *A multiscale study of MOFs as adsorbents in H_2 PSA purification*; Industrial & Engineering Chemistry Research 52 (29) (2013) 9946–9957

[64] S. Nandi, P. De Luna, T. D. Daff, J. Rother, M. Liu, W. Buchanan, A. I. Hawari, T. K. Woo and R. Vaidhyanathan; *A single-ligand ultra-microporous MOF for precombustion CO_2 capture and hydrogen purification*; Science advances 1 (11) (2015) e1500421

[65] Y. Zhou, Y. Shen, Q. Fu and D. Zhang; *CO Enrichment from Low-Concentration Syngas by a Layered-Bed VPSA Process*; Industrial & Engineering Chemistry Research

[66] F. Gao, Y. Wang and S. Wang; *Selective adsorption of CO on CuCl/Y adsorbent prepared using $CuCl_2$ as precursor: equilibrium and thermodynamics*; Chemical Engineering Journal 290 (2016) 418–427

[67] B. Li, G. He, X. Jiang, Y. Dai and X. Ruan; *Pressure swing adsorption/membrane hybrid processes for hydrogen purification with a high recovery*; Frontiers of Chemical Science and Engineering 10 (2) (2016) 255–264

[68] S. Sircar, W. Waldron, M. Rao and M. Anand; *Hydrogen production by hybrid SMR–PSA–SSF membrane system*; Separation and Purification Technology 17 (1) (1999) 11–20

[69] X. Feng, C. Y. Pan, J. Ivory and D. Ghosh; *Integrated membrane/adsorption process for gas separation*; Chemical engineering science 53 (9) (1998) 1689–1698

[70] J. Phair and S. Badwal; *Materials for separation membranes in hydrogen and oxygen production and future power generation*; Science and technology of advanced materials 7 (8) (2006) 792–805

[71] N. Al-Mufachi, N. Rees and R. Steinberger-Wilkens; *Hydrogen selective membranes: a review of palladium-based dense metal membranes*; Renewable and Sustainable Energy Reviews 47 (2015) 540–551

[72] P. Bernardo, E. Drioli and G. Golemme; *Membrane gas separation: a review/state of the art*; Industrial & Engineering Chemistry Research 48 (10) (2009) 4638–4663

[73] R. Swaidan, B. Ghanem and I. Pinnau; *Fine-tuned intrinsically ultramicroporous polymers redefine the permeability/selectivity upper bounds of membrane-based air and hydrogen separations* (2015)

[74] C. A. Scholes, G. W. Stevens and S. E. Kentish; *Membrane gas separation applications in natural gas processing*; Fuel 96 (2012) 15–28

[75] C. J. Orme, M. L. Stone, M. T. Benson and E. S. Peterson; *Testing of polymer membranes for the selective permeability of hydrogen*; Separation science and technology 38 (12-13) (2003) 3225–3238

[76] B. Castro-Dominguez, P. Leelachaikul, A. Takagaki, T. Sugawara, R. Kikuchi and S. T. Oyama; *Supported perfluorotributylamine liquid membrane for H_2/O_2 separation*; Journal of membrane science 448 (2013) 262–269

[77] P. Pinacci, E. Louradour, L. Wimbert, M. Gindrat, M. O. Jarligo, R. Vassen, A. Comite, J. Serra, J. Jewulski, L. Mancuso *et al.*; *Dense membranes for oxygen and hydrogen separation (DEMOYS): project overview and first results*; Energy Procedia 37 (2013) 1030–1038

[78] P. Leelachaikul, B. Castro-Dominguez, A. Takagaki, T. Sugawara, R. Kikuchi and S. T. Oyama; *Perfluorooctanol-based liquid membranes for H_2/O_2 separation*; Separation and Purification Technology 122 (2014) 431–439

[79] T. Yamaguchi, A. Takagaki, T. Sugawara, R. Kikuchi and S. T. Oyama; *Supported fluorocarbon liquid membranes for hydrogen/oxygen separation*; Journal of Membrane Science 520 (2016) 272–280

[80] R. W. Baker; *Future directions of membrane gas separation technology*; Industrial & Engineering Chemistry Research 41 (6) (2002) 1393–1411

[81] D. F. Sanders, Z. P. Smith, R. Guo, L. M. Robeson, J. E. McGrath, D. R. Paul and B. D. Freeman; *Energy-efficient polymeric gas separation membranes for a sustainable future: a review*; Polymer 54 (18) (2013) 4729–4761

[82] R. W. Baker; *Membrane technology* (2000); Wiley Online Library

[83] H. Ohya, V. Kudryavsev and S. I. Semenova; *Polyimide membranes: applications, fabrications and properties* (1997); CRC Press

[84] S. D. Kenarsari, D. Yang, G. Jiang, S. Zhang, J. Wang, A. G. Russell, Q. Wei and M. Fan; *Review of recent advances in carbon dioxide separation and capture*; Rsc Advances 3 (45) (2013) 22739–22773

[85] H. Lin, Z. He, Z. Sun, J. Kniep, A. Ng, R. W. Baker and T. C. Merkel; *CO_2-selective membranes for hydrogen production and CO_2 capture–Part II: Techno-economic analysis*; Journal of Membrane Science 493 (2015) 794–806

[86] T. C. Merkel, M. Zhou and R. W. Baker; *Carbon dioxide capture with membranes at an IGCC power plant*; Journal of membrane science 389 (2012) 441–450

[87] Y. Zhao and W. W. Ho; *CO_2-selective membranes containing sterically hindered amines for CO_2/H_2 separation*; Industrial & Engineering Chemistry Research 52 (26) (2012) 8774–8782

[88] S. R. Reijerkerk, M. H. Knoef, K. Nijmeijer and M. Wessling; *Poly (ethylene glycol) and poly (dimethyl siloxane): combining their advantages into efficient CO_2 gas separation membranes*; Journal of membrane science 352 (1) (2010) 126–135

[89] K. Ramasubramanian, Y. Zhao and W. Winston Ho; *CO_2 capture and H_2 purification: Prospects for CO_2-selective membrane processes*; AIChE Journal 59 (4) (2013) 1033–1045

[90] P. Li, Z. Wang, Z. Qiao, Y. Liu, X. Cao, W. Li, J. Wang and S. Wang; *Recent developments in membranes for efficient hydrogen purification*; Journal of Membrane Science 495 (2015) 130–168

[91] DOE/NETL; *Advanced Carbon Dioxide Capture R&D Program: Technology Update May 2013,Page B-158 to B-163*

[92] T. Merkel; MTR: Personal Communication; received 2016-04-21

[93] E. W. van Niel; *Biological processes for hydrogen production*; Anaerobes in Biotechnology pages 155–193

[94] W. Nuttall, B. Glowacki and S. Krishnamurthy; *Next Steps for Hydrogen-physics, technology and the future*

[95] S. Sharma and S. K. Ghoshal; *Hydrogen the future transportation fuel: from production to applications*; Renewable and sustainable energy reviews 43 (2015) 1151–1158

[96] J. Baltrusaitis; *Sustainable Ammonia Production* (2017)

[97] J. Z. Zhang, J. Li, Y. Li and Y. Zhao; *Hydrogen generation, storage and utilization* (2014); John Wiley & Sons

[98] M. Appl; *Ammonia: principles and industrial practice* (1999); Wiley Online Library

[99] M. van der Hoeven, Y. Kobayashi and R. Diercks; *Technology Roadmap: Energy and GHG Reductions in the Chemical Industry via Catalytic Processes*; International Energy Agency: Paris page 56

[100] M. Matzen, M. Alhajji and Y. Demirel; *Technoeconomics and sustainability of renewable methanol and ammonia productions using wind power-based hydrogen*; J Adv Chem Eng 5 (128) (2015) 2

[101] J. M. McEnaney, A. R. Singh, J. A. Schwalbe, J. Kibsgaard, J. C. Lin, M. Cargnello, T. F. Jaramillo and J. K. Nørskov; *Ammonia synthesis from N_2 and H_2O using a lithium cycling electrification strategy at atmospheric pressure*; Energy & Environmental Science 10 (7) (2017) 1621–1630

[102] F. Köleli and D. B. Kayan; *Low overpotential reduction of dinitrogen to ammonia in aqueous media*; Journal of Electroanalytical Chemistry 638 (1) (2010) 119–122

[103] H. Hirakawa, M. Hashimoto, Y. Shiraishi and T. Hirai; *Photocatalytic conversion of nitrogen to ammonia with water on surface oxygen vacancies of titanium dioxide*; Journal of the American Chemical Society 139 (31) (2017) 10929–10936

[104] X. Chen, N. Li, Z. Kong, W.-J. Ong and X. Zhao; *Photocatalytic fixation of nitrogen to ammonia: state-of-the-art advancements and future prospects*; Materials Horizons

[105] D. Seddon *et al.*; *Economics: Volatility in the methanol market*; Chemistry in Australia (Apr 2017) (2017) 36

[106] S. G. Jadhav, P. D. Vaidya, B. M. Bhanage and J. B. Joshi; *Catalytic carbon dioxide hydrogenation to methanol: a review of recent studies*; Chemical Engineering Research and Design 92 (11) (2014) 2557–2567

[107] I. Ganesh; *Conversion of carbon dioxide into methanol–a potential liquid fuel: Fundamental challenges and opportunities (a review)*; Renewable and Sustainable Energy Reviews 31 (2014) 221–257

[108] G. A. Olah; *Beyond oil and gas: the methanol economy*; Angewandte Chemie International Edition 44 (18) (2005) 2636–2639

[109] J. Haid and U. Koss; *Lurgi's Mega-Methanol technology opens the door for a new era in down-stream applications*; Studies in Surface Science and Catalysis 136 (2001) 399–404

[110] J.-P. Lange; *Methanol synthesis: a short review of technology improvements*; Catalysis Today 64 (1) (2001) 3–8

[111] J. Ott, V. Gronemann, F. Pontzen, E. Fiedler, G. Grossmann, D. Kersebohm, G. Weiss and C. Witte; *Ullmann's encyclopedia of industrial chemistry* (2012)

[112] É. S. Van-Dal and C. Bouallou; *Design and simulation of a methanol production plant from CO_2 hydrogenation*; Journal of cleaner production 57 (2013) 38–45

[113] M. Pérez-Fortes, J. C. Schöneberger, A. Boulamanti and E. Tzimas; *Methanol synthesis using captured CO_2 as raw material: techno-economic and environmental assessment*; Applied Energy 161 (2016) 718–732

[114] F. Pontzen, W. Liebner, V. Gronemann, M. Rothaemel and B. Ahlers; *CO_2-based methanol and DME–Efficient technologies for industrial scale production*; Catalysis Today 171 (1) (2011) 242–250

[115] J. Kim, C. A. Henao, T. A. Johnson, D. E. Dedrick, J. E. Miller, E. B. Stechel and C. T. Maravelias; *Methanol production from CO_2 using solar-thermal energy: process development and techno-economic analysis*; Energy & Environmental Science 4 (9) (2011) 3122–3132

[116] M. Peters, B. Köhler, W. Kuckshinrichs, W. Leitner, P. Markewitz and T. E. Müller; *Chemical technologies for exploiting and recycling carbon dioxide into the value chain*; ChemSusChem 4 (9) (2011) 1216–1240

[117] J. Kim, T. A. Johnson, J. E. Miller, E. B. Stechel and C. T. Maravelias; *Fuel production from CO_2 using solar-thermal energy: system level analysis*; Energy & Environmental Science 5 (9) (2012) 8417–8429

[118] Methanex; *Methanol current market price* (2017); URL: `https://www.methanex.com/our-business/pricing`; accessed 2017-07-25

[119] A. Kudo; *Development of photocatalyst materials for water splitting*; International Journal of Hydrogen Energy 31 (2) (2006) 197–202

[120] R. W. Baker and B. T. Low; *Gas separation membrane materials: a perspective*; Macromolecules 47 (20) (2014) 6999–7013

[121] V. Schröder and K. Holtappels; *Explosion characteristics of hydrogen-air and hydrogen-oxygen mixtures at elevated pressures*; in *International Conference on hydrogen safety, Congress Palace, Pisa, Italy* (2005)

[122] H. F. Coward and G. W. Jones; *Limits of flammability of gases and vapors*; Technical report; Bureau of Mines Washington DC (1952)

[123] I. A. Zlochower and G. M. Green; *The limiting oxygen concentration and flammability limits of gases and gas mixtures*; Journal of loss prevention in the process industries 22 (4) (2009) 499–505

[124] J. Dwyer Jr, J. G. Hansel and T. Philips; *Temperature influence on the flammability limits of heat treating atmospheres*; in *Proceedings of the 22nd heat treating society conference and the 2nd international surface engineering congress. Indianapolis* (2003) pages 24–28

[125] S. Rehn; *Flammability of hydrogen at sub-atmospheric pressures and reduced oxygen concentrations* (2014); Rutgers The State University of New Jersey-New Brunswick

[126] M. Scholz, T. Harlacher, T. Melin and M. Wessling; *Modeling gas permeation by linking nonideal effects*; Industrial & Engineering Chemistry Research 52 (3) (2012) 1079–1088

[127] T. Melin and R. Rautenbach; *Membranverfahren. Vol. 3* (2007)

[128] N. I. of Standards and Technology; *Thermophysical Properties of Fluid Systems* (2011); URL: `http://webbook.nist.gov/chemistry/fluid/`; accessed 2015-07-1

[129] E. Drioli and L. Giorno; *Comprehensive membrane science and engineering*; volume 1 (2010); Newnes

[130] M. R. Bussieck and S. Vigerske; *MINLP solver software*; Wiley encyclopedia of operations research and management science

[131] R. Misener and C. A. Floudas; *ANTIGONE: algorithms for continuous/integer global optimization of nonlinear equations*; Journal of Global Optimization 59 (2-3) (2014) 503–526

[132] M. Scholz, M. Alders, T. Lohaus and M. Wessling; *Structural optimization of membrane-based biogas upgrading processes*; Journal of Membrane Science 474 (2015) 1–10

[133] L. T. Biegler, I. E. Grossmann and A. W. Westerberg; *Systematic methods for chemical process design* (1997); Prentice Hall, Old Tappan, NJ (United States)

[134] B. Ohs, J. Lohaus and M. Wessling; *Optimization of membrane based nitrogen removal from natural gas*; Journal of Membrane Science 498 (2016) 291–301

[135] K. M. Guthrie; *Data and techniques for preliminary capital cost estimating*; Chemical Engineering 76 (6) (1969) 114

[136] DOE; *Fuel Cell Technologies Office: Multi-Year Research, Development, and Demonstration Plan (3.1 Hydrogen Production)* (2015); URL: `http://energy.gov/eere/fuelcells/downloads/fuel-cell-technologies-office-multi-year-research-development-and-22`; accessed 2015-08-21

[137] Eurostat; *Electricity prices by type of user (Medium Size Industries)* (2016); URL: `http://ec.europa.eu/eurostat/tgm/table.do?tab=table&init=1&language=en&pcode=ten00117&plugin=1`; accessed 2017-03-13

[138] A. Thyer, J. Kay and S. Gant; *Investigations into the flammability of propane/carbon dioxide, hydrogen/carbon dioxide and hydrogen/nitrogen mixtures*; in *Proc. IChemE Hazards XXI Conference, Manchester, UK* (2009) pages 9–12

[139] A. Di Benedetto, V. Di Sarli, E. Salzano, F. Cammarota and G. Russo; *Explosion behavior of $CH_4/O_2/N_2/CO_2$ and $H_2/O_2/N_2/CO_2$ mixtures*; international journal of hydrogen energy 34 (16) (2009) 6970–6978

[140] S. D. Emami, R. M. Kasmani, M. D. Hamid, C. R. C. Hassan and S. Z. Sulaiman; *Effect of inhibitor gases on hydrogen flame propagation in a confined tee pipe (Part I)*; Fuel 165 (2016) 50–58

[141] M. Tawarmalani and N. V. Sahinidis; *Convexification and global optimization in continuous and mixed-integer nonlinear programming: theory, algorithms, software, and applications*; volume 65 (2002); Springer Science & Business Media

[142] N. Sahinidis and M. Tawarmalani; *BARON: The GAMS Solver Manual*; GAMS Development Corporation, Washington, DC pages 9–20

[143] T. C. Merkel, H. Lin, X. Wei and R. Baker; *Power plant post-combustion carbon dioxide capture: an opportunity for membranes*; Journal of membrane science 359 (1) (2010) 126–139

[144] C. Pan; *Gas separation by permeators with high-flux asymmetric membranes*; AIChE journal 29 (4) (1983) 545–552

[145] N. v. d. Assen, L. J. MuÌĹller, A. Steingrube, P. Voll and A. Bardow; *Selecting CO_2 sources for CO_2 utilization by environmental-merit-order curves*; Environmental science & technology 50 (3) (2016) 1093–1101

[146] E. S. Rubin, J. E. Davison and H. J. Herzog; *The cost of CO_2 capture and storage*; International Journal of Greenhouse gas control 40 (2015) 378–400

[147] A. D. Ebner and J. A. Ritter; *State-of-the-art adsorption and membrane separation processes for carbon dioxide production from carbon dioxide emitting industries*; Separation Science and Technology 44 (6) (2009) 1273–1421

[148] R. P. Lively, M. E. Dose, L. Xu, J. T. Vaughn, J. Johnson, J. A. Thompson, K. Zhang, M. E. Lydon, J.-S. Lee, L. Liu *et al.*; *A high-flux polyimide hollow fiber membrane to minimize footprint and energy penalty for CO_2 recovery from flue gas*; Journal of membrane science 423 (2012) 302–313

[149] R. P. Lively, R. R. Chance, B. Kelley, H. W. Deckman, J. H. Drese, C. W. Jones and W. J. Koros; *Hollow fiber adsorbents for CO_2 removal from flue gas*; Industrial & Engineering Chemistry Research 48 (15) (2009) 7314–7324

[150] G. T. Rochelle; *Amine scrubbing for CO2 capture*; Science 325 (5948) (2009) 1652–1654

[151] K. Paustian, N. Ravindranath and A. van Amstel; *2006 IPCC Guidelines for National Greenhouse Gas Inventories*; Technical report (2006)

[152] A. Goeppert, M. Czaun, J.-P. Jones, G. S. Prakash and G. A. Olah; *Recycling of carbon dioxide to methanol and derived products–closing the loop*; Chemical Society Reviews 43 (23) (2014) 7995–8048

[153] M. Ramezan, T. J. Skone, N. y. Nsakala, G. Liljedahl, L. Gearhart, R. Hestermann and B. Rederstorff; *Carbon dioxide capture from existing coal-fired power plants*; National Energy Technology Laboratory, DOE/NETL Report (401/110907)

[154] M. Behrens; *Chemical hydrogen storage by methanol: challenges for the catalytic*

methanol synthesis from CO_2; Recycl. Catal

[155] Eurostat; *ECU/EUR exchange rates versus national currencies* (2016); URL: http://ec.europa.eu/eurostat/tgm/table.do?tab=table&init=1&plugin=1&language=en&pcode=tec00033; accessed 2017-03-14

[156] A. Aesar; *Copper based methanol synthesis catalyst* (2017); URL: https://www.alfa.com/en/catalog/045776/; accessed 2017-03-13

[157] M. Saito, T. Fujitani, M. Takeuchi and T. Watanabe; *Development of copper/zinc oxide-based multicomponent catalysts for methanol synthesis from carbon dioxide and hydrogen*; Applied Catalysis A: General 138 (2) (1996) 311–318

[158] H. Goehna and P. Koenig; *Producing methanol from CO_2*; CHEMTECH;(United States) 24 (6)

[159] D. Mignard and C. Pritchard; *Processes for the synthesis of liquid fuels from CO_2 and marine energy*; Chemical engineering research and Design 84 (9) (2006) 828–836

[160] A. M. De Groote and G. F. Froment; *Simulation of the catalytic partial oxidation of methane to synthesis gas*; Applied Catalysis A: General 138 (2) (1996) 245–264

[161] B. Cañete, C. E. Gigola and N. B. Brignole; *Synthesis gas processes for methanol production via CH_4 reforming with CO_2, H_2O, and O_2*; Industrial & Engineering Chemistry Research 53 (17) (2014) 7103–7112

[162] N. Haik-Beraud, S. Moreau, F. Jantet, J. Freysz and A. Moulin; *Purification of a mixture of H_2/CO by catalysis of the impurities* (2007); URL: https://www.google.com/patents/US20070003477; uS Patent App. 10/559,864

[163] H. Chen and D. Olsen; *Removing oxygen from hydrocarbon gases* (1995); URL: https://www.google.com/patents/US5446232; uS Patent 5,446,232